The University of Reading
Department of Mathematics

Three-dimensional Scattering Problems with applications to Optical Security Devices

by

Corinna Burkard

Thesis submitted for the degree of Doctor of Philosophy

March 2010

Abstract

Optical security devices such as those used on bank notes, passports and identification cards use the scattering of light. The mathematical discussion of the appropriate direct and inverse scattering problem can lead to new insights to understand and develop new security devices.

In this thesis we are concerned with the study of three-dimensional acoustic and electromagnetic scattering problems. To investigate the scattering effects in optical security devices we begin by studying the inverse three-dimensional rough surface problem using a potential approach which was first suggested by Kirsch and Kress for shape reconstructions of bounded domains. In contrast to the bounded domain case a rigorous analysis for the infinite rough surface approach cannot be carried out directly. We present a *multi-section* approach and prove convergence by using an analysis for the *semi-finite* approach. Studying also a time-domain rough surface reconstruction problem incorporates a more practical setting of shape reconstruction from time-domain measurements. The method we propose is based on the causality principle in contrast to earlier work of Chandler-Wilde and Lines, and by Luke and Potthast. We present numerical examples both for a frequency and a time-domain setting in three dimensions.

For further developments in optical security devices we suggest incorporating anisotropic materials which we discuss in terms of the three-dimensional electromagnetic scattering problem. We present a numerical integration scheme for the strong singularity of the involved integral operator. Furthermore, we develop a domain decomposition scheme which permits computations with several million unknowns. We include results from numerical experiments performed on a personal computer with 2 GB RAM and show the feasibility of using the domain decomposition approach.

Declaration

I confirm that this is my own work and the use of all material from other sources has been properly and fully acknowledged.

Corinna Burkard

Acknowledgements

First and foremost I would like to thank my supervisor Dr Roland Potthast for his constant support, guidance and enthusiasm throughout the past three years. His encouragement and expertise have enabled me to study a great topic and also to participate in many stimulating conferences and workshops.
I also thank all of my further supervisors, Prof Dr Simon Chandler-Wilde, Prof Dr Geoffrey Mitchell and the additional support from Dr Marko Lindner and Visiting Professor David Ezra for many interesting discussions and their inspiration.
I wish particularly to thank my Diplom-supervisor PD Dr Tilo Arens from the University of Karlsruhe who introduced me into the world of inverse and direct scattering theory and who drew my attention to the possibility to apply for a PhD studentship at the University of Reading.
I thank all my office mates and my friends at the Mathematics Department and elsewhere who made these three years tremendously enjoyable. Thank you for all your encouragement and support.
I owe special thanks to my boyfriend Yannick for his constant belief in me and in encouraging me in realising my dreams. I am deeply grateful for the love and support I have received from him, from my mum and dad, my childhood friend Jill and my sisters Victoria and Eva during the last three years.
Finally I would like to acknowledge the financial support of the Research Endowment Trust Fund (RETF).

Contents

Chapter 1

Introduction

1.1 From rough surface scattering to optical security devices

Optical security devices are widely used to secure documents like banknotes, passports, identity cards, credit cards or even CDs and DVDs. A presentation of different types of optically variable devices (OVDs), their functional principle and fabrication can be found in [53].

A mathematical discussion of such a device raises questions about how to formulate the problem setting and how to approach the computational complexity of such a 3D problem.

The *rough surface acoustic scattering problem* in three dimensions establishes a basis for the understanding of such optical security devices. By a *rough surface* we denote a surface which is usually a non-local perturbation of an infinite flat surface such that the surface lies within a finite distance of the original plane. The cross section of, for example, a *rainbow hologram*, possesses such a rough profile. Rainbow holograms are widely known and can typically be found on credit cards as a security tool. Hence, one of the possible approaches to the understanding of optical security devices is the discussion of the rough surface scattering problem. In particular, we consider the inverse problem which is to determine the shape of the surface from a knowledge of the near field measurements. We present two surface-reconstruction methods. This is

Part 1 of this thesis.

In addition, the optically *variable* device (OVD), see [53], could be enhanced by anisotropic scattering effects of electromagnetic waves. We approach the understanding of an optically variable device by the discussion of the electromagnetic anistropic scattering problem and its computational realisation. Here, as a consequence, scattering effects can be constructed and used for the development of new devices. The optical *variable* device can be seen as a medium where the matrix of *anisotropy*, given by

$$N(x) = \frac{1}{\epsilon_0}\left(\epsilon(x) + i\,\frac{\sigma(x)}{\omega}\right) \text{ for } x \in \mathbb{R}^3, \tag{1.1}$$

where $\epsilon = \epsilon(x)$ is the tensor of the *electric permittivity* and $\sigma = \sigma(x)$ is the tensor of the *electric conductivity*, possesses entries, which themselves are rough. For example, we could assume that $N_{i,j} \in BC^{n,\beta}(\mathbb{R}^3, \mathbb{C})$ for some $n \geq 1$ and $\beta \in (0, 1]$. We note that the constant ϵ_0 is known as the dielectric constant of the vacuum and ω is the frequency of the electromagnetic wave.

In Part 2 we are concerned with the latter approach. We discuss the scattering of electromagnetic waves in three-dimensions on an anisotropic strip and present an efficient numerical approach for the computational realisation. In particular, we consider a geometrical *domain decomposition approach* which enables us to compute numerical examples of electromagnetic scattering by anisotropic materials involving higher wavenumbers. We note that we restrict ourselves to the case where the entries of N are compactly supported and C^3-smooth. In this case a unique solution exists, see [42] and in [44].

1.2 Three-dimensional rough surface problems

In Part 1 we discuss the *inverse rough surface scattering problem* in the frequency domain. The purpose of this chapter is to introduce the direct rough surface scattering problem and to discuss its differences to the two-dimensional setting and to the bounded domain case. We begin with the presentation of the direct rough surface scattering problem and discuss how to establish a well-posed boundary integral equation in three-dimensions as carried out in [8] and [9]. In this chapter we provide the results of [8] and [9] and introduce the *multi-section method* for the rough surface problem as discussed

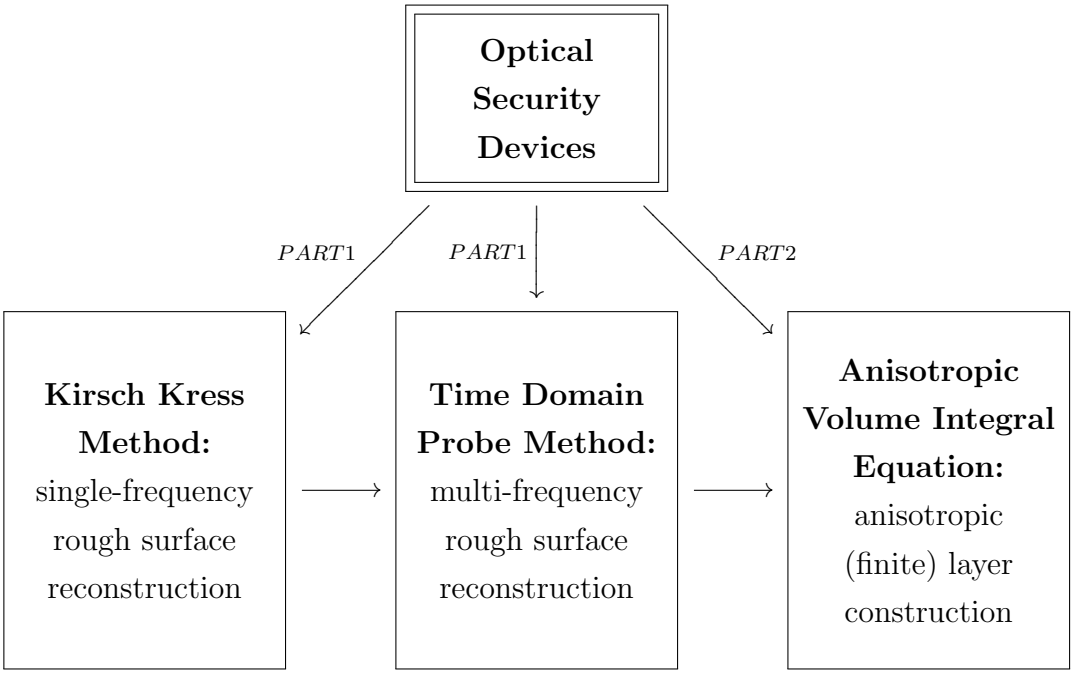

Figure 1.1: *The diagram shows the different parts of this thesis.*

in [27].

1.2.1 Rough surface scattering

We expect the *rough scattering surface* Γ to be the graph of some bounded continuous function $f : \mathbb{R}^2 \to \mathbb{R}$,

$$\Gamma := \Gamma_f = \left\{ x = (x_1, x_2, x_3) \in \mathbb{R}^3 : x_3 = f(x_1, x_2) \right\}, \tag{1.2}$$

where we further assume that there exist two constants $f_-, f_+ > 0$ with

$$f_- < f < f_+. \tag{1.3}$$

Additionally to assumption (1.3), we expect the rough surface to be the graph of a bounded *Hölder continuously differentiable* function $f \in BC^{1,\beta}(\mathbb{R}^2)$ for $0 < \beta \leq 1$. A Hölder continuous function is defined as follows.

DEFINITION 1.2.1 (uniformly Hölder continuous). *Let f be a real or complex valued function on a set $\Omega \subset \mathbb{R}^2$. If there exists a constant C with*

$$|f(x) - f(y)| \leq C|x - y|^\beta \tag{1.4}$$

for a Hölder exponent $0 < \beta \leq 1$, then f is called uniformly Hölder continuous. The linear space of all bounded and uniformly Hölder continuous functions defined on Ω with exponent β is called Hölder space $C^{0,\beta}(\Omega)$. This is a Banach space with norm

$$\|f\|_{0,\beta} := \sup_{x\in\Omega} |f(x)| + \sup_{x,y\in\Omega} \frac{|f(x) - f(y)|}{|x - y|^\beta}. \tag{1.5}$$

The Hölder space $C^{1,\beta}(\Omega)$ of uniformly Hölder continuously differentiable functions is the space of differentiable functions f for which the gradient of f belongs to $C^{0,\beta}(\Omega)$, note that we replace the absolute values in (1.5) by Euclidean norms. This is again a Banach space with norm

$$\|f\|_{1,\beta} := \sup_{x\in\Omega} |f(x)| + \|\nabla f\|_{0,\beta}\,. \tag{1.6}$$

Usually, rough surface scattering problems are posed in function spaces on the boundary, see for example [8],[9] for the three-dimensional case and [14], [16] for the two-dimensional case. In general, the integral operators involve integrals over a non-flat rough surface Γ_f. For this reason we need to define appropriate function spaces for functions $\varphi : \Gamma \to \mathbb{R}$ or $\mathbb{C}$. First, we make use of the following spaces of functions over $\mathbb{R}^d$ for $d = 1$ or $d = 2$.

Function spaces over $\mathbb{R}$ and over $\mathbb{R}^2$. We denote by $BC(\mathbb{R}^d)$, $d = 1, 2$, the space of all continuous and bounded functions $\varphi : \mathbb{R}^d \to \mathbb{R}$ or $\mathbb{C}$. If additionally, a function φ vanishes at infinity, i.e. $|\varphi(x)| \to 0$ for $|x| \to \infty$, then we denote this space by $BC_\infty(\mathbb{R}^d)$. Both spaces equipped with the norm

$$\|\varphi\|_{BC} := \sup_{x\in\mathbb{R}^d} |\varphi(x)| \tag{1.7}$$

are Banach spaces. By $BC(\mathbb{R}^d, \mathbb{R}^m)$, $d = 1, 2$, $m = 1, 2, 3$ we introduce the space of all continuous and bounded functions $\varphi : \mathbb{R}^d \to \mathbb{R}^m$ or $\mathbb{C}^m$. We also need the spaces of Lebesgue-integrable functions. Let $1 \leq p < \infty$. The space $L^p(\mathbb{R}^d)$ consists of all functions $\varphi : \mathbb{R}^d \to \mathbb{R}$ or $\mathbb{C}$ which are Lebesgue-measurable and for which the integral of $|\varphi|^p$ over $\mathbb{R}^d$ exists. This is a linear *space of equivalence classes* as we need to identify

two functions in $L^p(\mathbb{R}^d)$ whenever they are identical except for a null set, abbreviated usually by *almost everywhere* or abbreviated by *a.e.*. The L^p-spaces are equipped with the norms

$$\|\varphi\|_{L^p} := \left(\int_{\mathbb{R}^d} |\varphi(x)|^p \, dx \right)^{1/p}. \tag{1.8}$$

For $p = \infty$ we define the space of equivalence classes of *essentially bounded* functions defined by all functions with

$$\|\varphi\|_{L^\infty} := \inf \{c \in \mathbb{R} : |\varphi(x)| < c\} < \infty \tag{1.9}$$

and it is straightforward to see that $\|\cdot\|_{L^\infty}$ is a norm.

Function spaces on the boundary. We assume that a rough surface $\Gamma = \Gamma_f$ has the parametrization

$$\begin{aligned} F_f : \quad \mathbb{R}^2 &\to \mathbb{R}^3, \\ (x_1, x_2) &\to (x_1, x_2, f(x_1, x_2)), \end{aligned} \tag{1.10}$$

and that $F_f \in BC(\mathbb{R}^2, \mathbb{R}^3)$. Then, we define the space $BC(\Gamma)$ by

$$\varphi \in BC(\Gamma) :\Leftrightarrow \varphi \circ F_f \in BC(\mathbb{R}^2). \tag{1.11}$$

In a similar way, we can define the spaces $BC^k(\Gamma)$, $k \in \mathbb{N}$, $BC^{n,\beta}(\Gamma)$, for $n \in \mathbb{N}_0$, $\beta \in (0, 1]$ and the space $L^2(\Gamma)$. For φ in one of the above spaces the surface integral over Γ is given by

$$\int_\Gamma \varphi(y) \, ds(y) = \int_{\mathbb{R}^2} (\varphi \circ F_f)(y_1, y_2) \, J_f(y_1, y_2) \, d(y_1, y_2), \tag{1.12}$$

with the surface area element

$$J_f(y_1, y_2) = \sqrt{1 + |\nabla f(y_1, y_2)|^2}. \tag{1.13}$$

For a function $f \in BC^1(\mathbb{R}^2)$ the surface area element is bounded by

$$1 \le J_f(x_1, x_2) \le \sqrt{1 + L_f^2}$$

with the Lipschitz constant L_f,

$$L_f = \sup_{x,y \in \mathbb{R}^2} \frac{|f(x) - f(y)|}{|x - y|} = \sup_{x \in \mathbb{R}^2} |\nabla f(x)|.$$

We also introduce the isomorphism I_f for $f \in BC^{1,\beta}(\mathbb{R}^2)$, defined by

$$I_f : L^2(\Gamma_f) \to L^2(\mathbb{R}^2), \quad (I_f\varphi)(y_1, y_2) = \varphi(y_1, y_2, f(y_1, y_2)) \quad \text{for } (y_1, y_2) \in \mathbb{R}^2. \tag{1.14}$$

Then, we can associate an integral operator $A : L^2(\Gamma_f) \to L^2(\Gamma_g)$ of the form

$$A\varphi(x) := \int_{\Gamma_f} k(x, y)\varphi(y)\, ds(y) \quad \text{for } x \in \Gamma_g, \tag{1.15}$$

for $g, f \in BC^{1,\beta}(\mathbb{R}^2)$ and kernel $k : \Gamma_g \times \Gamma_f \to \mathbb{C}$ with the element $I_g A I_f^{-1}$ of the set of all bounded operators on $L^2(\mathbb{R}^2)$.

1.2.2 The direct scattering problem

In the forward problem we consider the scattering of an acoustic field by the rough surface Γ defined by (1.2) and let the *domain of propagation* be given by

$$\Omega := \left\{ x \in \mathbb{R}^3 : x_3 > f(x_1, x_2) \right\} . \tag{1.16}$$

To indicate the dependence on f we also use the notation Ω_f . The incident field is due to a *point source* at $z \in \Omega$ defined by $u^i(x) = \Phi(x, z)$, where Φ is the standard fundamental solution of the Helmholtz equation

$$\Phi(x, y) := \frac{1}{4\pi} \frac{e^{i\kappa|x-y|}}{|x - y|}, \quad x, y \in \mathbb{R}^3, x \neq y. \tag{1.17}$$

Here κ is the *wave number*, which is either positive or possesses positive real and imaginary part. The direct problem is to find the scattered field $u^s \in C^2(\Omega) \cap C(\overline{\Omega})$ such that the total field $u = u^i + u^s$ is a solution of the *Helmholtz equation*

$$\Delta u + \kappa^2 u = 0 \quad \text{in } \Omega. \tag{1.18}$$

Furthermore, the total field is required to satisfy the *Dirichlet boundary condition*

$$u = 0 \quad \text{on } \Gamma, \tag{1.19}$$

and the scattered field is supposed to be bounded, i.e.

$$|u^s(x)| \leq c, \quad x \in \Omega, \tag{1.20}$$

for some constant $c > 0$. In the case where the wave number is a positive real number, we follow [8] and require the *limiting absorbing principle*, i.e. that for sufficiently small $\epsilon > 0$ the solution with wave number $k_0 + i\epsilon$ exists and, denoting this solution temporarily with $u^{(k_0+i\epsilon)}$, the limit

$$u^{(k_0+i\epsilon)}(x) \longrightarrow u^{(k_0)}(x), \quad \epsilon \to 0, \tag{1.21}$$

is satisfied for every $x \in \Omega$.

Problem 1.2.2 (Direct Point Source Rough Surface Scattering Problem)**.** *Let u^i be an incident field due to a point source at the point $z \in \Omega$, i.e.*

$$u^i = \Phi(\cdot, z). \tag{1.22}$$

Then, we aim to find the total field $u = u^i + u^s \in C^2(\Omega) \cap C(\overline{\Omega})$, such that u solves the Helmholtz equation (1.18), the Dirichlet boundary condition (1.19), the scattered part u^s satisfies the bound (1.20) and, for $\kappa > 0$, the limiting absorbing principle (1.21) is valid.

We can convert this scattering problem into a boundary value problem seeking the scattered field in the form

$$u^s = v - \Phi(\cdot, z'), \tag{1.23}$$

where z' denotes the reflection of z in the x, y-plane, i.e. $z' = (z_1, z_2, -z_3)$. Then, the Dirichlet boundary condition of the direct scattering problem with the incident field (1.22) yields

$$u^s(x) = -\Phi(x, z), \quad x \in \Gamma,$$

and thus, the remainder v satisfies the boundary condition

$$v(x) = \Phi(x, z') - \Phi(x, z) = -G(x, z), \quad x \in \Gamma. \tag{1.24}$$

Furthermore, v satisfies also the bound (1.20) for some constant $\tilde{c} > 0$ as

$$|v(x)| \leq |u^s(x)| + |\Phi(x, z')| \leq c + \frac{1}{2f_-} \leq \tilde{c}, \quad x \in \Omega,$$

using that the distance $|x - z'|$ is always larger than $2f_-$ for the constant f_- from (1.3).

We remark that the total field u satisfies the direct scattering problem if and only if v solves the following boundary value problem, see [8].

Problem 1.2.3 (Boundary Value Problem)**.** *Find $v \in C^2(\Omega) \cap C(\overline{\Omega})$, which satisfies the Helmholtz equation (1.18), the boundary condition (1.24), the bound (1.20) and, for $\kappa > 0$, the limiting absorbing principle (1.21).*

The direct scattering problem can be reformulated in a well-posed integral equation in the sense that the integral equation possesses a unique solution which depends continuously on the right hand side, see [8],[9] and section 1.3.

1.2.3 Difficulties in extending the theory of BIE

For the rough surface scattering problem in *three dimensions*, there are a number of difficulties in extending the theory of boundary integral equation methods (BIE) from bounded to unbounded scatterers or from the two-dimensional case. Before we finish this chapter with an overview of the main results for the direct rough surface scattering problem by Chandler-Wilde, Potthast and Heinemeyer, [8],[9], and Heinemeyer, Lindner and Potthast, [27], we wish to illustrate these difficulties and give a brief outline of how to prove existence and uniqueness of the boundary integral equation given in [8],[9].

We begin with a brief discussion of the behavior of the boundary integral operators over an infinite surface. After that, we explicitly introduce the single and double layer potentials for the three-dimensional case as used in [8],[9]. Finally, we review the basic ideas and techniques which are used to derive the well-posed boundary integral equation for the direct scattering problem as presented in [8],[9]. In the following section we then summarise the main results of the last-mentioned articles.

Let us first consider a boundary integral operator of the form

$$K\varphi(\tilde{x}) := \int_{\Gamma_0} k(\tilde{x} - \tilde{y})\varphi(\tilde{y})\, ds(\tilde{y}), \quad \tilde{x} \in \mathbb{R}^d \tag{1.25}$$

over a flat surface $\Gamma_0 := \left\{\tilde{x} \in \mathbb{R}^d : \tilde{x}_d = 0\right\}$ and $d = 2, 3$. By (1.12) the integral reduces to

$$K\varphi(x) = \int_{\mathbb{R}^{d-1}} k(x - y)\varphi(y)\, dy, \quad x = (x_1, ..., x_{d-1}) \in \mathbb{R}^{d-1}. \tag{1.26}$$

We denote by small letters x, y the vectors $(x_1, ..., x_{d-1})$ and $(y_1, ..., y_{d-1}) \in \mathbb{R}^{d-1}$ as well as the projections $(x_1, ..., x_{d-1}, 0), (y_1, ..., y_{d-1}, 0) \in \mathbb{R}^d$ onto the plane Γ_0.

Weakly and strongly singular integral operators. We call an integral operator (1.26) with kernel $k : \mathbb{R}^d \times \mathbb{R}^d \to \mathbb{R}$ or $\mathbb{C}$, which is continuous for all $x \neq y$, *local weakly singular* if there exists a constant $c > 0$ and a $\lambda \in (0, d]$ with

$$|k(x-y)| \leq c|x-y|^{\lambda-d}, \quad x \in \mathbb{R}^d. \tag{1.27}$$

The integral operator is *strongly singular* if the integral kernel does not anymore satisfy (1.27) but the integral still exists in the sense of *Cauchy's principal value*, i.e. the limit

$$\lim_{\varepsilon \to 0} \int_{\mathbb{R}^d \setminus B_\varepsilon(x)} k(x-y)\varphi(y)\, ds(y)$$

for $B_\varepsilon(x)$ being the ball with radius ε and centre x exists.

If $x \in \Gamma_0$, then the integral operator (1.25) is not only singular *at infinity* in the sense that $x, y \to \infty$, but also whenever x equals y. We restrict the following computations to the situation where both x and y are in Γ_0.

Let us consider the kernel k to be the fundamental solution of the Helmholtz equation defined by

$$k(x-y) := \begin{cases} \Phi_2(x,y) = \frac{i}{4} H_0^1(\kappa|x-y|), & x, y \in \mathbb{R}^2, \\ \Phi_3(x,y) = \frac{1}{4\pi} \frac{e^{i\kappa|x-y|}}{|x-y|}, & x, y \in \mathbb{R}^3, \end{cases} \tag{1.28}$$

for $x \neq y$. The integral operator with this kernel is called *single layer potential*. Here, the function H_0^1 is the *Hankel function of the first kind of order zero*.

The layer potential where the kernel k is replaced by its normal derivative, i.e.

$$\frac{\partial \Phi_3(x,y)}{\partial \nu(y)}, \tag{1.29}$$

with normal vector ν pointing into the domain of propagation Ω, is called *double layer potential*.

A possible approach for the *(indirect) BIE formulation* is to represent the unknown function v of Problem 1.2.3 (or in general any other scattering problem) as either a single or double layer potential or a combination of both (Brakhage-Werner ansatz). By differentiation of the fundamental solution Φ with respect to x for a fixed y we see that Φ is a solution of the Helmholtz equation. The single or double layer potential approach can then be interpreted as a superposition of solutions of the Helmholtz

equation with respect to some 'weight function', the density. The idea is to find a density φ such that v satisfies the given boundary condition (1.24).

In the bounded domain case, the above kernels are the standard kernels for the single and double layer potentials. They are used for the formulation of the boundary integral equation for bounded continuous functions and Lebesgue-integrable functions, see [17]. For a non-bounded domain Γ_0 it is not clear if the single layer potential is well-defined on $BC(\Gamma_0)$ or $L^p(\Gamma_0)$.

We will show that the decay rate of the kernel defined in (1.28) is not enough for the single layer potential to be well defined for a bounded continuous density. In particular, we consider the integral

$$\int_{\Gamma_0 \cap \{B_N(x) \setminus B_\varepsilon(x)\}} \Phi_d(x,y)\varphi(y)\,dy \tag{1.30}$$

for $N \to \infty$ and $\varepsilon \to 0$ for bounded continuous densities φ and where $B_r(x)$ denotes a ball with radius r at the point x. In two dimensions we have, [17, (3.61)], that there exists a constant $c > 0$ with

$$|\Phi_2(x,y)| \le c \ln \frac{1}{|x-y|}, \tag{1.31}$$

for $|x-y| \to 0$. Furthermore, in three dimensions there exists a generic constant $C > 0$ with

$$|\Phi_3(x,y)| = C\frac{1}{|x-y|}. \tag{1.32}$$

Using the above (in-)equalities we obtain for fixed $N > 0$ that

$$\begin{aligned} \lim_{\varepsilon \to 0} \quad & \Big| \int_{\Gamma_0 \cap \{B_N(x) \setminus B_\varepsilon(x)\}} \Phi_2(x,y)\varphi(y)\,dy \Big| \le c \,\|\varphi\|_{BC} \lim_{\varepsilon \to 0} \int_\varepsilon^N r \ln(\frac{1}{r})\,dr \\ & = c \,\|\varphi\|_{BC} \lim_{\varepsilon \to 0} (\frac{1}{4}N - \frac{1}{2}N^2 \ln\frac{1}{N} - \frac{1}{4}\varepsilon^2 + \frac{1}{2}\varepsilon^2 \ln\frac{1}{\varepsilon}) < \infty, \end{aligned} \tag{1.33}$$

and, in three dimensions,

$$\begin{aligned} \lim_{\varepsilon \to 0} \quad & \Big| \int_{\Gamma_0 \cap \{B_1(x) \setminus B_\varepsilon(x)\}} \Phi_3(x,y)\varphi(y)\,dy \Big| \le C \,\|\varphi\|_{BC} \lim_{\varepsilon \to 0} \int_\varepsilon^1 r\frac{1}{r}\,dr \\ & = C \,\|\varphi\|_{BC} \lim_{\varepsilon \to 0} (N - \varepsilon) < \infty. \end{aligned} \tag{1.34}$$

This shows the integrability for $x = y$ for bounded continuous densities φ. Furthermore, we directly see that the above estimates for the fundamental solution do not suffice to show existence of the integrals for the limit $N \to \infty$.

In a next step we consider the integral (1.30) for the case of densities $\varphi \in L^q(\mathbb{R}^3)$ for $1 \leq q \leq \infty$. Usually, one would use the Hölder inequality to show that the integral of the form (1.30) exists.

THEOREM 1.2.4 (Hölder inequalitiy). *Let $1 \leq p < \infty$ and q with*

$$\frac{1}{p} + \frac{1}{q} = 1.$$

Let $\ell \in L^p(\mathbb{R}^d)$ and $f \in L^q(\mathbb{R}^d)$. Then, $\ell f \in L^1(\mathbb{R}^d)$ and it holds that

$$\int_{\mathbb{R}^d} |\ell(x) f(x)|\, dx \leq \left(\int_{\mathbb{R}^d} |\ell(x)|^p\, dx \right)^{1/p} \left(\int_{\mathbb{R}^d} |f(x)|^q\, dx \right)^{1/q}. \tag{1.35}$$

Proof. For a proof see for example [23], page 90. □

Here, we would like to illustrate the three-dimensional case. We obtain for $p > 2$

$$\begin{aligned} \int_{\Gamma_0 \cap \{B_N(x) \setminus B_\varepsilon(x)\}} |\Phi_3(x,y)|^p\, dy &= C \int_\varepsilon^N \frac{1}{r^p} r\, dr \\ &= C \left[\frac{1}{2-p} r^{2-p} \right]_\varepsilon^N = C \frac{1}{2-p} (N^{2-p} - \varepsilon^{2-p}), \end{aligned}$$

and, for the special cases $p = 2$,

$$\int_{\Gamma_0 \cap \{B_N(x) \setminus B_\varepsilon(x)\}} |\Phi_3(x,y)|^2\, dy = C(\ln N - \ln \varepsilon), \tag{1.36}$$

and for $p = 1$,

$$\int_{\Gamma_0 \cap \{B_N(x) \setminus B_\varepsilon(x)\}} |\Phi_3(x,y)|\, dy = C(N - \varepsilon). \tag{1.37}$$

For $p > 2$ we see that the limit for $N \to \infty$ exists, whereas the local singulariy at zero becomes hypersingular.

For $p = 1$ the local singularity is integrable and for $1 \leq p \leq 2$, the limit for N is not defined and we can interprete the non-integrability on $\mathbb{R}^2$ as a strong singularity.

We remark that in fact the limit of the integral (1.30) in three dimensions does not exist for L^p-densities, see [8] and references therein. Also, we note that in two dimensions, the decay of the Hankel function is also not fast enough for the single layer potential to exist as an improper integral. To show existence of (1.30) one could

consider rapidly decreasing densities φ. In particular, the integral (1.30) does converge if the density φ decreases sufficiently rapidly at infinity. Nevertheless, working with the *Schwartz space* $\mathcal{S}(\Gamma)$ of rapidly decaying functions implicates that we would have to work with a space with a rather unpleasant topological nature.

Instead of trying to chose an appropriate space, we look for a replacement of the kernel Φ_d, such that the above integral exists. To derive a well-defined operator we replace the fundamental solution Φ_d by the *Dirichlet Green's function for the half-space*

$$G_d(x,y) = \Phi_d(x,y) - \Phi_d(x,y'), \tag{1.38}$$

where $y' = (y_1, ..., y_{d-1}, -y_d)$. The single layer potential with kernel (1.38) still has the physical properties needed for the boundary integral equation formulation. In two dimensions the single layer potential with kernel (1.38) is well-defined for BC-densities. This follows from the estimates derived from the asymptotic behavior of the Hankel function (see for example, [55]),

$$|G_2(x,y)| \leq C(1 + |\ln|x-y||) \qquad \text{for } 0 < |x-y| \leq 1, \tag{1.39}$$

$$|G_2(x,y)| \leq c(1 + |x_1 - y_1|)^{-3/2} \quad \text{for } |x-y| \geq \rho, \tag{1.40}$$

where $\rho > 0$ is a constant and the constant $C > 0$ depends only on κ and the constant c depends on κ, x_2 and y_2. In three dimensions, using Taylor approximations for G_3 with respect to the third coordinate y_3 we obtain the asymptotic behavior, see [8],

$$|G_3(x,y)| \approx \frac{x_3 y_3 |\kappa|}{2\pi} \frac{e^{-\mathrm{Im}(\kappa)|x-y|}}{|x-y|^2}, \quad |y| \to \infty, \tag{1.41}$$

where this approximation holds in the sense that

$$|G_3(x,y) - \frac{x_3 y_3 |\kappa|}{2\pi} \frac{e^{-\mathrm{Im}(\kappa)|x-y|}}{|x-y|^2}| \leq C \frac{1}{|x-y|^3}, \tag{1.42}$$

for some constant $C > 0$. For $\kappa > 0$ we have

$$\begin{aligned} &\int_{B_N(x)\setminus B_1(x)} |G_3(x,y)|\, dy \\ &\qquad \approx \int_1^N \frac{1}{r^2} r\, dr = \ln N \to \infty \quad \text{for } N \to \infty, \end{aligned} \tag{1.43}$$

and hence the single layer potential is not well defined for bounded continuous densities. This is one major difference to boundary integral equation methods in two dimensions.

In [8] it is shown via Fourier techniques that the decay of $G_3(x,y)$ is in fact fast enough for the single layer potential to be well-defined for L^2-densities for every $x \in \overline{\Omega}$.

The Brakhage-Werner ansatz. We look for a solution of the boundary value problem, Problem 1.2.3, as the combined single- and double-layer potential

$$v(x) := u_1(x) - i\eta u_2(x) \tag{1.44}$$

with some parameter $\eta \geq 0$, where for a given function $\varphi \in L^2(\Gamma) \cap BC(\Gamma)$ we define the single- and double layer potentials by

$$u_1(x) := \int_\Gamma G_3(x,y)\varphi(y)\,dy, \quad x \in \mathbb{R}^3, \tag{1.45}$$

$$u_2(x) := \int_\Gamma \frac{\partial G_3(x,y)}{\partial \nu(y)}\varphi(y)\,dy, \quad x \in \mathbb{R}^3. \tag{1.46}$$

As shown in [8], seeking the solution of Problem 1.2.3 in the form (1.44) the boundary condition (1.24) leads to a boundary integral equation of the form

$$(\frac{1}{2}I + D - i\eta S)\varphi(x) = -G_3(x,z), \quad x \in \Gamma, \tag{1.47}$$

where the boundary integral operators are defined by

$$S\varphi(x) := \int_\Gamma G_3(x,y)\varphi(y)\,dy, \quad x \in \Gamma, \tag{1.48}$$

$$D\varphi(x) := \int_\Gamma \frac{\partial G_3(x,y)}{\partial \nu(y)}\varphi(y)\,dy, \quad x \in \Gamma. \tag{1.49}$$

S denotes the *single layer operator*, D is the *double layer operator*.

In particular, we have the following relation between the boundary value problem (Problem 1.2.3) and the boundary integral equation (1.47).

THEOREM 1.2.5. *Suppose that v is defined by (1.44) with $\varphi \in L^2(\Gamma) \cap BC(\Gamma)$. Then,*

1. *in the case $\mathrm{Im}(\kappa) > 0$, v satisfies the boundary value problem (Problem 1.2.3) if and only if φ satisfies the BIE (1.47);*

2. *in the case $\kappa > 0$, if v satisfies the boundary value problem (Problem 1.2.3), then φ satisfies (1.47). Conversely, if $\kappa > 0$, and if $\varphi^{(\kappa+i\varepsilon)} \in L^2(\Gamma) \cap BC(\Gamma)$ satisfies the integral equation (1.47) with κ replaced by $\kappa + i\varepsilon$, for all sufficiently small $\varepsilon > 0$, and,*

$$\left\|\varphi - \varphi^{(\kappa+i\varepsilon)}\right\|_{L^2(\Gamma)} \to 0 \text{ for } \varepsilon \to 0, \tag{1.50}$$

then v satisfies the boundary value problem.

Proof. The proof can be found in [8]. □

In the two-dimensional and the three-dimensional case the single and double layer potentials are not compact due to the infinite scattering surface and the low decay rate of the fundamental solution. Nevertheless, in two dimensions it is possible to generalise the Riesz-Fredholm theory of compact operators, see [15], and to prove existence and well-posedness. As pointed out in [8] these methods do not seem to be applicable in the three-dimensional case. In particular, the replacement of the standard fundamental solution by the Dirichlet Green's function for the half-space does not have the same preferable effects as in the two-dimensional case. On the one hand, this modification improves the behavior of the involved boundary integral operators at infinity, but, on the other hand, this modification also causes the kernels of the involved boundary integral operators to be strongly singular rather than weakly singular as in the two-dimensional case.

In [8], the case of a *mildly* rough surfaces in three dimensions is discussed. A mildly rough surface Γ_f is a rough surface which is sufficiently close to a flat surface, i.e. for a constant $h > 0$ we assume that $\|f - h\|_{1,\beta}$ is sufficiently small. The *mildly* rough surface scattering problem is well-posed, see [8]. This was shown by using the convolution type of the involved integral operators, computing the Fourier transform of the kernels and then employing operator perturbation arguments. In [9], these results are extended to the general case of a rough surface as a graph of a Hölder continuously differentiable function.

A numerical approach for the solution of the direct problem for which a complete convergence analysis could be carried out is due to Heinemeyer, Potthast, Lindner, see [27].

1.3 Main results for the direct rough scattering problem

Finally, we present the main results for the direct three-dimensional rough scattering problem obtained in the work of Chandler-Wilde, Heinemeyer and Potthast, [8] and [9]. We also outline the Multisection Method (MSM) which has been presented and

applied to the direct rough surface scattering problem in Heinemeyer, Lindner and Potthast, [27].

We first define the space $X := L^2(\Gamma) \cap BC(\Gamma)$. This space equipped with the norm

$$\|\varphi\|_X := \max\left\{\|\varphi\|_{BC}, \|\varphi\|_{L^2}\right\} \tag{1.51}$$

is a Banach space. For $C_1 > C_2 > 0$ let

$$B = B(C_1, C_2) := \left\{ f \in BC^{1,\beta}(\mathbb{R}^2) : C_1 < f(x_1, x_2), \|f\|_{1,\beta} \leq C_2 \right\}. \tag{1.52}$$

From now on, we assume that the rough surface Γ_f is given by a function $f \in B$.

THEOREM 1.3.1. *The single and double layer operators defined by (1.48) and (1.49) are bounded operators on $L^2(\Gamma)$ and on X.*

Proof. For a proof see [8]. □

THEOREM 1.3.2. *The operator $A := \frac{1}{2}I + D - i\eta S$, $\eta > 0$, is invertible as an operator on $L^2(\Gamma)$ and as an operator on X. Moreover, the BVP (Problem 1.2.3) has exactly one solution v defined by (1.44) where $\varphi \in X$ is given by*

$$\varphi(x) = A^{-1}(-G_3(x, z)), \quad x \in \Gamma. \tag{1.53}$$

Further, for some constant $c > 0$, independent of the point source $G_3(\cdot, z)$,

$$|v(x)| \leq c \|G_3(\cdot, z)\|_X, \quad x \in \overline{\Omega}. \tag{1.54}$$

Proof. For a proof see [9], Theorem 3.1. □

THEOREM 1.3.3. *The single layer operator defined by (1.48) depends continuously on the boundary Γ_f of the unbounded domain Ω_f in the sense that*

$$\sup_{f,g \in B, \|f-g\|_{BC^{1,\beta}(\mathbb{R}^2)} \leq \varepsilon} \left\| I_f S I_f^{-1} - I_g S I_g^{-1} \right\|_{L^2(\mathbb{R}^2) \to L^2(\mathbb{R}^2)} \to 0 \text{ for } \varepsilon \to 0, \tag{1.55}$$

where we make use of the isomorphism defined by (1.14). The same is true for the double layer potential given by (1.49).

Proof. For a proof see Theorem 5.6 in [8]. □

THEOREM 1.3.4. *For $\kappa > 0$ the single layer potential and the double layer potential satisfy the limiting absorption principle, (1.21).*

Proof. This follows from section 6 and Lemma 5.7 in [8]. □

The next definition specifies the Multisection Method.

DEFINITION 1.3.5. *Let Y be a Banach space and let $\{P_\rho\}_{\rho>0}$ be a family of projection operators with the properties*

(P1) $P_\rho P_\tau = P_\tau P_\rho$ *for all* $\rho \geq \tau > 0$,

(P2) $\|P_\rho\| = 1$ *for all* $\rho > 0$,

(P3) $P_\rho \varphi \longrightarrow \varphi$, *for* $\rho \to \infty$, *for all* $\varphi \in Y$.

Let $A : Y \to Y$ be a bounded linear operator, which is boundedly invertible on Y and possesses the property

$$\|(I - P_\rho)AP_\tau\| \to 0 \text{ as } \rho \to \infty \text{ for every fixed } \tau > 0. \tag{1.56}$$

Let $f \in Y$. We look for the unique solution of

$$A\varphi = f. \tag{1.57}$$

The Multisection Method (MSM) to approximate the solution φ of $A\varphi = f$ is defined as follows. For a given precision $\delta > 0$ and sufficiently large cutoff parameters τ and ρ, calculate a solution of

$$\text{(MSM)} \qquad \begin{cases} P_\tau \varphi = \varphi, \\ \|P_\rho A P_\tau \varphi - P_\rho f\| \leq \delta. \end{cases}$$

For the rough surface problem we define a projection operator

$$P_\tau : L^2(\mathbb{R}^2) \to L^2(\mathbb{R}^2), \quad \varphi(\boldsymbol{x}, \cdot) \mapsto \begin{cases} \varphi(\boldsymbol{x}, \cdot) & \text{if } \boldsymbol{x} = (x_1, x_2) \in [-\tau, \tau]^2, \\ 0 & \text{otherwise,} \end{cases} \tag{1.58}$$

where by (1.14) we consider P_τ as an operator on $L^2(\Gamma)$ as well. The projection sets a function to zero outside of the cylinder above the square

$$Q_\tau := \left\{ \boldsymbol{x} \in \mathbb{R}^2 : \max\{|x_1|, |x_2|\} < \tau \right\}.$$

We remark that the family of projection operators defined by (1.58) satisfies the conditions (P1)-(P3), see [27].

THEOREM 1.3.6. *For every precision $\delta > 0$ there is a constant $\tau_0 > 0$ such that the system (MSM) is solvable for every $\rho > 0$ and $\tau > \tau_0 = \tau_0(\delta) > 0$.*

Proof. For a proof see Theorem 3.8 in [27]. □

THEOREM 1.3.7. *For every $\varepsilon > 0$, there are functions $\delta_0, \tau_0 : \mathbb{R}_+ \to \mathbb{R}_+$ and $\rho_0 \mathbb{R}^3_+ \to \mathbb{R}^+$ such that if $\delta < \delta_0(\varepsilon)$, $\tau > \tau_0(\delta)$ and $\rho > \rho_0(\varepsilon, \delta, \tau)$, then every solution φ of the Multisection Method (MSM) is an approximation*

$$\|\varphi - \varphi_0\|_Y < \varepsilon \tag{1.59}$$

of the exact solution φ_0 of (1.57). Furthermore, the Multisection Method applied to the BIE (1.47) is convergent in the above sense.

Proof. This is shown in Theorem 3.10 and Theorem 3.12 in [27]. □

Part I

Inverse 3D Acoustic Rough Surface Scattering

Chapter 2

Preliminaries and tools for the inverse problem

We begin this section by introducing the notation we will use throughout Part 1.

By small letters x, y, z we usually denote points in $\mathbb{R}^3$. The coordinates for a point x are given by (x_1, x_2, x_3) and its reflection on the x, y-plane will be denoted by x' as abbreviation for $(x_1, x_2, -x_3)$. The orthogonal projection of a point $x \in \mathbb{R}^3$ onto $\mathbb{R}^2$, namely (x_1, x_2), will be abbreviated by $\tilde{x}$.

We recall that the definition of a rough surface is given by (1.2) and in the case of a flat surface of height c for a constant $c > 0$ we use the same notation, i.e. we write

$$\Gamma_c = \left\{ x \in \mathbb{R}^3 : x_3 = c \right\}. \tag{2.1}$$

In this case the propagation domain above Γ_c is also denoted by Ω_c.

The *finite section* of a rough surface $\Gamma = \Gamma_f$ is given by

$$\Gamma_{f,A} = \left\{ x \in \mathbb{R}^3 : x_3 = h, |x_1| \leq A, |x_2| \leq A \right\}, \tag{2.2}$$

where $A > 0$ denotes the truncation parameter.

In this section we concentrate on the properties of the single and double layer potentials in three dimensions, given by

$$S\varphi(x) := \int_\Gamma G(x, y)\varphi(y)\, ds(y), \quad x \in \mathbb{R}^3 \backslash \Gamma, \tag{2.3}$$

and

$$D\varphi(x) := \int_\Gamma \frac{\partial G(x,y)}{\partial \nu(y)} \varphi(y)\, ds(y), \quad x \in \mathbb{R}^3 \backslash \Gamma, \tag{2.4}$$

for densities $\varphi \in L^2(\Gamma)$. From now on, $G = G_3$ where G_3 is the Dirichlet Green's function for the Helmholtz equation in three dimensions defined in (1.38). By ν we denote the unit normal pointing into the domain Ω_f.

2.1 Mapping properties of the single layer potential

An essential tool for proving mapping properties of the single or double layer potential is the decomposition of the potentials in local and global parts to allow the study of the behavior of the kernels separately. We first recall an estimate for the Green's function for the half space, given in [8, (3.8)].

LEMMA 2.1.1. *There exists a constant $C = C(\delta) > 0$ such that*

$$|G(x,y)| \leq \frac{C(x_3+1)(y_3+1)}{|x-y|^2} \tag{2.5}$$

for all $x \neq y$ and for all $|x-y| > \delta$. Furthermore, the constant C of the bound (2.5) is given by $\frac{1}{\pi\delta}(1+|\kappa|)$. The estimate (2.5) holds also for the kernel of the double layer potential, given by $\frac{\partial G(x,y)}{\partial \nu(y)}$.

Proof. The bound (2.5) is presented in [8, (3.8)]. It also holds for the kernel of the double layer case, see (5.16) and the arguments before (5.16) in [8]. To see that the constant C is of the form $\frac{1}{\pi\delta}(1+|\kappa|)$, we can argue precisely as in the proof of Lemma 3.1 in [14]. In particular, let $r = |x-y|$ and $r' = |x-y'|$ and, using that

$$g(r) := \frac{d}{dr}\left(\frac{e^{i\kappa r}}{r}\right) = \frac{e^{i\kappa r} - i\kappa e^{i\kappa r}}{r^2}, \tag{2.6}$$

we obtain

$$\begin{aligned} |G(x,y)| &= \frac{1}{4\pi}\left|\frac{e^{i\kappa r}}{r} - \frac{e^{i\kappa r'}}{r'}\right| \leq \frac{1}{4\pi}|r-r'| \max_{r<s<r'} |g(s)| \\ &\leq \frac{1}{4\pi}\frac{4(1+x_3)(1+y_3)}{r+r'} \max_{r<s<r'} |g(s)| \\ &\leq \frac{(1+x_3)(1+y_3)}{\pi\delta}\frac{|(1-i\kappa)|}{r^2} \\ &\leq (1+|\kappa|)\frac{(1+x_3)(1+y_3)}{\pi\delta}\frac{1}{r^2}. \end{aligned} \tag{2.7}$$

From this the last statement follows. □

Using Taylor's expansion with respect to x_3 we obtain the following asymptotic behavior for the Green's function for the half space.

LEMMA 2.1.2. *There exists a constant $C > 0$ such that*

$$|G(x,y) + \frac{1}{2\pi} x_3 y_3 \frac{i\kappa\, e^{i\kappa|\tilde{x}-\tilde{y}|}}{|\tilde{x}-\tilde{y}|^2}| \leq C \frac{1}{|\tilde{x}-\tilde{y}|^3} \tag{2.8}$$

for all $\tilde{x} \neq \tilde{y}$, where $\tilde{x}$ and $\tilde{y}$ denote the orthogonal projections (x_1, x_2) and (y_1, y_2) of the points $x = (x_1, x_2, x_3)$ and $y = (y_1, y_2, y_3)$.

Proof. This is proven in [8]. □

In the following chapter we consider the single layer potential (2.3) over a flat surface $\Gamma = \Gamma_H$ for some constant function $H > 0$ and we will need the mapping properties of the single layer potential for the following cases.

(a) Let $\varphi \in L^2(\Gamma_H)$ and $x \in \Gamma_f$, where the surface $\Gamma = \Gamma_f$ lies above the test surface Γ_H where, additionally, $H > 0$ is a constant with $H < f_- < f(\tilde{x}) < f_+$.

(b) Let $\varphi \in L^2(\Gamma_H)$ and $x \in \Gamma_{h,A}$ for $H < h$ and for some truncation parameter $A > 0$.

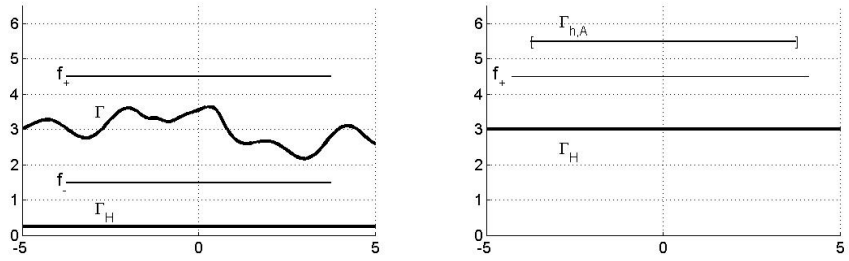

(a) (b)

Figure 2.1: *In Figure (a) we visualise case (a). Case (b) is shown in Figure (b).*

We note that these cases are motivated by the potential approach of the rough surface reconstruction scheme which will be the topic of the next chapter. In this chapter we prove the mapping properties for the case where S is a mapping from $L^2(\Gamma_g) \to L^2(\Gamma_f)$ for (non-intersecting) rough surfaces Γ_g and Γ_f.

We use the isomorphism (1.14) and the explanation below (1.14). In particular, we consider

$$\mathcal{S} : L^2(\mathbb{R}^2) \to L^2(\mathbb{R}^2) \tag{2.9}$$

defined by

$$\mathcal{S} := I_f S I_g^{-1}, \tag{2.10}$$

for $f, g \in B(\eta, C)$, see (1.52) for some constants $\eta, C > 0$. We split the operator

$$\mathcal{S}\psi(\tilde{x}) = \int_{\mathbb{R}^2} G((\tilde{x}, f(\tilde{x}), (\tilde{y}, g(\tilde{y})))J_g(\tilde{y})\psi(\tilde{y})\, d\tilde{y}, \quad \tilde{x} \in \mathbb{R}^2 \tag{2.11}$$

in two parts, the *global part*

$$\mathcal{S}_1\psi(\tilde{x}) = \int_{\mathbb{R}^2} \chi(|\tilde{x} - \tilde{y}|)G((\tilde{x}, f(\tilde{x}), (\tilde{y}, g(\tilde{y})))J_g(\tilde{y})\psi(\tilde{y})\, d\tilde{y}, \tag{2.12}$$

and the *local part*

$$\mathcal{S}_2\psi(\tilde{x}) = \int_{\mathbb{R}^2} (1 - \chi(|\tilde{x} - \tilde{y}|))G((\tilde{x}, f(\tilde{x})), (\tilde{y}, g(\tilde{y})))J_g(\tilde{y})\psi(\tilde{y})\, d\tilde{y}, \tag{2.13}$$

where $\tilde{x} = (x_1, x_2)$ and $\tilde{y} = (y_1, y_2)$ are in $\mathbb{R}^2$ and the continuous *cut-off function* is given by

$$\chi : [0, \infty) \to \mathbb{R},$$

with

$$\chi(t) = \begin{cases} 1 & , t \geq 1 \\ 0 & , t < \frac{1}{2} \end{cases}, \qquad \text{and } 0 \leq \chi(t) \leq 1 \text{ for all } t \geq 0. \tag{2.14}$$

This implies the decomposition $S = S_1 + S_2$ of the single layer potential given by (2.3), for $\Gamma = \Gamma_g$, where the global part S_1 is given by

$$S_1\varphi(x) = \int_{\Gamma_g} \chi(|\tilde{x} - \tilde{y}|)G(x, y)\varphi(y)\, ds(y), \tag{2.15}$$

and the local part S_2 is given by

$$S_2\varphi(x) = \int_{\Gamma_g} (1 - \chi(|\tilde{x} - \tilde{y}|))G(x, y)\varphi(y)\, ds(y), \tag{2.16}$$

and we are able to study the mapping properties separately. In the following pages we denote the kernel of S_1 by s_1 and the kernel of S_2 by s_2. The kernels of $\mathcal{S}_1$ and $\mathcal{S}_2$ are denoted by $\tilde{s}_1$ and $\tilde{s}_2$.

Remark. We refer to [8],[7] and to [26], [51] where the mapping properties of the single layer and double layer potential as operators from $L^2(\Gamma_f) \to L^2(\Gamma_f)$ are discussed.

LEMMA 2.1.3. *The local part S_2 is a bounded operator from $L^2(\Gamma_H) \to L^2(\Gamma_f)$ for every flat surface Γ_H of height $H > 0$ with $0 < H < f_-$ and $f_- < f(\tilde{x}) < f_+$ for all $\tilde{x} \in \mathbb{R}^2$.*

Proof. For $x = (\tilde{x}, f(\tilde{x})) \in \Gamma_f$ and $y = (\tilde{y}, \pm H) \in \Gamma_{\pm H}$ we observe from

$$(\tilde{x}, f(\tilde{x})) - (\tilde{x}, \pm H) \perp (\tilde{x}, \pm H) - (\tilde{y}, \pm H)$$

and from the Pythagorean theorem that

$$\begin{aligned} |x-y|^2 &= |(\tilde{x}, f(\tilde{x})) - (\tilde{x}, \pm H)|^2 + |(\tilde{x}, \pm H) - (\tilde{y}, \pm H)|^2 \\ &\geq |(\tilde{x}, f(\tilde{x})) - (\tilde{x}, \pm H)|^2 \\ &= |(0, 0, f(\tilde{x})) \mp H|^2 \geq (f_- - H)^2. \end{aligned} \tag{2.17}$$

We estimate the kernel of the local part s_2 by

$$|s_2(x,y)| \leq \tilde{\tilde{\ell}}(\tilde{x} - \tilde{y}) := \begin{cases} \frac{1}{(f_- - H)} & , |\tilde{x} - \tilde{y}| \leq 1 \\ 0 & , |\tilde{x} - \tilde{y}| > 1 \end{cases}, \quad \text{for } \tilde{x} \neq \tilde{y}, \tag{2.18}$$

for the case when $H < f_- < f$ and $x \in \Gamma_f$, $y \in \Gamma_{\pm H}$. We have $\tilde{\tilde{\ell}} \in L^1(\mathbb{R})^2$, and by Theorem A.0.1 we see that

$$\begin{aligned} \|S_2\varphi\|^2_{L^2(\Gamma)} &\leq \tilde{c} \int_{\mathbb{R}^2} | \int_{\mathbb{R}^2} \tilde{\tilde{\ell}}(\tilde{x} - \tilde{y}) \varphi(\tilde{y}, \pm H) d\tilde{y}|^2 \, d\tilde{x} \\ &\leq \tilde{c} \left\| \tilde{\tilde{\ell}} \right\|^2_{L^1(\mathbb{R}^2)} \|\varphi\|^2_{L^2(\Gamma_H)}, \end{aligned} \tag{2.19}$$

for some constant $\tilde{c} > 0$. Hence, the local part S_2 is a bounded operator from $L^2(\Gamma_H) \to L^2(\Gamma_f)$. □

LEMMA 2.1.4. *Let $f, g \in B(\eta, C)$, $0 < \eta < H$ and $C > 0$. Then, the local part S_2 is a bounded operator from $L^2(\Gamma_g) \to L^2(\Gamma_f)$ for Γ_f with either*

$$\Gamma_f \subset \Omega_g \text{ or } \Gamma_f \subset \Omega_g^- := \left\{ x \in \mathbb{R}^3 : x_3 < g(\tilde{x}) \right\}. \tag{2.20}$$

Proof. Let $x \in \Gamma_f$ and $y \in \Gamma_g$. Then, we set

$$x^* := (\tilde{x}, g(\tilde{x})),\ x_0 := (\tilde{x}, g(\tilde{y})), \tag{2.21}$$

and $\delta(\tilde{y}) := |g(\tilde{y}) - f(\tilde{y})|$. We now recall the estimates from [8] and [26] for the kernel of the single layer potential. In particular, from [26] following equation (2.18) we find that for $g \in B(\eta, C)$,

$$\begin{aligned}(|\tilde{x} - \tilde{y}|^2 + \delta(\tilde{y})^2)^{1/2} &= (|x_0 - y|^2 + |x^* - x|^2)^{1/2} \\ &\leq (1 + \|\nabla g\|_{BC(\Gamma_g)})|x - y| \leq C'|x - y|,\end{aligned} \tag{2.22}$$

for some constant $C' \geq (1 + \|\nabla g\|_{BC(\Gamma_g)})$. We have that $\delta(\tilde{y}) \geq \tilde{\delta} > 0$ for some constant $\tilde{\delta}$. Using the inequality (2.22), we see that there exists a constant

$$C'' = (1 + \|\nabla f\|^2_{BC(\Gamma_f)})^{1/2}/C' \tag{2.23}$$

such that the kernel s_2 of S_2 can be bounded by

$$|s_2(x, y)| \leq C'' \begin{cases} \tilde{\ell}(\tilde{x} - \tilde{y}) & , |\tilde{x} - \tilde{y}| \leq 1 \\ 0 & , |\tilde{x} - \tilde{y}| > 1 \end{cases}, \text{ for } x \in \Gamma_f,\ y \in \Gamma_g, \tag{2.24}$$

with $\tilde{\ell}$ defined by

$$\tilde{\ell}(\tilde{y}) := \frac{1}{(|\tilde{y}|^2 + \tilde{\delta}^2)^{1/2}}. \tag{2.25}$$

Using polar coordinates we see that

$$\int_{|\tilde{y}|<1} |\tilde{\ell}(\tilde{y})|\, d\tilde{y} \leq 2\pi \int_0^1 \frac{1}{(r^2 + \tilde{\delta}^2)^{1/2}} r\, dr = 4\pi \int_{\tilde{\delta}}^{1+\tilde{\delta}} z^{-1/2} dz \tag{2.26}$$

and the integral remains finite also in the case $\tilde{\delta} \to 0$. Hence, s_2 is bounded by a function which is in $L^1(\mathbb{R}^2)$ and, by Theorem A.0.1, the local operator is a bounded operator from $L^2(\Gamma_g) \to L^2(\Gamma_f)$. □

Now, we turn to the global part.

LEMMA 2.1.5. *Let Γ_f, Γ_g with $f, g \in B(\eta, C)$ such that (2.20) holds. Then, the global part of the single layer potential $S_1 : L^2(\Gamma_g) \to L^2(\Gamma_f)$ is a bounded operator.*

Proof. From the decomposition of G, (2.8), it follows that the kernel $\tilde{s}_1$ of the global part $\mathcal{S}_1$ can be written in the form

$$s_1(\tilde{x}, \tilde{y}) = \ell_1(\tilde{x}, \tilde{y}) + \ell(\tilde{x}, \tilde{y}) \tag{2.27}$$

with ℓ defined by

$$\ell(\tilde{x}, \tilde{y}) := J_g(\tilde{y}) \frac{1}{|\tilde{x} - \tilde{y}|^3} \chi(|\tilde{x} - \tilde{y}|) \tag{2.28}$$

and where ℓ_1 is a strongly singular part, given by

$$\ell_1(\tilde{x}, \tilde{y}) = \frac{i\kappa g(\tilde{y}) J_g(\tilde{y})\, f(\tilde{x})}{2\pi} \left(\frac{e^{i\kappa|\tilde{x}-\tilde{y}|}}{1 + |\tilde{x} - \tilde{y}|^2} \right). \tag{2.29}$$

We first observe, as $J_g(\tilde{y})$ can be bounded by a constant since $g \in B(\eta, C)$, that there exists a constant $C' > 0$ such that

$$|\ell(\tilde{x}, \tilde{y})| \leq C' \tilde{\ell}(|\tilde{x} - \tilde{y}|), \quad \tilde{x}, \tilde{y} \in \mathbb{R}^2, \tag{2.30}$$

with

$$\tilde{\ell}(\tilde{y}) := (1 + |\tilde{y}|)^{-3}. \tag{2.31}$$

The function $\tilde{\ell}$ is in $L^1(\mathbb{R}^2)$ as, using polar coordinates, we have

$$\int_{\mathbb{R}^2} (1 + |\tilde{y}|)^{-3}\, d\tilde{y} = \int_0^\infty (1 + r)^{-3} r\, dr < \infty.$$

From Theorem A.0.1, with r, $q = 2$ and $p = 1$, we obtain that the integral operator with kernel (2.28) is bounded from $L^2(\mathbb{R}^2) \to L^2(\mathbb{R}^2)$.

Next, we consider the strongly singular part (2.29) of the kernel of $\mathcal{S}_1$. In [8], Lemma 4.2, it has been shown that

$$\mathcal{F}\left(\frac{e^{i\kappa|\tilde{x}-\cdot|}}{1 + |\tilde{x} - \cdot|^2} \right) \in L^\infty(\mathbb{R}^2),$$

and, by Theorem A.0.5 and Lemma A.0.6, the operator with kernel ℓ_1 is a bounded operator from $L^2(\mathbb{R}^2) \to L^2(\mathbb{R}^2)$. Thus, we conclude that the global part is bounded from $L^2(\Gamma_g) \to L^2(\Gamma_f)$. □

We recall that $S = S_1 + S_2$ and, thus, by Lemma 2.1.4 and Lemma 2.1.5, we have shown the following result.

LEMMA 2.1.6. *Let Γ_g and Γ_f be rough surfaces with $g, f \in B(\eta, C)$ for some constant $0 < \eta < H$ and Γ_f satisfying (2.20). Then, the single layer potential is a bounded operator from $L^2(\Gamma_g)$ to $L^2(\Gamma_f)$.*

In a last step we prove that the single layer potential is a bounded operator from $L^2(\Gamma_H)$ to $L^2(\Gamma_{h,A})$. First, we show that the pointwise bound in [8, (5.15)], remains true in the case where the integral is taken over the flat surface Γ_H.

LEMMA 2.1.7. *For $\varphi \in L^2(\Gamma_H)$ it holds that*

$$|S\varphi(x)| \leq C \|\varphi\|_{L^2(\Gamma_H)} \tag{2.32}$$

for all $x \in \Gamma_h$.

Proof. From Lemma 2.1.1 we have that there is a constant $C > 0$ such that

$$|G(x,y)| \leq C \frac{(1+h)(1+H)}{|x-y|^2} \tag{2.33}$$

for $x \in \Gamma_{h,A}$ and $y \in \Gamma_H$. Applying the Cauchy-Schwarz inequality, we have that

$$|S\varphi(x)| \leq C(1+h)(1+H) \int_{\mathbb{R}^2} \left| \frac{1}{(|\tilde{x}-\tilde{y}|^2 + (h-H)^2)} \right|^2 d\tilde{y} \, \|\varphi\|^2_{L^2(\Gamma_H)} . \tag{2.34}$$

With

$$\begin{aligned} &\int_{\mathbb{R}^2} \left| \frac{1}{(|\tilde{x}-\tilde{y}|^2 + (h-H)^2)} \right|^2 d\tilde{y} = \int_0^\infty \frac{r}{(r^2 + (h-H)^2)^2} \, dr \\ &= \int_{h-H}^\infty \frac{1}{2r^2} \, dr < \infty \end{aligned}$$

we have shown the pointwise bound (2.32). □

We obtain

$$\|S\varphi\|^2_{L^2(\Gamma_{h,A})} = \int_{\Gamma_{h,A}} |S\varphi(x)|^2 \, ds(x) \leq C^2 \left\{ \int_{\Gamma_{h,A}} 1 \, ds(x) \right\} \|\varphi\|^2_{L^2(\Gamma_H)} ,$$

and hence, the single layer potential as an operator from $L^2(\Gamma_H)$ to $L^2(\Gamma_{h,A})$ is bounded. This is the statement of the following lemma.

LEMMA 2.1.8. *The single layer potential S is a bounded operator from $L^2(\Gamma_H)$ to $L^2(\Gamma_{h,A})$.*

2.2 Jump relations for L^2-densities

In this section we discuss the jump conditions of the single and double layer potential for L^2-densities. We also refer to [8] and [51].

THEOREM 2.2.1. *Let S be the single layer potential given by (2.3). Let D_f be given by*

$$D_f := \left\{ x \in \mathbb{R}^3 : 0 < x_3 < f \right\}, \tag{2.35}$$

and let $\varphi \in X := L^2(\Gamma_f) \cap BC(\Gamma_f)$ with norm defined in (1.51). Then, (i) $S\varphi \in C^2(\Omega_f \cup D_f)$ and satisfies the Helmholtz equation $\Delta(S\varphi) + \kappa^2 S\varphi = 0$ in $\Omega_f \cup D_f$, and (ii) the single-layer potential can be continuously extended from Ω_f to $\overline{\Omega_f}$ and from D_f to $\overline{D_f}$ with limiting value

$$\lim_{\varepsilon \to 0} S\varphi(x \pm \varepsilon \nu(x)) = S\varphi(x),\ x \in \Gamma_f.$$

For the double-layer potential given by (2.4) also (i) holds with $S\varphi$ replaced by $D\varphi$, and the double-layer potential can be continuously extended from Ω_f to $\overline{\Omega_f}$ and from D_f to $\overline{D_f}$ with limiting value

$$\lim_{\varepsilon \to 0} D\varphi(x \pm \varepsilon \nu(x)) = D\varphi(x) \pm \frac{1}{2}\varphi(x),\ x \in \Gamma_f.$$

Here, $\nu(x)$ denotes the unit normal in $x \in \Gamma_f$ directed into the domain Ω_f.

Proof. See Theorem 5.5 in [8]. □

THEOREM 2.2.2. *The jump relations hold for L^2-densities in the sense that*

$$\lim_{h \to 0} \left\| \int_\Gamma G(x \pm h\nu(\cdot), y)\varphi(y)\, ds(y) - S\varphi \right\|_{L^2(\Gamma)} = 0, \tag{2.36}$$

and

$$\lim_{h \to 0} \left\| \int_\Gamma \frac{\partial G(\cdot \pm h\nu(\cdot), y)}{\nu(y)} \varphi(y)\, ds(y) \pm \frac{1}{2}\varphi - D\varphi \right\|_{L^2(\Gamma)} = 0, \tag{2.37}$$

for $\varphi \in L^2(\Gamma)$.

Proof. We consider first the double layer case. As a shorthand notation we introduce

$$\Gamma^R := \Gamma \cap B_R(0), \tag{2.38}$$

for some ball B of radius R and centre 0. We define the double layer potential u_2 for $x \in \mathbb{R}^3 \backslash \Gamma$ by

$$u_2(x) = u_2^{(1)}(x) + u_2^{(2)}(x), \tag{2.39}$$

with

$$u_2^{(1)}(x) = \int_{\Gamma^R} \frac{\partial G(x,y)}{\nu(y)} \varphi^{(1)}(y)\, ds(y),$$

and

$$u_2^{(2)}(x) = \int_{\Gamma \backslash \overline{\Gamma^R}} \frac{\partial G(x,y)}{\nu(y)} \varphi^{(2)}(y)\, ds(y),$$

with $\varphi^{(1)}, \varphi^{(2)} \in L^2(\Gamma)$. Since supp $\varphi^{(1)} \subset \Gamma^R$ we have

$$D\varphi^{(1)}(x) = \int_{\Gamma_0} \frac{\partial G(x,y)}{\nu(y)} \varphi^{(1)}(y)\, ds(y) \tag{2.40}$$

for some finite surface patch Γ_0, which we can extend to a boundary of class $C^{1,\beta}$ of a bounded domain $D^+ \subset \overline{\Omega}$. In the same way it is possible to extend Γ_0 to a $C^{1,\beta}$-smooth boundary of a bounded domain $D^- \subset \mathbb{R}^3 \backslash \overline{\Omega}$. We can use the L^2-jump relations for bounded obstacles as presented in [29]. Let $\varepsilon > 0$. We find that there exists $\delta = \delta(R) > 0$ such that

$$\left\| \int_{\Gamma^R} \frac{\partial G(\cdot + h\nu(\cdot))}{\nu(y)} \varphi(y)\, ds(y) \pm \frac{1}{2}\varphi - D\varphi \right\|^2_{L^2(\Gamma^R)} < \frac{\varepsilon}{4}, \tag{2.41}$$

for all $h < \delta$. As seen in [8], from the estimates for the local and global part of the double layer potential, the image $D_h^{\pm}\varphi$, given by

$$D_h^{\pm}\varphi := \int_{\Gamma} \frac{\partial G(\cdot \pm h\nu(\cdot), y)}{\nu(y)} \varphi(y)\, ds(y),$$

is in $L^2(\Gamma)$ uniformly for $h \in [0,1]$. This means that there exists an $R_0 = R_0(\varepsilon) > 0$ such that

$$\int_{\Gamma \backslash \Gamma^\rho} |D_h^{\pm}\varphi|^2 ds(x) < \frac{\varepsilon}{4}, \tag{2.42}$$

for all $\rho > R_0$ and all $h \in [0,1]$. Since $\varphi \in L^2(\Gamma)$, also $\|\varphi\|^2_{L^2(\Gamma \backslash \Gamma^\rho)} < \frac{\varepsilon}{4}$ for all sufficiently large $\rho > 0$. As $R > 0$ was arbitrary we find that, by using the triangle inequality for $\psi_h := D_h^{\pm}\varphi \pm \frac{1}{2}\varphi + D\varphi$,

$$\begin{aligned} \|\psi_h\|^2_{L^2(\Gamma)} &= \|\psi_h\|^2_{L^2(\Gamma^\rho)} + \|\psi_h\|^2_{L^2(\Gamma \backslash \Gamma^\rho)} \\ &\leq \|\psi_h\|^2_{L^2(\Gamma^\rho)} + \left\|D_h^{\pm}\varphi\right\|^2_{L^2(\Gamma \backslash \Gamma^\rho)} + \frac{1}{2}\|\varphi\|^2_{L^2(\Gamma \backslash \Gamma^\rho)} + \|D\varphi\|^2_{L^2(\Gamma \backslash \Gamma^\rho)} \\ &< \varepsilon, \end{aligned} \tag{2.43}$$

for some $h < \delta(\rho)$ and $\rho > R_0(\varepsilon)$. For the single layer potential we argue exactly as we did for the double layer potential, noting that, by the bounds given in [8] and presented in this Chapter, (2.42) also holds for the single layer potential uniformly for all $h \in [0, 1]$. □

2.3 Some further properties

We note that the single layer potential (2.3) is a C^∞-smooth solution of the Helmholtz equation in the domain Ω_f and $\mathbb{R}^3 \backslash \overline{\Omega_f}$. This follows immediatly from differentiation of the kernel. Let us consider weak solutions of the Helmholtz equation in the strip

$$D_H := \left\{ x \in \mathbb{R}^3 : 0 < x_3 < H \right\}, \tag{2.44}$$

i.e. we consider $u \in H^1(D_H)$ to be a solution of

$$\int_{D_H} (\nabla u \cdot \overline{\nabla v} + \kappa^2 u \overline{v})\, dx = 0 \text{ for all } v \in H_0^1(D_H) \tag{2.45}$$

with the trace $\gamma u \in H^{\frac{1}{2}}(\partial D_H)$. We define $H^1_{loc}(D_H)$ as the space of locally H^1-functions in the sense that for every compact set $D \subset D_H$ we have that $u \in H^1_{loc}(D_H)$ if and only if $u|_D \in H^1(D)$.
We say κ^2 is an eigenvalue of the Laplacian in the weak sense if

$$\int_{D_H} (\nabla u \overline{\nabla v})\, dx = -\kappa^2 \int_{D_H} (u \overline{v})\, dx \text{ for all } v \in H_0^1(D_H). \tag{2.46}$$

We also remark the following properties.

Lemma 2.3.1. *The single layer potential S, given by (2.3), satisfies*

$$S\varphi(x') = -S\varphi(x)\,,\ x \in \mathbb{R}^3 \backslash (\Gamma_f \cap \Gamma_{-f}), \tag{2.47}$$

for every $\varphi \in L^2(\Gamma_f)$.

Proof. Let x with $x_3 \geq 0$ be fixed and let $x' = (x_1, x_2, -x_3)$ with $x_3 \neq f(\tilde{x})$ and $y = (y_1, y_2, y_3) \in \Gamma_f$. We observe that

$$\begin{aligned} |x' - y| &= ((x_1 - y_1)^2 + (x_2 - y_2)^2 + (-x_3 - y_3)^2)^{\frac{1}{2}} \\ &= ((x_1 - y_1)^2 + (x_2 - y_2)^2 + (x_3 - (-y_3))^2)^{\frac{1}{2}} = |x - y'| \end{aligned}$$

and $|x' - y'| = |x - y|$, so that

$$G(x', y) = \Phi(x', y) - \Phi(x', y') = \Phi(x, y') - \Phi(x, y) = -G(x, y)\,.$$

Thus, $S\varphi(x') = -S\varphi(x)$. The same arguments hold for the choice of x with $x_3 < 0$ and $x_3 \neq -f(\tilde{x})$. □

Chapter 3

A multi-section approach for rough surface reconstruction via the Kirsch-Kress scheme

In this chapter we present the reconstruction of a three-dimensional rough surface from the knowledge of its near field pattern via a potential approach. The results of this chapter are published, see [5].

Using single layer potentials for the solution of shape reconstruction problems was first suggested by Kirsch and Kress in the case of bounded obstacles, [31], [32] and [33]. The basic idea consists of the reformulation of the inverse problem as a nonlinear optimisation problem. In particular, the problem is broken up in two parts. The first part treats the ill-posedness by constructing the scattered field from the knowledge of the far or near field pattern via a potential approach. This means that instead of solving a non-linear operator equation of the form $\mathcal{F}(\partial D) = u_\infty$ for the (far or near) field operator $\mathcal{F}$ which maps the boundary ∂D to the far or near field data u_∞, we try to represent the scattered field by a potential. This leads to an operator equation of the form $S\varphi = u_\infty$ with a linear integral operator S and a density φ. The second part addresses the nonlinearity by determining the unknown boundary of the scattering obstacle as the location of the zeros of the total field.

In the bounded obstacle case, the measurements are often taken on a surface surrounding the obstacle. The results of Kirsch and Kress remain valid if we only know the

far field pattern on a nonempty open subset of the measurements surface (the so-called *limited aperature problem*), this was shown by Zinn after modification of the far field integral operator, see [56]. In 2002, the ideas of Kirsch and Kress had been applied to the periodic grating problem by Elschner and Yamamoto, [22]. At the same time the inverse problem for periodic diffraction gratings had been discussed via several other approaches, see for example [1] (Factorization Method) or [3]. Furthermore, a new version of the Kirsch-Kress method for bounded obstacles has been proposed by Schulz and Potthast in 2006, [48], using the *range test* to fully separate the linear ill-posed and nonlinear well-posed part of the reconstruction with complete convergence analysis.

For bounded obstacles or periodic settings the Kirsch-Kress scheme is well settled and theoretically explored. However, the analysis for the rough surface case is significantly different from the bounded obstacle case, since the difficulties from the forward problem carry over to the inverse problem.

In *two dimensions* much progress on the forward rough surface scattering problem has been made by a generalised Fredholm theory, see for example [13], [14], [55], [11]. The study of the corresponding inverse problem can be found in [20], [21], and using the *point source method* in [10] and [36].

Frequency-domain problems are widely studied, for the rough surface case in one and two dimensions we refer to [8], [9], [11], [14], [55], [15], [16]. There exist many methods to solve the inverse problem, most of which have been worked out for the bounded obstacle case. For example, iterative methods update some reconstruction using gradients or the Fréchet derivative with respect to the unknown boundaries [12], [41], [17]. The Point Source Method [10] and the Kirsch-Kress Method [17] reconstruct the full field and then use the boundary condition to find the unknown shape. Probe Methods as introduced by Ikehata, [28], Potthast, Nakamura and others, compare [46], usually define some indicator function via particular incident fields which can be used to construct or visualise the unknown shapes or objects. As examples for further approaches we name Sampling Methods, [6], [44], Range Tests, [49], [48], and Factorization Methods, [24], a survey is given in [46] and in [45]. The inverse rough surface problem in two dimensions in the frequency domain is for example discussed by DeSanto and Wombell, [20], [21], and for the periodic case by Elschner and Yamamoto, [22].

For the numerical realisation of the rough surface case we employ the multi-section approach presented by E. Heinemeyer, M. Lindner and R. Potthast, [27].

We begin this chapter by introducing the inverse rough surface problem. After that, we proceed with the rough surface reconstruction problem via a potential approach. We assume to know the location of the source (the incident field u^i) and we restrict ourselves to the case of Dirichlet boundary condition. We solve this inverse problem via a single layer potential approach, using the Dirichlet Green's function for the half-space instead of the standard fundamental solution for the Helmholtz equation. First, we present the basic setting of the rough surface inverse problem and study properties of the single layer potential approach. The next three sections investigate the ideas of Kirsch and Kress via (A) a fully infinite, (B) a semi-finite approach and (C) a multi-section approach to carry out a full rigorous analysis for the inverse rough surface reconstruction problem. We will show that the analysis of Kirsch and Kress cannot be carried out for (A) or (C) directly, but using an analysis for the semi-finite case (B) we will prove convergence for the practically relevant case (C).

At the end, we will show reconstructions carried out by the multi-section approach.

3.1 The inverse scattering problem

For the inverse problem we assume the knowledge of the total field on a *finite section* of Γ_h given by

$$\Gamma_{h,A} = \left\{ x \in \mathbb{R}^3 : x_3 = h, |x_1| \leq A, |x_2| \leq A \right\} \tag{3.1}$$

for a constant $A > 0$ under the condition that we have the a-priori information $h > f_+$ to assure that there are no intersections between Γ_h and the unknown surface Γ given by (1.2) where we further assume that $f \in BC^{1,\beta}(\mathbb{R}^2)$ is in $B(f_-, C)$ defined by (1.52) for some constant $C > 0$ and $f_- > 0$.

Let U be the space of all surfaces Γ_f defined by (1.2) with $f \in B(f_-, C)$. We equip this space with the $C^{1,\beta}$-norm and understand *convergence of a sequence of surfaces* $(\Gamma_{f_n})_{n\in\mathbb{N}}$ to a *limit surface* Γ_f in the sense that $\|f_n - f\|_{C^{1,\beta}} \to 0$ for $n \to \infty$.

We formulate the inverse problem as follows.

Problem 3.1.1 (The Inverse Problem)**.** *Suppose we know the incident field* $u^i = \Phi(\cdot, z)$

and the scattered field u^s on the surface patch $\Gamma_{h,A}$. We assume that the total field u satisfies the Dirichlet boundary condition $u = 0$ on the unknown surface Γ. Then, we try to find

(α) the scattered field u^s and

(β) the surface Γ

such that u is the solution of the direct problem, Problem 1.2.2, and $u - u^i$ coincides with $u^s(x)$ for all $x \in \Gamma_{h,A}$.

Remark. The inverse problems (α) and (β) are strongly related, since the total field u is only defined in the region above Γ and, thus, its reconstruction in general also involves the reconstruction of Γ. On the other side, the reconstruction of Γ as the set of zeros of the total field relies on the reconstruction of the total field or its extension into the set below the surface Γ, respectively, without the knowledge of Γ.

3.2 An infinite approach for the rough surface case

The main idea of the Kirsch-Kress Method is to search for an approximation of the total field via a single layer potential ansatz over some auxiliary surface Γ_t. Here, we first formulate an *infinite approach* (A) in which both the unknown surface Γ as well as the *test surface* on which the single-layer potential is defined is infinite. To this end we employ a test surface on height $0 < t < f_-$ defined by

$$\Gamma_t = \left\{ x \in \mathbb{R}^3 : x_3 = t \right\}. \tag{3.2}$$

For $\varphi \in L^2(\Gamma_t)$ we define the single layer potential via

$$S\varphi(x) := \int_{\Gamma_t} G(x,y)\varphi(y)\, ds(y) \text{ for all } x \in \mathbb{R}^3 \backslash \Gamma_t. \tag{3.3}$$

Here, the kernel G is the Dirichlet Green's function for the Helmholtz equation in three dimensions, defined in (1.38) for $d = 3$. The restrictions of the measurements u^s onto the surface patch $\Gamma_{h,A}$ can be seen as the image of the projection $P_A u^s \in L^2(\Gamma_{h,A})$ of the scattered field u^s, where the projection operator is defined by (1.58). We employ

the *ansatz* (1.23) with unknown function φ and seek the measurement data $v = v|_{\Gamma_{h,A}}$ as a single layer potential (3.3). This leads to the equation

$$S\varphi(x) = v(x), \quad x \in \Gamma_{h,A}. \tag{3.4}$$

Since S is a compact operator from $L^2(\Gamma_t) \to L^2(\Gamma_{h,A})$, as we will see in Lemma 3.2.4, equation (3.4) is ill-posed and we need to employ a regularisation strategy.

To solve $S\varphi = v$ on $\Gamma_{h,A}$ we apply the *Tikhonov regularisation*, i.e. we solve

$$\alpha\varphi + S^*S\varphi = S^*v, \tag{3.5}$$

with a regularisation parameter $\alpha > 0$. Then, we approximate the function v in the domain $\mathbb{R}^3\backslash\Gamma_t$, via

$$v(x) = S\varphi(x), \quad x \in \mathbb{R}^3\backslash\Gamma_t\,. \tag{3.6}$$

Now, using the ansatz (1.23), we obtain an approximation u of the total field via

$$u = u^i + u^s = u^i + S\varphi - \Phi(\cdot, z') = S\varphi + G(\cdot, z). \tag{3.7}$$

The zeros of the exact total field represent the location of the scattering field in case of Dirichlet boundary condition. Therefore, we seek the scattering surface as a minimum of the approximation u in a norm sense.

One key difficulty for the convergence of the reconstructions by the infinite approach (A) is the fact that the surface Γ_t is not compact. Bounded sequences in $L^2(\Gamma_t)$ do not have convergent subsequences. And since the kernel of S is slowly decaying, influence from functions supported far away can be strong. To avoid the problems and obtain convergence of reconstructions we will study potentials supported on a bounded subset $[-B, B] \times [-B, B] \times \{t\}$ of Γ_t. This leads to the semi-finite approach (B) below.

For the justification of the convergence for reconstructing the total field via the single layer potential ansatz we remark that the single layer potential S given by (3.3) fulfills the *limiting absorbing principle*, (1.21), see Theorem 1.3.4.

THEOREM 3.2.1. *The single layer potentials*

$$S : L^2(\Gamma_t) \to L^2(\Gamma_{h,A})$$

and

$$S : L^2(\Gamma_t) \to L^2(\Gamma)$$

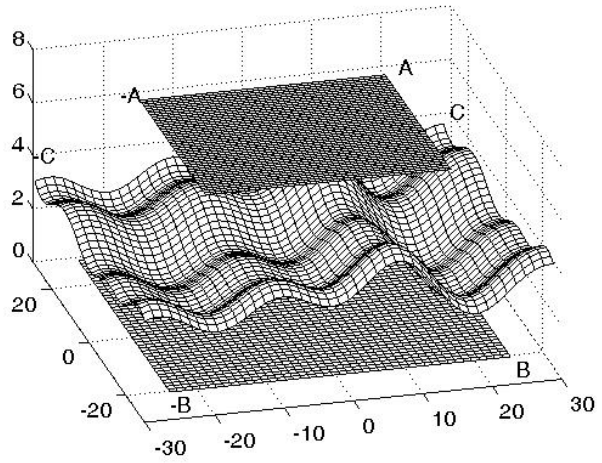

Figure 3.1: *The inverse problem settings with the different finite sections under consideration. The variable A controls the size of the measurement domain, B is the size of the support of the single-layer potential for field approximation, C controls the area for the fit of the unknown scattering surface. The case $C = \infty$ corresponds to the semi-finite approach, $C < \infty$ is used for the multi-section approach.*

for every rough scattering surface $\Gamma = \Gamma_f$ are injective and have dense range provided that κ^2 is not an eigenvalue of the negative Laplacian operator in the strip D_t given by

$$D_t := \{x \in \mathbb{R}^3 : 0 < x_3 < t\} \tag{3.8}$$

where we consider functions in $H^1(D_t)$ which are weak solutions of the eigenvalue equation (2.46) with Dirichlet boundary condition.

Proof. First, we show that $S : L^2(\Gamma_t) \to L^2(\Gamma_{h,A})$ is injective. Consider a density $\varphi \in L^2(\Gamma_t)$ such that $S\varphi(x) = 0, \quad x \in \Gamma_{h,A}$. Then, the function

$$v(x) := S\varphi(x), \quad x \in \mathbb{R}^3, \tag{3.9}$$

satisfies $v = 0$ on Γ_h due to the analyticity of v on Γ_h. We note that $v|_{\Gamma_t} \in L^2(\Gamma_t)$. Moreover, v is well-defined in Ω_t and $\mathbb{R}^3 \backslash \overline{\Omega_t}$, see [8], [51]. The function v solves the homogeneous boundary value problem 1.2.3 in the domain Ω_h above the surface Γ_h. According to the uniqueness theorem, Theorem 2.4 in [8] for mildly rough surfaces and L^2-densities, v must be the trivial solution $v \equiv 0$ in the upper half-space Ω_h. Then,

by analyticity, it is zero in the half space Ω_t above Γ_t. From the L^2-jump relations, Theorem 2.2.2, we conclude $S\varphi = 0$ for almost all $x \in \Gamma_t$. Further $S\varphi(x) = 0$ for $x_3 = 0$ as the kernel $G(x, y) = 0$ for $x \in \Gamma_0$. Thus, v is solution of the homogeneous Dirichlet problem in the strip D_t. By the estimates given in [9], proof of Lemma 3.3, we find that v is in the standard Sobolev space $H^1(D_t)$. According to our assumptions and the definition of eigenvalues in a weak sense of the Laplacian, see (2.46), we obtain from Theorem 3.2.2 that $v = 0$ in D_t. The jump conditions, Theorem 2.2.2, finally imply

$$\varphi(x) = \frac{\partial v}{\partial x_3}|_+(x) - \frac{\partial v}{\partial x_3}|_-(x) = 0 \text{ almost everywhere on } \Gamma_t.$$

Therefore, the operator $S : L^2(\Gamma_t) \to L^2(\Gamma_{h,A})$ and also $S : L^2(\Gamma_t) \to L^2(\Gamma_h)$ are both injective.

Second, we show the denseness of the range of the operator $S : L^2(\Gamma_t) \to L^2(\Gamma_{h,A})$. By $\overline{S(L^2(\Gamma_t))} = N(S^*)^\perp$ it is sufficient to show the injectivity of the adjoint operator

$$S^* : L^2(\Gamma_{h,A})) \to L^2(\Gamma_t).$$

Assume that for an element $\varphi \in L^2(\Gamma_{h,A})$ we have $(S^*\varphi)(y) = 0$ for all $y \in \Gamma_t$. Then we obtain

$$v(y) := \overline{S^*\varphi(y)} = \int_{\Gamma_{h,A}} G(x, y)\overline{\varphi(x)}ds(x) = 0 \text{ for all } y \in \Gamma_t.$$

Now, with the same arguments as in the first part of the proof we derive $\varphi = 0$ on $\Gamma_{h,A}$. Hence, S^* is injective and the single layer potential $S : L^2(\Gamma_t) \to L^2(\Gamma_{h,A})$ has dense range in $L^2(\Gamma_{h,A})$.

Third, the proof for the case $S : L^2(\Gamma_t) \to L^2(\Gamma)$ is carried out with the same arguments.

□

The choice of Γ_t is at our disposal. Therefore, we can choose Γ_t such that κ^2 is not a Dirichlet eigenvalue for the negative Laplacian in the strip D_t. That this is possible is shown by the following result.

THEOREM 3.2.2. *If $Im(\kappa) > 0$ or $\kappa \in \mathbb{R}$ with $\kappa t < \sqrt{2}$, then on the strip D_t there are no (weak) eigenvalues in $H^1(D_t)$ of the negative Laplace operator where we understand the eigenvalue equation in the sense of (2.46).*

Proof. Let $Im(\kappa) > 0$. Then, Green's first theorem and the boundary conditions $u = 0$ on ∂D_t imply

$$0 = \int_{D_t} (\Delta u + \kappa^2 u)\overline{u} dx = \int_{D_t} \kappa^2 |u|^2 - |\nabla u|^2 \, dx. \tag{3.10}$$

Hence, taking the imaginary part of

$$\kappa^2 \|u\|^2_{L^2(D_t)} = \|\nabla u\|^2_{L^2(D_t)} \tag{3.11}$$

yields $u = 0$ in D_t, i.e. $-\Delta u = \kappa^2 u$ in D_t with homogeneous boundary conditions possesses only the trivial solution.

Now, we turn to the case when $\kappa > 0$. Let $\tilde{x} \in \mathbb{R}^2$ be arbitrary and define $g(x_3) := u(\tilde{x}, x_3)$. We estimate

$$|g(x_3)|^2 = |\int_0^{x_3} \frac{\partial g}{\partial x_3}(\xi) d\xi|^2 \leq \int_0^{x_3} |\frac{\partial g}{\partial x_3}(\xi)|^2 d\xi \cdot \int_0^{x_3} 1 \, d\xi \leq x_3 \int_0^t |\frac{\partial g}{\partial x_3}(\xi)|^2 \, d\xi. \tag{3.12}$$

Thus we have

$$\int_0^t |g(x_3)|^2 dx_3 \leq \frac{t^2}{2} \int_0^t |\frac{\partial g(x_3)}{\partial x_3}|^2 dx_3. \tag{3.13}$$

With (3.11) and (3.13) we then derive

$$\begin{aligned} \|\nabla u\|^2_{L^2(D_t)} &= \kappa^2 \|u\|^2_{L^2(D_t)} = \kappa^2 \int_{\mathbb{R}^2} \int_0^t |u(\tilde{x}, x_3)|^2 \, dx_3 \, d\tilde{x} \\ &\leq \frac{\kappa^2 t^2}{2} \int_{D_t} |\frac{\partial u(\boldsymbol{x}, x_3)}{\partial x_3}|^2 dx \leq \frac{\kappa^2 t^2}{2} \|\nabla u\|^2_{L^2(D_t)}, \end{aligned}$$

which we rearrange to

$$(1 - \frac{\kappa^2 t^2}{2}) \|\nabla u\|^2_{L^2(D_t)} \leq 0. \tag{3.14}$$

Hence, if $2 - \kappa^2 t^2 > 0$, u must be the trivial solution in D_t. □

The above statement implies that we can choose the test surface with sufficiently small height $t > 0$, such that no eigenvalues appear. Next, we will study the properties of the operator $S : L^2(\Gamma_{t,B}) \to L^2(\Gamma)$. We first obtain its injectivity and denseness of range using the above results.

COROLLARY 3.2.3. *For every scattering surface Γ which does not intersect Γ_t, the operator $S : L^2(\Gamma_{t,B}) \to L^2(\Gamma)$ is injective and has dense range in $L^2(\Gamma)$ provided that κ^2 is not an eigenvalue of the negative Laplacian operator in the strip D_t.*

Proof. For $B = \infty$ the results are stated in Theorem 3.2.1. Since $L^2(\Gamma_{t,B}) \subset L^2(\Gamma_t)$, injectivity is trivial. Denseness follows from the fact that the injectivity of the adjoint $S^* : L^2(\Gamma) \to L^2(\Gamma_{t,B})$ is obtained from the injectivity of $S^* : L^2(\Gamma) \to L^2(\Gamma_t)$ by an analyticity argument on Γ_t. □

LEMMA 3.2.4. *For constants $A, B > 0$ the operators*

(i) $S : L^2(\Gamma_{t,B}) \to L^2(\Gamma_{h,A})$,

(ii) $S : L^2(\Gamma_{t,B}) \to L^2(\Gamma)$,

(iii) $S : L^2(\Gamma_t) \to L^2(\Gamma_{h,A})$,

are compact. Furthermore, there exists a constant $c > 0$ such that

$$\|(I - P_C)SP_B\|_{L^2(\Gamma_t)\to L^2(\Gamma)} \leq c\,\frac{B}{C}, \tag{3.15}$$

holds for every $C > 2B$ and for the projections P_C and P_B defined via (1.58).

Proof. (i) $S : L^2(\Gamma_{t,B}) \to L^2(\Gamma_{h,A})$ is given by

$$S\varphi(x) = \int_{\Gamma_{t,B}} G(x,y)\varphi(y)ds(y) \text{ for } x \in \Gamma_{h,A}. \tag{3.16}$$

By the definition of a finite section of a rough surface, (2.2), $\Gamma_{h,A}$ and $\Gamma_{t,B}$ are both compact sets. Moreover, S possesses a continuous kernel $G : \Gamma_{h,A} \times \Gamma_{t,B} \to \mathbb{C}$. We conclude that $G(\cdot,\cdot) \in L^2(\Gamma_{h,A} \times \Gamma_{t,B})$ and hence, $S : L^2(\Gamma_{t,B}) \to L^2(\Gamma_{h,A})$ is compact.

(ii) The following steps are based on Lemma 3.2 in [27]. Let $\varphi \in L^2(\Gamma_t)$ and define $\psi(\tilde{y}) = \varphi(\tilde{y}, t)$. We further use

$$|\tilde{x}|_\infty := \max\{|x_1|, |x_2|\}. \tag{3.17}$$

With the coordinate transform onto $\mathbb{R}^2$ we have that

$$\begin{aligned}&\|(I - P_C)SP_B\varphi\|^2_{L^2(\Gamma)}\\ &= \int_{|\tilde{x}|_\infty \geq C} \Big| \int_{|\tilde{y}|_\infty < B} G\left((\tilde{x}, f(x)), (\tilde{y}, t)\right) \psi(\tilde{y}) \sqrt{1 + |\nabla f(y)|^2}\, d\tilde{y}\Big|^2 d\tilde{x}\end{aligned}$$

and the Cauchy-Schwarz inequality yields

$$\begin{aligned}&\|(I-P_C)SP_B\varphi\|^2_{L^2(\Gamma)}\\&\leq C'\int_{|\tilde{x}|_\infty\geq C}\left\{\int_{|\tilde{y}|_\infty<B}|G\left((\tilde{x},f(x)),(\tilde{y},t)\right)|^2\,d\tilde{y}\right\}d\tilde{x}\;\|\varphi\|^2_{L^2(\Gamma_t)},\end{aligned}\tag{3.18}$$

for some constant $C'=(1+\|\nabla f\|^2_{0,\beta})$. Here, we used that $f\in B(f_-,C)$ is bounded by a constant, $\|f\|_{1,\beta}\leq C$ and, thus, also $\|\nabla f\|_{0,\beta}$ is bounded.

With the decay of the Green's function, by Lemma 2.1.1, and the property

$$|\tilde{x}-\tilde{y}|_\infty\leq|x-y|,$$

there exists a constant $\tilde{c}$ such that

$$|G(x,y)|\leq\frac{\tilde{c}}{|\tilde{x}-\tilde{y}|^2_\infty}\text{ for }x\in\Gamma,y\in\Gamma_t.$$

We assume that $C>2B$, then from

$$|\tilde{x}|_\infty\geq C>2B>2|\tilde{y}|_\infty,$$

we obtain

$$|\tilde{x}-\tilde{y}|_\infty\geq|\tilde{x}|_\infty-|\tilde{y}|_\infty\geq\frac{|\tilde{x}|_\infty}{2}.$$

This yields

$$\begin{aligned}\|(I-P_C)SP_B\|^2_{L^2(\Gamma_t)\to L^2(\Gamma)}&\leq C'\int_{|\tilde{x}|_\infty\geq C}\int_{|\tilde{y}|_\infty<B}|G\left((\tilde{x},f(x)),(\tilde{y},t)\right)|^2\,d\tilde{y}\,d\tilde{x}\\&\leq C'\int_{|\tilde{x}|_\infty\geq C}\int_{|\tilde{y}|_\infty<B}\frac{\tilde{c}^2}{|\tilde{x}-\tilde{y}|^4_\infty}\,d\tilde{y}\,d\tilde{x}\\&\leq c^2B^2\int_{r=C}^{\infty}\frac{1}{r^4}r\,dr\\&\leq c^2B^2\frac{1}{C^2},\end{aligned}\tag{3.19}$$

for some constant $c>0$. We have shown (3.15) and found a sequence $(P_NSP_B)_{N\in\mathbb{N}}$ of compact operators which is norm-convergent towards the operator SP_B, which proves (ii).

(iii) Following the arguments in (ii) the adjoint operator $S^*:L^2(\Gamma_{h,A})\to L^2(\Gamma_t)$ is compact and hence, $S:L^2(\Gamma_t)\to L^2(\Gamma_{h,A})$ is compact as the adjoint of a compact operator. This completes the proof. □

3.3 A semi-finite approach

In this section we study a semi-finite Kirsch-Kress type functional which tries to find the unknown scattering surface by the simultaneous minimisation of the *Tikhonov functional*

$$J_{B,\alpha}(\varphi) = \|SP_B\varphi - v\|^2_{L^2(\Gamma_{h,A})} + \alpha \|P_B\varphi\|^2_{L^2(\Gamma_t)}, \tag{3.20}$$

over the set U of all surfaces Γ defined by (1.2), and the minimisation of

$$\|G(\cdot, z) + SP_B\varphi\|_{L^2(\Gamma)} \tag{3.21}$$

which corresponds to the search for a surface on which the total field vanishes.

In our *semi-finite approach* we restrict the minimisation in (3.20) onto densities of the form $P_B\varphi$ for a fixed truncation parameter $B > 0$ but we leave the minimisation of (3.21) defined on an infinite domain, see figure 3.1. We point out that the numerical minimisation with respect to infinite surfaces Γ in (3.21) is not possible. Nevertheless, the semi-finite approach establishes the basis for a further study of the *multi-section approach* as a method which is numerically implementable.

If the scattered field is not analytically extensible up to the whole domain above Γ_t, then the equation (3.4) is not solvable and the single layer potential does not converge towards the scattered field in the neighbourhood of the unknown surface. To overcome this issue, following Kirsch and Kress we combine the Tikhonov minimisation problem (3.20) and the minimisation of the total field (3.21) into one optimisation problem. For alternative solutions we refer to [48]. We consider the minimisation of the *semi-finite* cost functional

$$\begin{aligned} \mu_{B,\alpha}(\varphi, \Gamma) &= \|SP_B\varphi - v\|^2_{L^2(\Gamma_{h,A})} \\ &\quad + \alpha \|P_B\varphi\|^2_{L^2(\Gamma_t)} + \gamma \|G(\cdot, z) + SP_B\varphi\|^2_{L^2(\Gamma)}, \end{aligned} \tag{3.22}$$

with $\varphi \in L^2(\Gamma_t)$, $\Gamma \in U$ and a coupling parameter γ, for which we may assume $\gamma = 1$ for theoretical purposes.

We choose $\mathcal{U}$ to be a compact subset of U and we assume that the true surface Γ is contained in $\mathcal{U}$.

Definition 3.3.1 (compact imbedding). *Let X, Y be Banach spaces with $X \subset Y$. Then, X can be compactly imbedded in Y if X is a subspace of Y with continuous identity $I : X \to Y$, $I(x) = x$ and I is a compact linear mapping.*

Example for a compact $\mathcal{U}$. To construct an example of such a compact subset $\mathcal{U}$ of U we can consider functions which are C^2-smooth on $\mathbb{R}^2$ with a norm bounded by some constant $C > 0$. We have that, for $D \subset \mathbb{R}^3$ compact, the imbedding

$$I : \tilde{X} := \left\{ f \in C^2(D) : \|f\|_{C^2} \leq C \right\} \to C^{1,\beta}(D)$$

is compact, see for example [17]. The set $\{f \in C^2(\mathbb{R}^2) : \|f\|_{C^2} \leq C\}$ is *locally compact* in the sense that its restriction to any compact subset of $C^{1,\beta}(\mathbb{R}^2)$ is compact. Now, with the assumption that the functions further satisfy a certain decay-property at infinity, we have found a compact subset of U. Clearly, this strong assumption of the behavior at infinity limits our theory. To avoid this demand we would need to discuss the setting for locally compact sets. We limit ourselves to the case of a compact set $\mathcal{U}$ and leave the case of locally compact sets to future research.

We first discuss the continuous dependence of the total field on the scattering surface Γ_f on compact subsets of Ω_f.

THEOREM 3.3.2. *Let $(\Gamma_{f_n})_{n\in\mathbb{N}}$ be a convergent sequence in $\mathcal{U}$ with $\Gamma_{f_n} \to \Gamma_f \in \mathcal{U}$. Let u_n resp. u denote the solutions of the Helmholtz equation in the upper half-spaces bounded by Γ_{f_n} and Γ_f respectively. Assume that the continuous boundary values of u_n on Γ_{f_n} are L^2-convergent to the boundary values of u on Γ_f, i.e.*

$$\lim_{n\to\infty} \int_\Gamma |u_n(\tilde{x}, f_n(\tilde{x})) - u(\tilde{x}, f(x))|^2 \, d\tilde{x} = 0. \tag{3.23}$$

Then, the sequence (u_n) converges to u uniformly on compact subsets of

$$\left\{ x = (\tilde{x}, x_3) \in \mathbb{R}^3 : x_3 > f(\tilde{x}) \right\}.$$

Proof. We split the solution u and u_n of the exterior Dirichlet problem with boundary values $u = b$ for $x \in \Gamma_f$ and $u_n = b_n$ for $x \in \Gamma_{f_n}$ in two parts, namely $u = v - G(\cdot, z)$ resp. $u_n = v_n - G(\cdot, z)$ and represent the remainder v and v_n in a combination of a single and double layer potential, compare Chapter 1 and Theorem 1.3.2. We have

$$v(x) = \int_{\Gamma_f} \frac{\partial G(x,y)}{\partial \nu(y)} \varphi(y) ds(y) - i\eta \int_{\Gamma_f} G(x,y)\varphi(y) ds(y) \text{ for } x \in \Omega_f, \tag{3.24}$$

and

$$v_n(x) = \int_{\Gamma_{f_n}} \frac{\partial G(x,y)}{\partial \nu(y)} \varphi_n(y) ds(y) - i\eta \int_{\Gamma_{f_n}} G(x,y)\varphi_n(y) ds(y) \text{ for } x \in \Omega_{f_n}, \tag{3.25}$$

with densities $\varphi \in L^2(\Gamma_f) \cap BC(\Gamma_f)$ and $\varphi_n \in L^2(\Gamma_{f_n}) \cap BC(\Gamma_{f_n})$. Here, ν is the normal vector of Γ_{f_n} resp. Γ_f pointing upwards and $\eta > 0$ is a coupling parameter. The boundary conditions are given by

$$\begin{aligned} v_n(x) &= G(x,z) + b_n(x) \text{ for } x \in \Gamma_{f_n}, \\ v(x) &= G(x,z) + b(x) \text{ for } x \in \Gamma_f. \end{aligned}$$

From the jump conditions, Theorem 2.2.1, we obtain the two integral equations

$$\begin{aligned} \varphi(x) \;+\; 2\int_{\Gamma_f} \frac{\partial G(x,y)}{\partial \nu(y)} \varphi(y)\, ds(y) \\ +2i\eta \int_{\Gamma_f} G(x,y)\varphi(y)\, ds(y) = 2G(x,z) \text{ for } x \in \Gamma_f, \end{aligned} \tag{3.26}$$

and

$$\begin{aligned} \varphi_n(x) \;+\; 2\int_{\Gamma_{f_n}} \frac{\partial G(x,y)}{\partial \nu(y)} \varphi_n(y)\, ds(y) \\ +2i\eta \int_{\Gamma_{f_n}} G(x,y)\varphi_n(y)\, ds(y) = 2G(x,z) \text{ for } x \in \Gamma_{f_n}. \end{aligned} \tag{3.27}$$

Let $\psi(\tilde{x}) := \varphi(\tilde{x}, f(\tilde{x}))$ and $\psi_n(\tilde{x}) := \varphi(\tilde{x}, f_n(\tilde{x}))$ and define

$$\begin{aligned} K_n\psi_n(\tilde{x}) &:= 2\int_{\mathbb{R}^2} \frac{\partial G((\tilde{x}, f_n(\tilde{x})), y)}{\partial \nu(y)} \psi_n(\tilde{y}) J_{f_n}(\tilde{y})\, d\tilde{y}, \\ S_n\psi_n(\tilde{x}) &:= 2\int_{\mathbb{R}^2} G((\tilde{x}, f_n(\tilde{x})), y)\psi_n(\tilde{y}) J_{f_n}(\tilde{y})\, d\tilde{y}, \\ K_0\psi(\tilde{x}) &:= 2\int_{\mathbb{R}^2} \frac{\partial G((\tilde{x}, f(\tilde{x})), y)}{\partial \nu(y)} \psi(y) J_f(\tilde{y})\, d\tilde{y}, \\ S_0\psi(\tilde{x}) &:= 2\int_{\mathbb{R}^2} G((\tilde{x}, f(\tilde{x})), y)\psi(y) J_f(\tilde{y})\, d\tilde{y}. \end{aligned}$$

The integral transformation of the boundary integral equations onto $\mathbb{R}^2$ leads to

$$\psi_n(\tilde{x}) + (K_n - i\eta S_n)\psi_n(\tilde{x}) = g_n(\tilde{x}) \text{ for } \tilde{x} \in \mathbb{R}^2 \tag{3.28}$$

and

$$\psi(\tilde{x}) + (K_0 - i\eta S_0)\psi(\tilde{x}) = g(\tilde{x}) \text{ for } \tilde{x} \in \mathbb{R}^2, \tag{3.29}$$

with the right hand sides

$$g(\tilde{x}) := 2G((\tilde{x}, f(\tilde{x})), z) + b(\tilde{x}, f(\tilde{x}))$$

and

$$g_n(\tilde{x}) := 2G((\tilde{x}, f_n(\tilde{x})), z) + b_n(\tilde{x}, f_n(\tilde{x}))$$

for $\tilde{x} \in \mathbb{R}^2$. Now we use Theorem 3.4 in [9] to observe that $I + K_n - i\eta S_n$ is invertible on $L^2(\mathbb{R}^2)$ and it holds that

$$\begin{aligned}&\left\|(I + K_n - i\eta S_n)^{-1}\right\|_{L^2(\mathbb{R}^2)\to L^2(\mathbb{R}^2)}\\ &\leq \frac{1}{2}\left(1 + \left[\frac{3\kappa^2\mathcal{L}^{1/2}}{\eta^2}(5\mathcal{L}^{1/2} + 6\mathcal{L}) + 6(\mathcal{L}^{1/2} + 3\mathcal{L})^2\right]^{\frac{1}{2}}\right),\end{aligned}$$

with $\mathcal{L} = 1 + L_n^2$ for the Lipschitz constant L_n of f_n. As $0 \leq L_n \to L$ for $n \to \infty$, there exists a constant $c > 0$ such that $\|(I + K_n - i\eta S_n)^{-1}\|_{L^2(\mathbb{R}^2)\to L^2(\mathbb{R}^2)} \leq c$ and hence, $(I + K_n - i\eta S_n)^{-1}$ is uniformly bounded. With

$$\begin{aligned}(I + K_n - i\eta S_n)(\psi_n - \psi) &= g_n - (g - (K_0 - i\eta S_0)\psi) + (K_n - i\eta S_n)\psi\\ &= g_n - g + ((K_0 - i\eta S_0) - (K_n - i\eta S_n))\psi,\end{aligned}$$

we obtain

$$\begin{aligned}\|\psi_n - \psi\| \quad \leq \quad & c\,\|g_n - g\|_{L^2(\mathbb{R})^2}\\ &+c\,\|K_n - i\eta S_n - (K - i\eta S)\|_{L^2(\mathbb{R}^2)\to L^2(\mathbb{R}^2)}\,\|\psi\|_{L^2(\mathbb{R}^2)}\,.\end{aligned}$$

The continuous dependence of the boundary integral operators on the surface, see Theorem 1.3.3, and the convergence $g_n \to g$ yields the norm-convergence of $\psi_n \to \psi$. This shows that also

$$\|\varphi_n\|_{L^2(\Gamma_{f_n})} \to \|\varphi\|_{L^2(\Gamma_f)}\,.$$

Substituting the densities in the above ansatz, we derive the convergence of the solutions u_n to u on compact subsets of $\{x \in \mathbb{R}^3 : x_3 > f(\tilde{x})\}$ by means of the Cauchy-Schwarz inequality. This completes the proof. □

We are now prepared to define *optimal surfaces* and show their existence.

DEFINITION 3.3.3. *Given the incident field $u^i = \Phi(\cdot, z)$, the measured field $v \in L^2(\Gamma_{h,A})$ and a regularisation parameter $\alpha > 0$, we call a surface $\Gamma_0 \in \mathcal{U}$ optimal if there exists a density $\varphi_0 \in L^2(\Gamma_t)$ such that φ_0 and Γ_0 minimize the cost functional (3.22), i.e.*

$$m_B(\alpha) := \inf_{\Gamma\in\mathcal{U},\varphi\in L^2(\Gamma_t)} \mu_{B,\alpha}(\varphi, \Gamma) = \mu_{B,\alpha}(\varphi_0, \Gamma_0). \tag{3.30}$$

THEOREM 3.3.4. *For each $\alpha > 0$ there exists an optimal surface $\Gamma \in \mathcal{U}$.*

Proof. Let $(\varphi_n, \Gamma_{f_n})_{n\in\mathbb{N}}$ be a minimizing sequence in $L^2(\Gamma_t) \times \mathcal{U}$, that means that the sequence fulfills

$$\mu_{B,\alpha}(\varphi_n, \Gamma_{f_n}) \longrightarrow \inf_{\Gamma\in\mathcal{U},\varphi\in L^2(\Gamma_t)} \mu_{B,\alpha}(\varphi, \Gamma), \quad n \to \infty.$$

Since $\mathcal{U}$ is compact, there exists a subsequence of surfaces in $\mathcal{U}$ with $\Gamma_{f_{n_j}} \to \Gamma$ for $j \to \infty$ and some surface $\Gamma \in \mathcal{U}$, without loss of generality we denote this subsequence with $(\Gamma_{f_n})_{n\in\mathbb{N}}$. Furthermore, the definition of the cost functional yields

$$\alpha \left\|P_B\varphi_n\right\|^2_{L^2(\Gamma_t)} \leq \mu_{B,\alpha}(\varphi_n, \Gamma_{f_n}) \longrightarrow m_B(\alpha), \quad n \to \infty,$$

and hence,

$$\left\|P_B\varphi_n\right\|_{L^2(\Gamma_t)} \leq c, \tag{3.31}$$

for some constant $c > 0$ depending on α. We consider the sequence $(P_B\varphi_n)_{n\in\mathbb{N}}$. Because every bounded sequence possesses a weakly convergent subsequence, see Theorem B.0.14, there exists a subsequence w.l.o.g. $(P_B\varphi_n)_{n\in\mathbb{N}}$ with $P_B\varphi_n \rightharpoonup P_B\varphi$. Since $S : L^2(\Gamma_{t,B}) \to L^2(\Gamma_{h,A})$ is compact by Lemma 3.2.4, we derive the convergence of the first term in the cost functional, i.e.

$$\left\|SP_B\varphi_n - v\right\|_{L^2(\Gamma_{h,A})} \to \left\|SP_B\varphi - v\right\|_{L^2(\Gamma_{h,A})} \text{ for } n \to \infty. \tag{3.32}$$

We now consider the integral operator $S^{(n)} : L^2(\Gamma_{t,B}) \to L^2(\Gamma_{f_n})$ defined by

$$S^{(n)}P_B\varphi(x) = \int_{\Gamma_{t,B}} G(x,y)P_B\varphi(y)ds(y) \text{ for } x \in \Gamma_{f_n}. \tag{3.33}$$

We make use of the isomorphism I_f for $f \in B(f_-, C)$, defined in (1.14) and assosciate the operator $S := S_f : L^2(\Gamma_t) \to L^2(\Gamma_f)$ with the element

$$\tilde{S}_f := I_f S_f I_t^{-1} \tag{3.34}$$

of the set of all bounded operators on $L^2(\mathbb{R}^2)$.

With the boundedness (3.31) and with the surface area element $J_t = 1$ we obtain

$$\begin{aligned}
&\left\|\tilde{S}^{(n)}P_B\varphi_n - \tilde{S}P_B\varphi\right\|_{L^2(\mathbb{R}^2)} \\
&\quad= \left\|\tilde{S}^{(n)}P_B\varphi_n - \tilde{S}P_B\varphi_n + \tilde{S}P_B\varphi_n - \tilde{S}P_B\varphi\right\|_{L^2(\mathbb{R}^2)} \\
&\quad\leq c\left\|\tilde{S}^{(n)}P_B - \tilde{S}P_B\right\|_{L^2(\mathbb{R}^2)\to L^2(\mathbb{R}^2)} + \left\|SP_B\varphi_n - SP_B\varphi\right\|_{L^2(\Gamma)}.
\end{aligned} \tag{3.35}$$

Since $S : L^2(\Gamma_{t,B}) \to L^2(\Gamma)$ is a compact operator by Lemma 3.2.4, S maps a weakly convergent sequence into a strongly convergent sequence, see Theorem B.0.14, we obtain that

$$\|SP_B\varphi_n - SP_B\varphi\|_{L^2(\Gamma)} \longrightarrow 0 \text{ for } n \to \infty\,. \tag{3.36}$$

Let $\varepsilon > 0$ and set $\psi(\tilde{y}) := P_B\varphi(\tilde{y}, t)$ for all $\tilde{y} \in \mathbb{R}^2$. Then, we find that

$$\begin{aligned}
&\left\|\tilde{S}^{(n)}P_B\psi - \tilde{S}P_B\psi\right\|^2_{L^2(\mathbb{R}^2)} \\
&\leq C\,\|\psi\|^2_{L^2(\mathbb{R}^2)} \int_{\mathbb{R}^2}\int_{|\tilde{y}|_\infty \leq B} |J_{f_n}(\tilde{x})G(\tilde{x}, f_n(\tilde{x}), \tilde{y}, t) \\
&\qquad\qquad -J_f(\tilde{x})G(\tilde{x}, f(\tilde{x}), \tilde{y}, t)|^2 d\tilde{y}\,d\tilde{x},
\end{aligned} \tag{3.37}$$

for some constant $C > 0$. We split the above integral expression in two parts I_1 and I_2, depending on a parameter $R > 0$ and n, with

$$\begin{aligned}
I_1(R,n) \;:=\; &\int_{|\tilde{x}|_\infty \leq R}\int_{|\tilde{y}|_\infty \leq B} |J_{f_n}(\tilde{x})G(\tilde{x}, f_n(\tilde{x}), \tilde{y}, t) \\
&\qquad -J_f(\tilde{x})G(\tilde{x}, f(\tilde{x}), \tilde{y}, t)|^2 d\tilde{y}\,d\tilde{x},
\end{aligned}$$

and

$$\begin{aligned}
I_2(R,n) \;:=\; &\int_{|\tilde{x}|_\infty > R}\int_{|\tilde{y}|_\infty \leq B} |J_{f_n}(\tilde{x})G(\tilde{x}, f_n(\tilde{x}), \tilde{y}, t) \\
&\qquad -J_f(\tilde{x})G(\tilde{x}, f(\tilde{x}), \tilde{y}, t)|^2 d\tilde{y}\,d\tilde{x}.
\end{aligned}$$

By the pointwise convergence of $f_n \to f$ for every $\tilde{x} \in \mathbb{R}^2$ and the compactness of $\{\tilde{x}, \tilde{y} \in \mathbb{R}^2 : |\tilde{x}|_\infty \leq R,\, |\tilde{y}|_\infty \leq B\}$ we see that

$$\begin{aligned}
|I_1(R,n)| \;&\leq\; \pi^2 2B^2 \frac{1}{R^2} \sup_{\tilde{x}:|\tilde{x}|_\infty \leq R}\ \sup_{\tilde{y}:|\tilde{y}|_\infty \leq B} |J_{f_n}(\tilde{x})G(\tilde{x}, f_n(\tilde{x}), \tilde{y}, t) \\
&\qquad\qquad -J_f(\tilde{x})G(\tilde{x}, f(\tilde{x}), \tilde{y}, t)| \\
&<\; \frac{\varepsilon}{2}
\end{aligned} \tag{3.38}$$

for some $n > n_0(\varepsilon, R)$. Arguing exactly as in (3.19) we find that

$$\begin{aligned}
|I_2(R,n)| \;&\leq\; \int_{|\tilde{x}|_\infty > R}\int_{|\tilde{y}|_\infty \leq B} |J_{f_n}(\tilde{x})G(\tilde{x}, f_n(\tilde{x}), \tilde{y}, t)|^2 d\tilde{y}\,d\tilde{x} \\
&\qquad\qquad + \int_{|\tilde{x}|_\infty > R}\int_{|\tilde{y}|_\infty \leq B} |J_f(\tilde{x})G(\tilde{x}, f(\tilde{x}), \tilde{y}, t)|^2 d\tilde{y}\,d\tilde{x} \\
&<\; \frac{\varepsilon}{4} + \frac{\varepsilon}{4}.
\end{aligned} \tag{3.39}$$

for a sufficiently large $R = R(\varepsilon)$. Hence, for all $\tilde{R} > R(\varepsilon)$ and $n > n_0(\varepsilon, R(\varepsilon))$, we have $|(I_1 + I_2)| < \varepsilon$. As $\varepsilon > 0$ was arbitrary, combining (3.38), (3.39), (3.36) and (3.35), we have shown the convergence

$$S^{(n)} P_B \varphi_n \to S P_B \varphi \tag{3.40}$$

for $n \to \infty$.

With the definition of the cost functional we derive

$$\begin{aligned} m_B(\alpha) &= \lim_{n\to\infty} (\|SP_B\varphi_n - v\|^2_{L^2(\Gamma_{h,A})} + \alpha \|P_B\varphi_n\|^2_{L^2(\Gamma_t)} \\ &\quad + \left\|G(\cdot,z) - S^{(n)}P_B\varphi_n\right\|^2_{L^2(\Gamma_{f_n})}) \\ &= \lim_{n\to\infty} \left\{\alpha \|P_B\varphi_n\|^2_{L^2(\Gamma_t)}\right\} \\ &\quad + \|SP_B\varphi - v\|^2_{L^2(\Gamma_{h,A})} + \|G(\cdot,z) - SP_B\varphi\|^2_{L^2(\Gamma)}, \end{aligned} \tag{3.41}$$

and thus, using $m_B(\alpha) \leq \mu_{B,\alpha}(\varphi, \Gamma)$ for the limits φ, Γ of the (sub)sequences φ_n and Γ_{f_n}, we have

$$\begin{aligned} \lim_{n\to\infty} \left\{\alpha \|P_B\varphi_n\|^2_{L^2(\Gamma_t)}\right\} &= m_B(\alpha) - \|SP_B\varphi - v\|^2_{L^2(\Gamma_{h,A})} \\ &\quad - \|G(\cdot,z) + SP_B\varphi\|^2_{L^2(\Gamma)} \\ &\leq \mu_{B,\alpha}(\varphi,\Gamma) - \|SP_B\varphi - v\|^2_{L^2(\Gamma_{h,A})} \\ &\quad - \|G(\cdot,z) + SP_B\varphi\|^2_{L^2(\Gamma)} \\ &= \alpha \|P_B\varphi\|^2_{L^2(\Gamma_t)}. \end{aligned} \tag{3.42}$$

The weak convergence leads to

$$\begin{aligned} 0 \leq \lim_{n\to\infty} \|P_B\varphi_n - P_B\varphi\|^2_{L^2(\Gamma_t)} &= \lim_{n\to\infty} \left\{\|P_B\varphi_n\|^2 - 2\mathrm{Re}\,\langle P_B\varphi_n, P_B\varphi\rangle\right\} + \|P_B\varphi\|^2 \\ &= \lim_{n\to\infty} \left\{\|P_B\varphi_n\|^2\right\} - \|P_B\varphi\|^2 \leq 0, \end{aligned}$$

i.e. $P_B\varphi_n$ converges strongly to $P_B\varphi$. We conclude

$$\mu_{B,\alpha}(\varphi_n, \Gamma_{f_n}) \longrightarrow \mu_{B,\alpha}(\varphi, \Gamma),$$

which is the statement of the theorem. □

THEOREM 3.3.5. *The cost functional converges to zero, i.e. $m_B(\alpha) \to 0$, for $\alpha \to 0$.*

Proof. Let $\epsilon > 0$ and let $\Gamma_0 \in \mathcal{U}$ be the true surface. The single layer potential $S : P_B(L^2(\Gamma_{t,B})) \to L^2(\Gamma_0)$ has dense range, see Theorem 3.2.1. Thus, there exists a density $P_B\varphi \in L^2(\Gamma_{t,B}))$ such that

$$\|SP_B\varphi + G(\cdot, z)\|_{L^2(\Gamma_0)} < \epsilon.$$

We have with the ansatz (1.23) for the remainder v that

$$\|SP_B\varphi - v\|_{L^2(\Gamma_{h,A})} = \|SP_B\varphi - u^s - \Phi(\cdot, z')\|_{L^2(\Gamma_{h,A})}\,. \tag{3.43}$$

Since $u^i + u^s = 0$ on Γ_0 and, by Theorem 3.3.2, the boundary values of the total field u on $\Gamma_{h,A}$ depend continuously on the boundary values on Γ_0 we have

$$\begin{aligned} \|SP_B\varphi - v\|_{L^2(\Gamma_{h,A})} &\leq \tilde{c}\,\|SP_B\varphi + G(\cdot, z)\|_{L^2(\Gamma_0)} \\ &\leq \tilde{c}\,\epsilon, \end{aligned} \tag{3.44}$$

for a constant $\tilde{c} > 0$. We get

$$\begin{aligned} m_B(\alpha) &\leq \mu_{B,\alpha}(\varphi, \Gamma_0) \\ &= \|SP_B\varphi - v\|^2_{L^2(\Gamma_{h,A})} + \alpha\,\|P_B\varphi\|^2_{L^2(\Gamma_t)} + \|SP_B\varphi + G(\cdot, z)\|^2_{L^2(\Gamma_0)} \\ &\leq \tilde{c}^2\epsilon^2 + \alpha\,\|P_B\varphi\|^2_{L^2(\Gamma_t)} + \epsilon^2 \overset{\alpha\to 0}{\longrightarrow} (1 + \tilde{c}^2)\epsilon^2, \end{aligned} \tag{3.45}$$

and since $\epsilon > 0$ is arbitary we have proven the theorem. □

THEOREM 3.3.6 (Convergence of the semi-finite Kirsch-Kress Method). *Let the true surface be in $\mathcal{U}$ and let (α_n) be a null sequence and (Γ_{f_n}) be the corresponding sequence of optimal surfaces for the regularisation parameter α_n. Then, there exists a convergent subsequence of (Γ_{f_n}). Every limit point Γ^* of Γ_{f_n} represents a surface which solves the inverse problem, i.e. on which the total field for the prescribed incident field satisfies the Dirichlet boundary condtion.*

Proof. Because of the compactness of $\mathcal{U}$ there exists a convergent subsequence (Γ_{f_n}) of optimal surfaces with

$$\Gamma_{f_n} \to \Gamma^* \in \mathcal{U} \text{ for } n \to \infty.$$

Let now Γ^* be such a limit point. Let u^* be the solution of the direct scattering problem (Problem 1.2.2) with the scattering surface Γ^* and incident field $u^i = \Phi(\cdot, z)$. Then, $(u^*)^s$ fulfills the boundary value problem (Problem 1.2.3) with boundary condition

$$(u^*)^s = -u^i \text{ on } \Gamma^*. \tag{3.46}$$

Since Γ_{f_n} is an optimal surface there exists a density φ_n such that

$$\mu(\varphi_n, \Gamma_{f_n}) = m(\alpha_n).$$

We define u_n by

$$u_n(x) := -SP_B\varphi_n(x) - \Phi(x, z') \text{ for } x \in \Omega_{f_n}, \tag{3.47}$$

where Ω_{f_n} is the upper half space with boundary Γ_{f_n}. The continuous extension of the single layer potential on the boundary implies that u_n is the solution of the boundary value problem (Problem 1.2.3) with the boundary condition

$$u_n = -SP_B\varphi_n - \Phi(\cdot, z') \text{ on } \Gamma_{f_n}. \tag{3.48}$$

Theorem 3.3.5 yields

$$\begin{aligned} \|SP_B\varphi_n + G(\cdot, z)\|_{L^2(\Gamma_{f_n})} &= \|u_n + \Phi(\cdot, z)\|_{L^2(\Gamma_{f_n})} \\ &= \left\|u_n + u^i\right\|_{L^2(\Gamma_{f_n})} \longrightarrow 0 \text{ for } n \to \infty, \end{aligned} \tag{3.49}$$

and by Theorem 3.3.2 and (3.46), we have the convergence

$$u_n \to (u^*)^s \tag{3.50}$$

on compact subsets of the open exterior of Γ^*.

We remind that we have the relation (1.23) $u^s = v - \Phi(\cdot, z')$ for the remainder v and the scattered field u^s of the true surface. Then, Theorem 3.3.5 implies

$$\begin{aligned} \|SP_B\varphi_n - v\|_{L^2(\Gamma_{h,A})} &= \|u_n + \Phi(\cdot, z') - u^s - \Phi(\cdot, z')\|_{L^2(\Gamma_{h,A})} \\ &= \|u_n - u^s\|_{L^2(\Gamma_{h,A})} \longrightarrow 0 \text{ for } n \to \infty, \end{aligned}$$

that means

$$u_n \to u^s \text{ on } \Gamma_{h,A}. \tag{3.51}$$

Hence, from (3.50) and (3.51) we derive

$$u^s = (u^*)^s \text{ on } \Gamma_{h,A}.$$

Due to the analyticity of $(u^s)^*$ we obtain $u^s = (u^*)^s$ in the whole plane Γ_h. Now $(u^s)^*$ and u^s both solve the Dirichlet boundary value problem (Problem 1.2.2) in the exterior domain Ω_{f_h} and from this, and the uniqueness result for this problem, we

deduce $u^s = (u^*)^s$ in Ω_{f_h}. Further, using the analyticity of $(u^*)^s$ in the whole domain Ω^* we see that $(u^*)^s$ is an analytic extension of u^s into the whole domain Ω^*, which is a solution of the Dirichlet boundary problem in Ω^*, whence

$$u^s = (u^*)^s \text{ on } \Gamma^* ,$$

such that the total field $u = u^s + u^i$ satisfies $u = 0$ on Γ^*. □

3.4 The Multi-Section approach for the optimisation problem

Here, we study the reconstruction of a finite section of the unknown surface using a compactly supported density. To this end, we define the *multi-section cost functional*

$$\begin{aligned} \mu_{B,C,\alpha}(\varphi,\Gamma) &= \|SP_B\varphi - v\|^2_{L^2(\Gamma_{h,A})} + \alpha \|P_B\varphi\|^2_{L^2(\Gamma_t)} \\ &\quad + \|P_C G(\cdot,z) - P_C S P_B \varphi\|^2_{L^2(\Gamma)} , \end{aligned} \tag{3.52}$$

for $\varphi \in L^2(\Gamma_t)$, $\Gamma \in \mathcal{U}$ and truncation parameters $B, C > 0$.

At this point we can also understand why we did not directly study the multi-section functional. The crucial point is that we cannot expect the continuous dependence of the measurements $v|_{\Gamma_{h,A}}$ on the boundary values on the *finite* section of the scattering surface Γ. However, using the knowledge of the properties of the semi-finite approach leads to the convergence result for the infimum of the multi-section cost functional. Here, we first estimate the difference between the semi-finite and the multi-section approach with some truncation parameter $C > 0$ and some regularisation parameter $\alpha > 0$. Then, we conclude this section with the convergence result for the multi-section approach.

THEOREM 3.4.1. *For every $\alpha > 0$ and $C, B > 0$ there exists an optimal surface, i.e. there exists a surface $\Gamma_0 \in \mathcal{U}$ and a density $\varphi_0 \in L^2(\Gamma_t)$ such that*

$$\mu_{B,C,\alpha}(\varphi_0,\Gamma_0) = \inf_{\varphi\in L^2(\Gamma_t),\ \Gamma\in\mathcal{U}} \mu_{B,C,\alpha}(\varphi,\Gamma). \tag{3.53}$$

Proof. Let $(\varphi_n, \Gamma_{f_n})$ be a minimizing sequence of $\mu_{B,C,\alpha}$. By exactly the same arguments as in the proof of Theorem 3.3.4, we see that there exists a convergent subsequence of (Γ_{f_n}) and a weakly convergent subsequence of $(P_B\varphi_n)$ with limits Γ and $P_B\varphi$.

Without loss of generality we denote these subsequences by (Γ_{f_n}) and resp. $(P_B\varphi_n)$. Let $S^{(n)}$ defined as in (3.33). Then, we deduce from the strong convergence (3.40) that also

$$\left\|P_C(G(\cdot,z)-S^{(n)}P_B\varphi_n)\right\|^2_{L^2(\Gamma_{f_n})} \to \|P_C(G(\cdot,z)-SP_B\varphi)\|^2_{L^2(\Gamma_0)}\,, \tag{3.54}$$

where $P_CS^{(n)}P_B$ converges to P_CSP_B in the sense that

$$\left\|P_C\tilde{S}^{(n)}P_B - P_C\tilde{S}P_B\right\|_{L^2(\mathbb{R}^2)\to L^2(\mathbb{R}^2)} \to 0 \text{ for } n\to 0.$$

Now, we can apply the same proof as in Theorem 3.3.4 to conclude $\mu_{B,C,\alpha}(\varphi_n,\Gamma_n)\to \mu_{B,C,\alpha}(\varphi,\Gamma)$. □

We note that, in general, the optimal surface Γ_0 defined as in Theorem 3.4.1 will not be uniquely determined. From the definition of the functional $\mu_{B,C,\alpha}$ and $\mu_{B,\alpha}$ we first observe the following relation. For every $B,C>0$, $\Gamma\in\mathcal{U}$ and $\varphi\in L^2(\Gamma_t)$ it holds that

$$\mu_{B,C,\alpha}(\varphi,\Gamma)+\|(I-P_C)(G(\cdot,z)+SP_B\varphi)\|^2_{L^2(\Gamma)} = \mu_{B,\alpha}(\varphi,\Gamma). \tag{3.55}$$

To show the convergence of the infimum of the multi-section cost functional, we discuss the properties of the remainder $\|(I-P_C)(G(\cdot,z)+SP_B\varphi)\|^2_{L^2(\Gamma)}$ for an optimal surface Γ and the associated density $\varphi\in L^2(\Gamma_t)$ for the cost functional $\mu_{B,C,\alpha}$.

LEMMA 3.4.2. *Let $m_{B,C}(\alpha)$ denote the infimum of the multi-section cost functional*

$$m_{B,C}(\alpha) = \inf_{\varphi\in L^2(\Gamma_t),\Gamma\in\mathcal{U}} \mu_{B,C,\alpha}(\varphi,\Gamma). \tag{3.56}$$

Then, we have the convergence

$$\lim_{\alpha\to 0} m_{B,C}(\alpha) = 0 \text{ for every fixed } C>0. \tag{3.57}$$

Proof. Let Γ_B and φ_B be optimal for the semi-finite cost functional, i.e.

$$m_B(\alpha) = \inf_{\varphi\in L^2(\Gamma_t),\Gamma\in\mathcal{U}} \mu_{B,\alpha}(\varphi,\Gamma) = \mu_{B,\alpha}(\varphi_B,\Gamma_B).$$

The relation (3.55) of the multi-section cost functional and the semi-finite cost functional implies

$$\begin{aligned} m_B(\alpha) &= \mu_{B,C,\alpha}(\varphi_B,\Gamma_B)+\|(I-P_C)(G(\cdot,z)+SP_B\varphi_B\|^2_{L^2(\Gamma_B)} \\ &\geq m_{B,C}(\alpha)\geq 0. \end{aligned} \tag{3.58}$$

Thus, with the convergence of the cost functional $m_B(\alpha)$ towards 0 for $\alpha \to 0$, see Theorem 3.3.5, we have the convergence result (3.57). □

LEMMA 3.4.3. *Let Γ be an optimal surface for $\mu_{B,C,\alpha}$ as defined in Theorem 3.4.1 and $\varphi \in L^2(\Gamma_t)$ be the corresponding density. Then, for $C > \min\{2B, 2|\tilde{z}|_\infty\}$ and $0 < \alpha \leq 1$, there exists a constant $\eta > 0$ such that*

$$\|(I - P_C)(G(\cdot, z) + SP_B\varphi))\|^2_{L^2(\Gamma)} \leq \eta \frac{1}{\alpha C^2} \tag{3.59}$$

holds.

Proof. With the decay property of the Green's function , see Lemma 2.1.2, there exists a constant c with

$$|G(x,z)| \leq \frac{c}{|x-z|^2} \leq \frac{c}{|\tilde{x}-\tilde{z}|^2_\infty} \leq \frac{c}{(|\tilde{x}|_\infty - |\tilde{z}|_\infty)^2}, \tag{3.60}$$

where $x, y \in \Gamma$ and $\tilde{x}, \tilde{z} \in \mathbb{R}^2$. Further, the assumption on C yields

$$(r - |z|_\infty)^2 \geq r^2/4$$

for $r > C$ and we conclude

$$\begin{aligned}
\|(I - P_C)G(\cdot, z)\|^2_{L^2(\Gamma)} &= \int_\Gamma |(I - P_C)G(x,z)|^2 ds(x) \\
&\leq c^2 \int_{|\tilde{x}|_\infty \geq C} \frac{1}{(|\tilde{x}|_\infty - |\tilde{z}|_\infty)^4} d\tilde{x} \\
&\leq 4c^2 \int_C^\infty \frac{1}{(r - |\tilde{z}|)^4} r \, dr \\
&\leq 4c^2 \int_C^\infty \frac{1}{r^3} \, dr = 2c^2 \frac{1}{C^2} = \frac{\rho^2}{C^2},
\end{aligned} \tag{3.61}$$

for $\rho^2 = 2c^2$. For an optimal density φ (depending on α) of $\mu_{B,C,\alpha}$ from (3.57) and the relation (3.55) given $\tau > 0$ there is a constant $\alpha_0 > 0$ such that

$$\alpha \, \|P_B\varphi\|^2_{L^2(\Gamma_t)} \leq m_{B,C}(\alpha) \leq \tau$$

for all $\alpha < \alpha_0$. Lemma 3.2.4 and the property $P_B^2 = P_B$ of the projection operator now

implies

$$\begin{aligned}\|(I-P_C)\left(G(\cdot,z)+SP_B\varphi\right))\|_{L^2(\Gamma)} &\leq \|(I-P_C)G(\cdot,z)\|_{L^2(\Gamma)} \\ &\quad + \|(I-P_C)SP_B(P_B\varphi)\|_{L^2(\Gamma)} \\ &\leq \frac{\rho}{C} + \|(I-P_C)SP_B\|_{L^2(\Gamma_t)\to L^2(\Gamma)}\,\|P_B\varphi\|_{L^2(\Gamma_t)} \\ &\leq \frac{\rho}{C} + \frac{\sigma}{C}\sqrt{\frac{\tau}{\alpha}},\end{aligned}$$

where $\sigma = cB$ with c from Lemma 3.2.4. Thus, we have

$$\begin{aligned}\|(I-P_C)(G(\cdot,z)+SP_B\varphi))\|^2_{L^2(\Gamma)} &\leq (\frac{\rho}{C} + \frac{\sigma}{C}\sqrt{\frac{\tau}{\alpha}})^2 \\ &\leq \frac{\eta}{\alpha C^2} \qquad (3.62)\end{aligned}$$

with some constant $\eta > 0$ for α sufficiently small. □

LEMMA 3.4.4. *We have the convergence*

$$\lim_{C\to\infty} m_{B,C}(\alpha) = m_B(\alpha) \text{ for every fixed } \alpha > 0. \qquad (3.63)$$

Proof. Using that there exists an optimal surface $\Gamma_{B,C}$ and an associated density $\varphi_{B,C}$, see corollary 3.4.1, we derive with the relation (3.55)

$$\begin{aligned}m_{B,C}(\alpha) &= \mu_{B,\alpha}(\varphi_{B,C},\Gamma_{B,C}) - \|(I-P_C)(G(\cdot,z)+SP_B\varphi_{B,C}))\|^2_{L^2(\Gamma_{B,C})} \\ &\geq m_B(\alpha) - \|(I-P_C)(G(\cdot,z)+SP_B\varphi_{B,C}))\|^2_{L^2(\Gamma_{B,C})}\,. \qquad (3.64)\end{aligned}$$

Thus, from (3.58) and (3.64) and Lemma 3.4.3 we conclude (3.63). □

THEOREM 3.4.5 (Convergence of the Multi-Section Method). *Let (α_n) be a null sequence and (C_n) a monotonically increasing sequence of real positive numbers such that*

$$\alpha_n C_n^2 \to \infty \text{ for } n\to\infty, \qquad (3.65)$$

and let Γ_{f_n} be the corresponding sequence of optimal surfaces for the regularisation parameter α_n and truncation parameter C_n. Then, there exists a convergent subsequence of (Γ_{f_n}) and every limit point Γ^* represents a surface on which the total field satisfies the Dirichlet boundary condtion.

Proof. As in the proof of Theorem 3.3.6, because of the compactness of $\mathcal{U}$, there exists a convergent subsequence (Γ_{f_n}) of optimal surfaces with

$$\Gamma_{f_n} \to \Gamma^* \in \mathcal{U} \text{ for } n \to \infty,$$

and let u^* be the solution of the direct scattering problem (Problem 1.2.2) with the scattering surface Γ^* and incident field $u^i = \Phi(\cdot, z)$. Then, $(u^*)^s$ fullfills the boundary value problem (Problem 1.2.3) with boundary condition

$$(u^*)^s = -u^i \text{ on } \Gamma^*. \tag{3.66}$$

Since Γ_{f_n} is an optimal surface there exists a density φ_n such that

$$\mu_{B,C_n,\alpha_n}(\varphi_n, \Gamma_{f_n}) = m_{B,C_n}(\alpha_n).$$

We define u_n by

$$u_n(x) := SP_B\varphi_n(x) - \Phi(x, z') \text{ for } x \in \Omega_{f_n}, \tag{3.67}$$

where Ω_{f_n} is the upper half space with boundary Γ_{f_n}. The continuous extension of the single layer potential on the boundary implies that u_n is the solution of the boundary value problem (Problem 1.2.3) with the boundary condition

$$u_n = SP_B\varphi_n - \Phi(\cdot, z') \text{ on } \Gamma_{f_n}. \tag{3.68}$$

We have

$$\begin{aligned} \left\|u_n + u^i\right\|_{L^2(\Gamma_{f_n})} &= \|SP_B\varphi_n + G(\cdot, z)\|_{L^2(\Gamma_{f_n})} \\ &= \|P_{C_n}\left(SP_B\varphi_n + G(\cdot, z)\right)\|_{L^2(\Gamma_{f_n})} \\ &\quad + \|(I - P_{C_n})\left(SP_B\varphi_n + G(\cdot, z)\right)\|_{L^2(\Gamma_{f_n})}. \end{aligned} \tag{3.69}$$

It holds that

$$\begin{aligned} \|P_{C_n}\left(SP_B\varphi_n + G(\cdot, z)\right)\|_{L^2(\Gamma_{f_n})} &\leq m_{B,C_n}(\alpha_n) \\ &\leq m_B(\alpha_n) \to 0 \text{ for } n \to \infty, \end{aligned} \tag{3.70}$$

and, with Lemma 3.4.3 and the assumption (3.65) we obtain

$$\|(I - P_{C_n})\left(SP_B\varphi_n + G(\cdot, z)\right)\|_{L^2(\Gamma_{f_n})} \to 0 \text{ for } n \to \infty. \tag{3.71}$$

and thus, from (3.69),

$$\left\|u_n + u^i\right\|_{L^2(\Gamma_{f_n})} \to 0. \tag{3.72}$$

By Theorem 3.3.2 and (3.66), we have the convergence

$$u_n \to (u^*)^s \tag{3.73}$$

on compact subsets of the open exterior of Γ^*. We remind that we have the relation (1.23) $u^s = v - \Phi(\cdot, z')$ for the remainder v and the scattered field u^s of the true surface. Then, the convergence of the semi-finite cost functional implies

$$\begin{aligned} \|P_A(u_n - u^s)\|_{L^2(\Gamma_{h,A})} &= \|P_A(SP_B\varphi_n - \Phi(\cdot, z') - u^s)\|_{L^2(\Gamma_{h,A})} \\ &= \|P_A S P_B \varphi_n - P_A v\|_{L^2(\Gamma_{h,A})} \\ &\leq m_{B,C_n}(\alpha_n) \leq m_B(\alpha_n) \longrightarrow 0 \text{ for } n \to \infty, \end{aligned}$$

that means

$$u_n \to u^s \text{ on } \Gamma_{h,A}. \tag{3.74}$$

Hence, we derive from (3.73) and (3.74) and the same arguments used in the proof of Theorem 3.3.6 that

$$u^s = (u^*)^s \text{ on } \Gamma_{h,A}.$$

This implies

$$(u^*)^s = u^s \text{ on } \Gamma^*,$$

such that the total field $u = u^s + u^i$ satisfies $u = 0$ on Γ^*. □

3.5 Numerical realisation

In this last section we show an example for the numerical realisation of the multi-section method using the measurement data which we calculated following [27].

We solve the multi-section version of the Tikhonov normal equation, given by

$$P_C(\alpha I + S^* P_A S) P_B \varphi = P_C S^* P_A f. \tag{3.75}$$

We apply Nystroem's Method to approximate the Tikhonov normal equation, using standard numerical quadrature for the evaluation of the integral (c.f. [34]). In particular, we choose a uniform grid $\mathcal{G}_{\mathcal{B}}$ for $[-B, B]^2$ and a uniform grid $\mathcal{G}_{\mathcal{A}}$ for $[-A, A]^2$ with

M grid points $\tilde{y}_\xi \in \mathcal{G}_\mathcal{B}$ for $\xi = 1, ..., M$, and N grid points $\tilde{x}_\eta \in \mathcal{G}_\mathcal{A}$ for $\eta = 1, ..., N$. We approximate $P_A S P_B : L^2(\Gamma_{t,B}) \to L^2(\Gamma_{h,A})$ by a discretisation of the associated integral operator $P_A I_h S P_B I_t^{-1} \varphi$,

$$(P_A I_h P_B S I_t^{-1} \varphi)(\tilde{x}_\eta, h) = \int_{[-B,B]^2} G(\tilde{x}_\eta, h, \tilde{y}, t) \varphi(\tilde{y}, t)\, d\tilde{y} \tag{3.76}$$

$$\approx \sum_{j=1}^{M} a_j G((\tilde{x}_\eta, h), (\tilde{y}_j, t)) \varphi(\tilde{y}_j, h), \tag{3.77}$$

for $x_\eta \in \mathcal{G}_\mathcal{A}$ and quadrature weights a_j, $j = 1, ..., M$. We also choose a uniform grid $\mathcal{G}_\mathcal{C}$ for $[-C, C]^2$ with K grid points

$$\tilde{x}_\ell \in \mathcal{G}_\mathcal{C},\ \ell = 1, ..., K.$$

The discretisation of the truncated adjoint operator $(P_C I_t S^* I_h^{-1} \psi)(\tilde{x}_\ell, h)$ is then given by

$$(P_C I_t S^* I_h^{-1} \psi)(\tilde{x}_\ell, t) = \sum_{j=1}^{N} a_j \overline{G((\tilde{x}_j, h), (\tilde{x}_\ell, t))} \psi(\tilde{x}_j, h),\ \ell = 1, ..., K, \tag{3.78}$$

and we have

$$\begin{aligned} &P_C(\alpha I_t I I_h^{-1} + I_t S^* P_A I_h S)(P_B I_t^{-1} \varphi)(\tilde{x}_\ell, t) \\ &\approx \alpha \varphi(\tilde{x}_\ell, t) + \sum_{j=1}^{N} a_j \overline{G((\tilde{x}_j, h), (\tilde{x}_\ell, t))} \left(\sum_{i=1}^{M} a_i G((\tilde{x}_j, h), (\tilde{y}_i, t)) \boldsymbol{\varphi}(\tilde{y}_i, t) \right), \end{aligned}$$

for $\ell = 1, ..., K$. Furthermore, we choose a rectangular grid $\mathcal{G}$ which covers a finite section of the unknown scattering surface and evaluate the total field via $u = u^i + S\varphi - \Phi(\cdot, z)$ for all gridpoints in $\mathcal{G}$. In a second step, we look for a minimum surface of the total field.

In the following examples, see Figures 3.2 - 3.6, the point source is located at the point $(-3, 0, 12)$ and the wave number is given by $\kappa = 1$. As Tikhonov regularisation parameter we choose $\alpha = 10^{-6}$. We further choose $A = 15$ and the measurement plane with height $h = 8$ or $h = 11$. We use 26×27 data points. The test surface has height $t = 0.2$ and the Tikhonov regularisation parameter is $\alpha = 10^{-6}$. To compare the average error between the reconstructed surface Γ_{f_r} and the original surface Γ_f we compute the L^2-norm of $f - f_r$ given by

$$\mathcal{E} = \left(\frac{1}{K} \sum_{i=1}^{K} |(f - f_r)(\tilde{x}_i)|^2 \right)^{\frac{1}{2}}, \tag{3.79}$$

where K is the total number of discretisation points $\tilde{x}_i \in \mathcal{G}_C$.

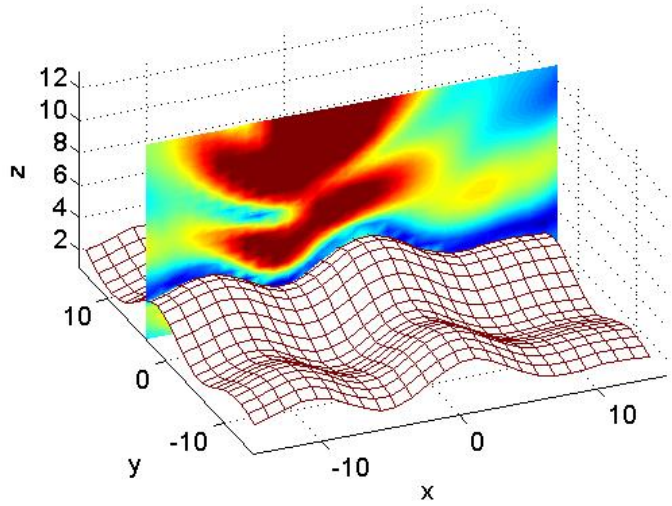

Figure 3.2: *The solution of the forward problem, with a slice of the absolute values of the total field.*

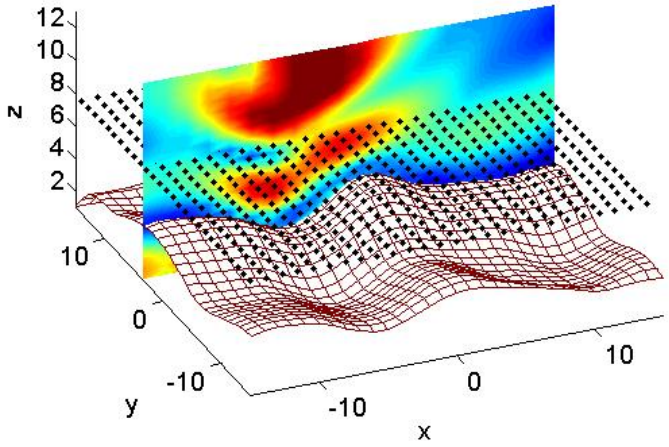

Figure 3.3: *We show a reconstruction of the total field by the knowledge of the measured values on subset of a plane parallel to the x, y-plane, here with height $h = 8$, and a section of the reconstructed surface.*

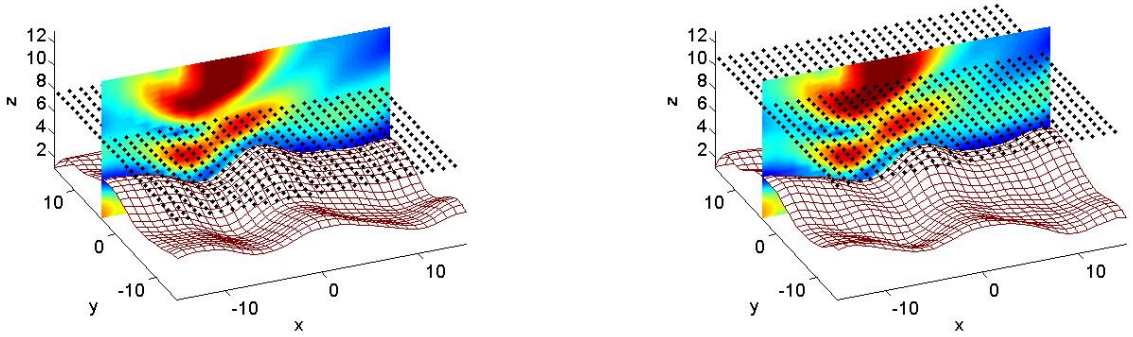

Figure 3.4: *Here, we added 1% noise and show the results for the measurement heights $h = 8$ and $h = 11$.*

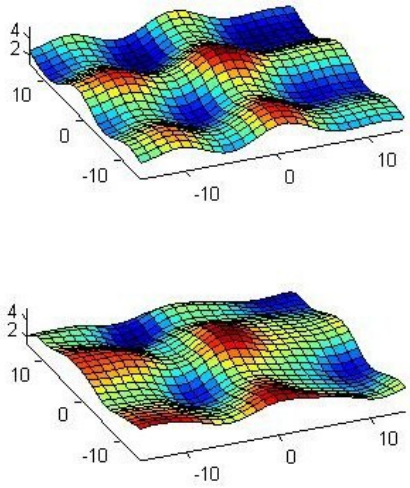

Figure 3.5: *(a)*

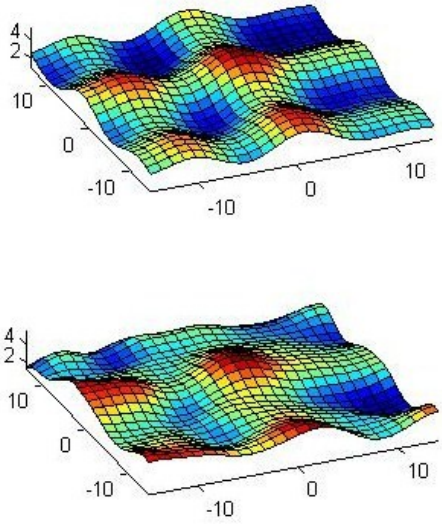

Figure 3.6: *(b)*

We show the results of the reconstruction with 1% *(Figure (a)) and* 5% *of noise (Figure (b)). In both pictures, (a) and (b), the surface on the top is the original surface and below is shown its reconstruction.*

Noise	$\mathcal{E}$	truncated $\mathcal{E}$
1%	0.62728	0.49617
3%	0.6958	0.53084
5%	0.83253	0.7624
7%	0.90339	0.82143
9%	0.9608	0.85689

Table 3.1: *We present the results for the reconstruction of the rough surface shown in Figure 3.2 for different levels of noise for a fixed height* $h = 8$ *for the measurement plane. The truncated* $\mathcal{E}$ *excludes values of* f *and* f_r *for discretisation points near the boundary, i.e. points with* $\max|\tilde{x}_1| > C_1$ *and* $\max|\tilde{x}_2| > C_2$ *for some constants* $C_1, C_2 > 0$*. In particular, in this table we excluded the two outer rows of discretisation points.*

Chapter 4

A time-domain Probe Method

In this section we develop a *time-domain Probe Method* (TDPM) for the reconstruction of a rough surface. The results presented in this chapter have been published in [4]. The basic idea of the time-domain Probe Method is to use pulses in the time domain and the time-dependent response of the scatterer to reconstruct its location and shape.

In particular, we consider the scattering of a time-dependent pulse from a rough surface in three dimensions. In acoustic applications time-domain measurements are usually relatively easy to obtain whereas pure frequency-domain methods do not take full advantage of the data which are available. The method we present here takes full time-measurements into account. It incorporates the principle of causality in time-domain scattering problems in contrast to recent work of Chandler-Wilde and Lines [10] and by Luke and Potthast [38] in which the two-dimensional and the bounded domain case are discussed. The time-domain Probe Method is a full time-domain scheme: it is based on causality and thus it naturally incorporates the knowledge of scattered fields for many frequencies.

The method can be seen as an extension of the probing methods presented by Ikehata, Potthast, Nakamura, Sini and others. The approach will not rely on a particular probe in the time domain, but will in principle work with a large variety of incident time-dependent fields. Also, the probing fields do not need to have a singularity of any type. This avoids numerical instabilities which is one of the key problems for the realisation of the time-domain probe schemes. In contrast to engineering schemes from travel-time tomography we use a full reconstruction of the time-dependent scattered

field U^s which is exploited for reconstructing the unknown surfaces.

As a part of the probing procedure we employ the time-domain field reconstruction problem by frequency-domain inverse methods and Fast Fourier Transform (FFT) via a single layer potential approach as first used by Kirsch and Kress in 1986, [17], and discussed in Chapter 3 of this thesis. An alternative has been developed with the Point Source method by Chandler-Wilde and Lines, [10]. Here, we need to employ the Dirichlet Green's function for the half-space instead of the standard free-space fundamental solution for the Helmholtz equation as it has been carried out for the forward problem, [8], [9] and presented in Chapter 1.

For the time-domain probe method the actual boundary condition is not explicitly used in the reconstruction algorithm. All arguments will be analogous for other type of boundary conditions. Here, we will only investigate the case of the Dirichlet boundary condition in detail and leave other boundary conditions to future research.

4.1 The time-domain problem

In this section we formulate the *time-domain problem* as the time-dependent counterpart of the frequency-domain problem given by Problem 1.2.2. In the frequency-domain problem we consider the scattering of an acoustic field from the rough surface Γ as introduced in Chapter 1 and whenever we wish to explicitly denote the dependence on κ we write $u(\cdot, \kappa)$ for the solution u of Problem 1.2.2.

We begin with the construction of an incident pulse, which serves as a time-dependent incident field before we state the time-domain problem.

Let $g \in C_c^n(\mathbb{R})$ be a compactly supported, bounded n-times continuously differentiable function for some $n \in \mathbb{N}$. We obtain by Lemma A.0.2

$$|\mathcal{F}g(\xi)| \leq M(1 + |\xi|)^{-n} \text{ for all } \xi \in \mathbb{R}, \tag{4.1}$$

for some constant $M > 0$. In the following we consider the Fourier transform $\mathcal{F}$ with respect to frequency or time, respectively, using capital letters for the time-dependent fields and small letters in the frequency-domain, i.e. we use the notation

$$v(x, \kappa) := (\mathcal{F}^{-1}V(x, \cdot))(\kappa) = \int_{-\infty}^{\infty} e^{is\kappa} V(x, s)\, ds, \quad x \in \Omega, \tag{4.2}$$

and

$$V(x,t) = (\mathcal{F}v(x,\cdot))(t), \quad x \in \Omega,\, t \in \mathbb{R}.$$

Then, we define the incident pulse by

$$U^i(x,t) = \mathcal{F}\Big(\Phi(x,z,\cdot)(\mathcal{F}^{-1}g)(\cdot)\Big)(t), \quad t \in \mathbb{R},\, x \neq z, \tag{4.3}$$

on a rough surface with the free-space fundamental solution defined by (1.17). Here, we again use the notation $\Phi(x,y,\kappa)$ for $\Phi(x,y)$. We note that $\mathcal{F}$ is a unitary operator i.e. $\mathcal{F}^*\mathcal{F} = \mathcal{F}\mathcal{F}^* = 2\pi I$ for the adjoint operator $\mathcal{F}^*$ of $\mathcal{F}$. Furthermore, we recall that $\mathcal{F}^{-1}g = \frac{1}{2\pi}\mathcal{F}^*g$ in the sense of Theorem A.0.4. We have

$$\begin{aligned} 4\pi U^i(x,t) &= \frac{1}{|x-z|}\int_{-\infty}^{\infty} e^{is(|x-z|-t)}(\mathcal{F}^{-1}g)(s)ds \\ &= \frac{1}{|x-z|}\mathcal{F}(\mathcal{F}^{-1}g(\cdot))(|x-z|-t) \\ &= \frac{1}{|x-z|}\frac{1}{2\pi}\mathcal{F}(\mathcal{F}^*g(\cdot))(|x-z|-t) \\ &= \frac{1}{2\pi|x-z|}g(|x-z|-t) \text{ for } t \in \mathbb{R},\, x \neq z, \end{aligned} \tag{4.4}$$

and, hence, for every fixed $x \in \mathbb{R}^3$, $U^i(x,\cdot)$ is compactly supported and C^n-smooth in time $t \in \mathbb{R}$. Moreover, U^i depends for every fixed time t only on the distance $|x-z|$. Hence, whenever $U^i(x,t) > 0$ for some fixed time t and point x, this then implies that $U^i(y,t) > 0$ for all y with $|y-z| = |x-z|$ at the same time t. For this reason we say that U^i is a *spherical pulse*.

Throughout this chapter we set the wave speed equal to one. The time-domain problem is formulated as follows.

Problem 4.1.1 (The direct problem in the time-domain)**.** *Given an incident pulse $U^i(x,z,t)$ by (4.3) which is C^n-smooth and compactly supported with respect to time, find a solution $U^s \in (C^2(\Omega) \cap C^1(\overline{\Omega})) \times (C^n(\mathbb{R}) \cap L^2(\mathbb{R}))$, of*

$$\Delta U^s(x,t) - \frac{\partial^2}{\partial t^2}U^s(x,t) = 0,\, x \in \Omega_f, \quad t \in \mathbb{R} \tag{4.5}$$

$$U^s(x,t) = -U^i(x,z,t), \quad x \in \Gamma_f,\, t \in \mathbb{R}. \tag{4.6}$$

We assume that the (inverse) Fourier transform $u^s(x,\kappa)$ of $U^s(x,t)$ uniformly satisfies the boundedness condition *(compare [8])*

$$|u^s(x,\kappa)| \leq c\,, \quad x \in \Omega, \tag{4.7}$$

with some constant c for any fixed κ, $\mathrm{Im}(\kappa) \geq 0$, *and we demand* u^s *to satisfy a* limiting absorption principle *(see (1.21)).*

The *time-domain wave* U is a real-valued mapping $U : \Omega \times \mathbb{R} \to \mathbb{R}$ and it holds that $(\mathcal{F}^{-1}U(x,\cdot))(\kappa) = \overline{(\mathcal{F}^{-1}U(x,\cdot))(-\kappa)}$. Further, in three-dimensions (in contrast to the two-dimensional case) there are no difficulties arising at $\kappa = 0$ as the fundamental solution $\Phi(x, y, \kappa)$ has no singularity in $\kappa = 0$. For this reason we may assume that $\kappa \in \mathbb{R}$.
Let $U(x,t)$ be a solution of the wave equation (4.5) in free space and $t \in \mathbb{R}$. Then, using $U(x,t) = \mathcal{F}u(x,\cdot)(t)$, for $x \in \Omega_f$, we deduce that

$$\begin{aligned} 0 &= \Delta_x \mathcal{F}u(x,\cdot)(t) - \frac{\partial^2}{\partial t^2}\mathcal{F}u(x,\cdot)(t) \\ &= \int_{-\infty}^{\infty} \Delta u(x,s)e^{-its}\,ds + \int_{-\infty}^{\infty} s^2 u(x,s)e^{-its}\,ds. \end{aligned} \tag{4.8}$$

By an application of the inverse Fourier transform to (4.8), we see that $u(x,s)$ satisfies the Helmholtz equation with respect to x, i.e. $\Delta u(\cdot,s) + s^2 u(\cdot,s) = 0$ in Ω_f, for almost all $s \in \mathbb{R}$. Furthermore, by applying the Fourier transform with respect to time to the boundary condition (4.6) we arrive at the Dirichlet boundary condition for the frequency-domain problem, see Problem 1.2.2, and we have

$$u^i(x,\kappa) = (\mathcal{F}^{-1}U^i(x,\cdot))(\kappa) = \Phi(x,z,\kappa)(\mathcal{F}^{-1}g)(\kappa) = -u^s(x,\kappa), \quad x \in \Omega. \tag{4.9}$$

Thus, the incident field is now due to a point source multiplied by a constant

$$c_\kappa = (\mathcal{F}^{-1}g)(\kappa) \tag{4.10}$$

depending on g and κ. We remark that boundary conditions other than (4.6) can be considered and by an application of the Fourier transform we obtain the corresponding boundary condition in the frequency-domain as seen in (4.9) for the Dirichlet case.

Under the above setting we obtain uniqueness and solvability of the time-domain problem, given by Problem 4.1.1, for a sufficiently smooth g by combining uniqueness and solvability of the frequency problems and the bounds on the inverse as worked out in [9] by an application of the Fourier transform. This is the statement of the following lemma.

LEMMA 4.1.2. *Let* $g \in C^n(\mathbb{R})$ *for some* $n \geq 6$. *Then, Problem 4.1.1 possesses exactly one solution.*

Proof. We first prove uniqueness. Let U_1 and U_2 with $U_1 \neq U_2$ be two solutions of Problem 4.1.1. Then, the difference $U = U_1 - U_2$ is a solution of the homogenuous problem, i.e. U solves Problem 4.1.1 with incident field $U^i = 0$ for all $t \in \mathbb{R}$ and $x \in \Gamma$. Then, for almost all $\kappa > 0$, the inverse Fourier transform u defined by $u(x) := (\mathcal{F}^{-1}U(x,\cdot))(\kappa)$ is a solution of the boundary value problem, Problem 1.2.3, with boundary condition $u = 0$ on Γ_f. Hence, from Theorem 1.3.2, $u(\cdot,\kappa) = 0$ in Ω, for almost all κ, and therefore, also $U = 0$. The existence of a solution U of the time-domain problem, Problem 4.1.1, follows from the existence of the solutions of the boundary value problem (Problem 1.2.3). In particular, we have that every solution of Problem 1.2.3 with boundary condition (4.9), for a given $\kappa > 0$, satisfies the bound,

$$|u(x,\kappa)| \leq C_1(1+\frac{\kappa}{\eta})c_\kappa \, \|G(\cdot,z,\kappa)\|_{L^2(\Gamma_f)}, \quad x \in \Omega_f, \tag{4.11}$$

see [7], Theorems 2.2 and 3.4, for some constant $C_1 > 0$, which only depends on the Lipschitz constant of the function f and the constant c_κ given by (4.10). Here, $\eta > 0$ is the coupling parameter of the boundary integral approach, see (1.47). By Lemma 2.1.1 there exist constants $\tilde{C}, C > 0$ such that

$$\|G(\cdot,z,\kappa)\|^2_{L^2(\Gamma_f)} \leq \tilde{C}(1+|\kappa|)^2(z_3+1)^2 \int_1^\infty \frac{1}{r^4} r\, dr < C(1+|\kappa|)^2.$$

Inserting the above estimate into (4.11) we find that for some constant $\tilde{C} > 0$,

$$|u(x,\kappa)| \leq \tilde{C}(1+\frac{\kappa}{\eta})(1+|\kappa|)^2(1+|\kappa|)^{-n}, \quad x \in \Omega_f, \tag{4.12}$$

where we also used the bound (4.1) for c_κ. For $\kappa < 0$ we set $u(s,\kappa) := \overline{u(x,-\kappa)}$. Without loss of generality we set $\eta = 1$ to see that

$$\int_{-\infty}^{\infty} |u(x,s)|^2\, ds \leq C \int_{-\infty}^{\infty} |\frac{(1+|s|)^4}{(1+|s|)^n}|^2\, ds < \infty, \tag{4.13}$$

for some constant $C > 0$ and for $n \geq 6$. Hence, $U(x,\cdot) := (\mathcal{F}u)(x,\cdot) \in L^2(\mathbb{R})$ is a solution of the wave equation in Ω_f (compare (4.8)), and, by construction of U, the boundary condition and the assumptions about the Fourier transform of U hold. □

4.2 A retarded potential formulation

Often, time-domain solutions to scattering problems are represented by time-domain integral equations [2], [37], [19]. To formulate such a time-domain integral equation it

is possible to consider the Green's representation Theorem for the frequency-domain case and employ the Fourier transform to obtain a Green's representation formula for the time-domain fields. This is the statement of the following lemma.

LEMMA 4.2.1 (Retarded Green's formulation). *Let $D \subset \mathbb{R}^3$ be an open subset with C^2-smooth boundary. Let $U \in (C^2(D) \cap C^1(\overline{D})) \times (C^n(\mathbb{R}) \cap L^2(\mathbb{R}))$ be a solution of the wave equation. Then, it holds that*

$$\begin{aligned} U(x,t) &= \int_{\partial D} \nu(y) \cdot \left(\frac{-i\kappa(x-y)}{4\pi|x-y|^2} - \frac{(x-y)}{4\pi|x-y|^3}\right) U(y, t-|x-y|) \\ &\quad + \frac{1}{4\pi|x-y|}\, \nu(y) \cdot \nabla_y U(y, t-|x-y|)\, ds(y) \end{aligned} \tag{4.14}$$

for every $x \in D$, $t > 0$.

Proof. Let $u(x,\kappa) := \mathcal{F}^{-1}U(x,\cdot)(\kappa)$ and note that $u(x,-\kappa) = \overline{u(x,\kappa)}$. By the Green's representation Theorem for solutions of the Helmholtz equation for $\kappa > 0$, see [17], we obtain the representation for $U(x,t)$ in the time-domain,

$$\begin{aligned} U(x,t) &= \int_0^\infty e^{-i\kappa t} \int_{\partial D} \frac{\partial \Phi}{\partial \nu(y)}(x,y,\kappa) u(y,\kappa) + \Phi(x,y,\kappa) \frac{\partial u}{\partial \nu}(y,\kappa)\, ds(y)\, d\kappa \\ &+ \int_{-\infty}^0 e^{-i\kappa t} \overline{\int_{\partial D} \frac{\partial \Phi}{\partial \nu(y)}(x,y,-\kappa) u(y,-\kappa) + \Phi(x,y,-\kappa) \frac{\partial u}{\partial \nu}(y,-\kappa)\, ds(y)\, d\kappa} \\ &= \int_0^\infty e^{-i\kappa t} \int_{\partial D} \frac{\partial \Phi}{\partial \nu(y)}(x,y,\kappa) u(y,\kappa) + \Phi(x,y,\kappa) \frac{\partial u}{\partial \nu}(y,\kappa)\, ds(y)\, d\kappa \\ &+ \int_{-\infty}^0 e^{-i\kappa t} \int_{\partial D} \frac{\partial \Phi}{\partial \nu(y)}(x,y,\kappa) \overline{u(y,-\kappa)} + \Phi(x,y,\kappa) \overline{\frac{\partial u}{\partial \nu}(y,-\kappa)}\, ds(y)\, d\kappa \\ &= \int_{\partial D} \mathcal{F}\left(\frac{\partial \Phi}{\partial \nu(y)}(x,y,\cdot) u(y,\cdot)\right)(t) \\ &\qquad + \mathcal{F}\left(\Phi(x,y,\cdot) \frac{\partial u}{\partial \nu(y)}(y,\cdot)\right)(t)\, ds(y) \end{aligned} \tag{4.15}$$

for $x \in D$. In order to simplify the above formula, we need to study the Fourier transforms of $\Phi(x,y,\cdot)$ and $\nabla_y \Phi(x,y,\cdot))$ with respect to the wave number. We have

$$\begin{aligned} \mathcal{F}\left(\Phi(x,y,\cdot)\right)(t) &= \frac{1}{4\pi|x-y|} \int_{-\infty}^\infty e^{-is(t-|x-y|)} ds \\ &= \frac{1}{4\pi|x-y|} \delta(t-|x-y|) \end{aligned} \tag{4.16}$$

for the distribution δ, see for example [50]. We further compute

$$\begin{aligned}
&\mathcal{F}\Big(\nu(y)\cdot\nabla_y\Phi(x,y,\cdot)\Big)(t)\\
&\quad=\nu(y)\cdot(x-y)\left(\frac{-i\kappa}{4\pi|x-y|^2}-\frac{1}{4\pi|x-y|^3}\right)\int_{-\infty}^{\infty}e^{-is(t-|x-y|)}\,ds\\
&\quad=-\nu(y)\cdot(x-y)\left(\frac{-i\kappa}{4\pi|x-y|^2}-\frac{1}{4\pi|x-y|^3}\right)\delta(t-|x-y|). \qquad (4.17)
\end{aligned}$$

Inserting this into (4.15) we find that

$$\begin{aligned}
&U(x,t)=\\
&\int_{\partial D}\left[\nu(y)\cdot(x-y)\left(\frac{-i\kappa}{4\pi|x-y|^2}-\frac{1}{4\pi|x-y|^3}\right)\delta(\cdot-|x-y|)*U(y,\cdot)\right](t)\\
&\qquad+\left[\frac{1}{4\pi|x-y|}\delta(\cdot-|x-y|)*(\nu(y)\cdot\nabla_y U(y,\cdot))\right](t)\,ds(y) \qquad (4.18)
\end{aligned}$$

and as the delta function acts as an identity under convolution, the theorem follows. □

We see that $U(x,t)$ for a particular fixed point (x,t) in space and time does depend on all values of $U(y,t-|x-y|)$ for all y on some surrounding boundary ∂D. The time $t^*:=t-|x-y|$ is a point in time before the particular time t, the potential

$$\mathcal{R}\varphi(x,t):=\int_{\partial D}\frac{\varphi(y,t-|x-y|)}{|x-y|}\,ds(y) \qquad (4.19)$$

for some density φ is also known as *retarded potential*.

Corollary 4.2.2 (Range of Influence). *Let D be any subset of Ω and $t>0$ and let the wave speed be $c=1$. Then, the values of the total field U on the boundary of*

$$D_t\cap\Omega \qquad (4.20)$$

with

$$D_t:=\big\{x\in\mathbb{R}^3:d(x,D)<t\big\} \qquad (4.21)$$

at time $t^*=0$ in the case if $D_t\subset\Omega$, and for all times $t^*\in[0,t]$ in the case $D_t\cap(\mathbb{R}^3\backslash\Omega)\neq\varnothing$, uniquely determines the field $U^s(x,t)$ in D of Problem 4.1.1. Here, d denotes the Euclidean distance defined by $d(x,D):=\inf_{z\in D}|x-z|$.

Proof. Let $D \subset \Omega$ and we choose $t > 0$ such that $D_t \subset \Omega$. By Theorem 4.2.1 we can represent the scattered field by

$$\begin{aligned} U^s(x,t) &= \int_{\partial D_t} \nu(y) \cdot \left(\frac{-i\kappa(x-y)}{4\pi|x-y|^2} - \frac{(x-y)}{4\pi|x-y|^3} \right) U(y, t-|x-y|) \\ &\quad + \frac{1}{4\pi|x-y|} \nu(y) \cdot \nabla_y U(y, t-|x-y|)\, ds(y) - U^i(x,t) \\ &= \int_{\partial D_t} \nu(y) \cdot \left(\frac{-i\kappa(x-y)}{4\pi|x-y|^2} - \frac{(x-y)}{4\pi|x-y|^3} \right) U(y, 0) \\ &\quad + \frac{1}{4\pi|x-y|} \nu(y) \cdot \nabla_y U(y, 0)\, ds(y) - U^i(x,t) \end{aligned}$$

for $x \in D$. Hence, whenever U and $\nabla_x U(x, \cdot)$ vanish at time $t = 0$ on the boundary ∂D_t, and $U^i(x,t)$ vanishes in x for the fixed time t, then also the scattered field must vanish. This means that the scattered field at the point (x,t) is only influenced by the behavior of the total field $U(x,0)$ on the boundary of D_t and the incident field U^i at (x,t).

It remains to show that the statement is true for the case where $t > 0$ is a point in time such that $D_t \cap (\mathbb{R}^3 \backslash \Omega) \neq \varnothing$. We set $\tilde{D}_t = D_t \cap (\mathbb{R}^3 \backslash \Omega)$ and use the retarded Green's representation of U to find that

$$\begin{aligned} U^s(x,t) &= \int_{\partial \tilde{D}_t} \nu(y) \cdot \left(\frac{-i\kappa(x-y)}{4\pi|x-y|^2} - \frac{(x-y)}{4\pi|x-y|^3} \right) U(y, t-|x-y|) \\ &\quad + \frac{1}{4\pi|x-y|} \nu(y) \cdot \nabla_y U(y, t-|x-y|)\, ds(y) - U^i(x,t). \end{aligned} \tag{4.22}$$

We see that if the incident field $U^i(x,t) = 0$ and if

$$U(y, t-|x-y|) = 0 \text{ and } \nabla_y U(y, t-|x-y|) = 0 \text{ for all } y \in \partial \tilde{D}_t, \tag{4.23}$$

then also the scattered field U^s vanishes in (x,t). It holds that

$$0 \leq t - |x-y| \leq t \text{ for } y \in \partial \tilde{D}_t$$

and hence, (4.23) reduces to the assumption that U and $\nabla_y U$ vanish for all times $t^* \in [0,t]$ on the boundary $\partial \tilde{D}_t$. □

We remark that the boundary of the cone $\{x : |x - x_0| \leq t\}$ for some fixed $x_0 \in \Omega$ is also denoted by *characteristic lines*. Here, the characteristic lines are the lines

$$|x - x_0| = t, \quad t \geq 0 \tag{4.24}$$

shown in Figure 4.1 (a) and the domain D_t is the maximal domain from which points in D can be reached by an influence travelling along the characteristics in the time interval $[0, t]$. The above lemma physically represents a *causality principle*, which states

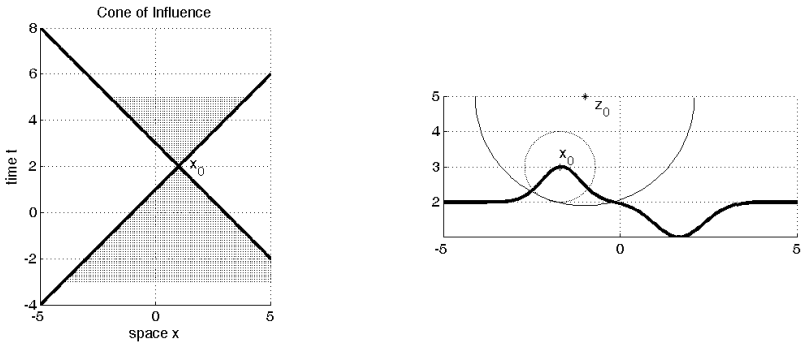

(a) (b)

Figure 4.1: *We visualise the characteristics of the wave equation, where we used a wave speed $c = 1$. (a) The field at the point $x_0 = (1, 2)$ is influenced by the field in the dotted region below. It is influencing the field in the dotted cone above x_0. If the field is zero in the lower cone, then it must be zero at x_0. (b) Consider an incident field emerging from z_0 which reached x_0 at time T. The image shows the situation at $T + \delta T$, where the sphere of influence of the incident field is visualised by the large circle. The scattered field arising at T from x_0 can reach the sphere indicated by the dotted smaller circle.*

that whenever there are no sources to influence the total field before some particular point in time t, then, the total field will not change at the specific time t.

4.3 A time-dependent Probe Method

For simulation and inversion we employ calculations using FFT and frequency-domain methods. Starting from a retarded potential approach for the rough surface scattering problem we will see that this approach is linked via the Fourier transform to the single layer approach for the frequency-domain which we presented in Chapter 3.

Let Γ^* be some surface with $\Gamma^* \subset \overline{\Omega}$ and let Ω^* be the propagation domain above

Γ^*. Then, the retarded single layer approach is to find φ such that it solves the *retarded boundary integral equation*

$$\mathcal{S}\varphi = U^s \text{ on } \Gamma_{h,A}, \tag{4.25}$$

in the time-domain with $\Gamma_{h,A}$ given by

$$\Gamma_{h,A} = \left\{x \in \mathbb{R}^3 : x_3 = h, |x_1| \leq A, |x_2| \leq A\right\} \tag{4.26}$$

for constants $h, A > 0$ and where we define

$$(\mathcal{S}\varphi)(x,t) := \frac{1}{4\pi} \int_{\Gamma^*} \left(\frac{\varphi(y, t-|x-y|)}{|x-y|} - \frac{\varphi(y', t-|x-y'|)}{|x-y'|} \right) ds(y) \tag{4.27}$$

for $x \in \Omega^*, t \in \mathbb{R}$. For an investigation of numerical methods to solve the retarded boundary integral equation for bounded surfaces, i.e. $\Gamma^* = \partial\Omega$ where Ω is a bounded subset of $\mathbb{R}^3$, we refer for example to [19]. A complete theoretical background using Laplace transforms can be found in [2] and in [37].

An application of the FFT with respect to time to equation (4.25) leads to the standard single-layer boundary integral equation in the frequency-domain for all frequencies $\kappa \in \mathbb{R}$. We solve this problem for κ in a uniform grid of points and employ the inverse FFT to obtain an approximate solution to the retarded integral equation. For more details about equivalence and estimates we refer to the arguments worked out in [38]. We also refer to [47] where this equivalence has been used to construct a time-domain filter for field reconstruction from a family of frequency-domain filters.

4.3.1 Field reconstructions in the time-domain

We begin this section by recalling the field reconstruction problem in the frequency-domain as discussed in Chapter 3. In particular, given measurements of the total field $u(\cdot,\kappa) = u^i(\cdot,\kappa) + u^s(\cdot,\kappa)$ for a single fixed wavenumber $\kappa > 0$ on a finite surface patch $\Gamma_{h,A}$ given by (4.26) for a constant $A > 0$ the task is to reconstruct $u^s(x,\kappa)$ in Ω. In this chapter, we particularly make use of the following frequency-domain problem.

Problem 4.3.1 (The Field Reconstruction Problem, frequency-domain)**.** *Suppose we know the incident field $u^i(\cdot,\kappa) = \Phi(\cdot,z,\kappa)$ in $\mathbb{R}^3 \setminus \{z\}$ and the scattered field $u^s(\cdot,\kappa)$ on the plane $\Gamma_{h,A}$ for a fixed wavenumber κ with $\mathrm{Im}(\kappa) \geq 0$. Then, we try to find the total field such that u is the solution of the direct problem (1.2.2) and $(u-u^i)(\cdot,\kappa)$ coincides with $u^s(x,\kappa)$ for all $x \in \Gamma_{h,A}$.*

As in Chapter 3 we approximate the total field $u(\cdot,\kappa)$ via a single layer potential ansatz over some auxiliary surface $\Gamma^* \subset \overline{\Omega}$. For $\varphi \in L^2(\Gamma^*)$ the single layer potential is defined via

$$S\varphi(x,\kappa) := \int_{\Gamma^*} G(x,y,\kappa)\varphi(y)\, ds(y) \tag{4.28}$$

for all $x \in \mathbb{R}^3$. We proceed as in the approach given in Chapter 3, i.e. we make the ansatz

$$u^s(\cdot,\kappa) = v(\cdot,\kappa) - \Phi(\cdot,z',\kappa) \tag{4.29}$$

and seek the projection $P_A v$ of the remainder v in a single layer potential. Moreover, we follow Chapter 3 and restrict our approach to compactly supported densities $P_B\varphi$, i.e. we solve $P_A S P_B \varphi(x) = P_A v(x)$ on $\Gamma_{h,A}$ by Tikhonov regularisation

$$\alpha P_B\varphi(\cdot,\kappa) + S^* P_A S P_B \varphi(\cdot,\kappa) = S^* P_A v(\cdot,\kappa) \text{ on } \Gamma_{h,A}\,, \tag{4.30}$$

with a regularisation parameter $\alpha > 0$. In the following we indicate the dependence on the regularisation parameter $\alpha > 0$ by the subscript α. Then, we approximate the function v in the domain Ω^* above Γ^* via

$$v_\alpha(x,\kappa) = S P_B \varphi_\alpha(x,\kappa), \quad x \in \overline{\Omega^*}\,. \tag{4.31}$$

Using the ansatz (4.29), we obtain an approximation u_α of the total field via

$$u_\alpha(\cdot,\kappa) = S P_B \varphi_\alpha(\cdot,\kappa) + G(\cdot,z,\kappa), \tag{4.32}$$

in the frequency-domain.

We use the knowledge of U^s on $\Gamma_{h,A}$ for $t \in \mathbb{R}$ to reconstruct the field and moreover the unknown surface via the help of Fourier transforms. In particular, for every $\kappa \in \mathbb{R}$ we can evaluate the Fourier transform of U^s with respect to time for all $x \in \Gamma_{h,A}$. The Fourier transform of the time-domain data can be used as frequency-domain data, i.e. $(\mathcal{F}^{-1}U^s(x,\cdot))(\kappa)$ on $\Gamma_{h,A}$ for every fixed κ, serves as measurement data for the frequency-domain problem. Thus, we can incorporate the single layer potential approach for the reconstruction of the frequency-dependent field. We are now prepared to introduce the inverse time-domain problem. To this end we assume to know the measurements of the scattered field through time on the measurement surface, that is

$$U^s(x,t) \text{ for all } x \in \Gamma_{h,A},\ t \in \mathbb{R}. \tag{4.33}$$

The inverse time-domain problem is given as follows.

Problem 4.3.2. *Suppose we know the incident pulse U^i, which is C^3-smooth and compactly supported with respect to time, and the scattered field U^s on the surface patch $\Gamma_{h,A}$ for all $t \in \mathbb{R}$. Then, we try to find the total field such that U is the solution of the direct problem, Problem 4.1.1, and $(U - U^i)$ coincides with U^s for all $x \in \Gamma_{h,A}$ and $t \in \mathbb{R}$.*

Next, we present an algorithm for the reconstruction of the field U^s above Γ^* from the given time-domain data (4.33) based on the single layer approach in the frequency-domain. In particular, we employ the idea to use the Tikhonov regularisation (4.30) in the frequency-domain and reconstruct the time-domain field through the use of the Fourier transform.

Algorithm 1 (Field Reconstructions)**.** *We reconstruct the time-dependent scattered field $U^s(x,t)$ for $x \in \Omega^*$ and $t \in \mathbb{R}$ by frequency-domain methods via the Fourier transform as follows: Let $\alpha > 0$ the regularisation parameter of the Tikhonov regularisation.*

1. *For $\kappa > 0$ evaluate $v(x,\kappa) := (\mathcal{F}^{-1}U^s(x,\cdot))(\kappa)$, $x \in \Gamma_{h,A}$. Further, we set $v^s(x,-\kappa) := \overline{(\mathcal{F}^{-1}U^s(x,\cdot))(\kappa)}$.*
2. *For every $\kappa \in \mathbb{R}\setminus\{0\}$, reconstruct the scattered field $u^s = (u-u^i)(x,\kappa)$ for $x \in \Omega$, by use of the approach (4.29), i.e. reconstruct $v = v_\alpha$ of $u^s = v - \Phi(\cdot,z')$ by a single layer potential approach and Tikhonov regularisation, given by (4.30).*
3. *Evaluate U^s via $U^s(x,t) = \mathcal{F}v_\alpha(x,\cdot)(t)$.*

First, we note that we excluded zero frequencies as in acoustic scattering zero frequencies are not physical. As $v_\alpha(\cdot,0)$ is a null set with respect to frequency we can alter the value of $v_\alpha(x,0)$ by setting $v_\alpha(x,0) = 0$ without altering the value of the integral $(\mathcal{F}v_\alpha(x,\cdot))$.

In the frequency-domain potential approach, we used a single-layer potential defined on some finite part Γ_B^* of Γ^*. In the next section we will show convergence of this finite section method to the true solution for the infinite surface Γ^*.

4.3.2 Surface reconstruction in the time-domain

We are now prepared to formulate the time-domain probe method for the reconstruction of the unknown scattering surface from the knowledge of time-measurements on a

surface patch $\Gamma_{h,A}$ above the scattering surface.

DEFINITION 4.3.3. *For a point $x \in \Omega$ we define the* first hitting time *with respect to the incident field U^i by*

$$T(x) := \inf\{t \in \mathbb{R} : |U^i(x,t)| > 0\}. \tag{4.34}$$

For $\tilde{x} = (x_1, x_2) \in \mathbb{R}^2$ define

$$x_\lambda := (x_1, x_2, h - \lambda)\,,\ 0 < \lambda < h\,, \tag{4.35}$$

which is called a vertical needle. *Then the* first hitting parameter λ_* *is defined as*

$$\lambda_* := \sup_{x_\lambda \in \Omega} \lambda. \tag{4.36}$$

We use a grid of size $h_\lambda > 0$ for the discretisation of the vertical probing, i.e. we employ

$$\lambda_\xi := h_\lambda \cdot \xi, \quad \xi = 0, 1, 2, ... \tag{4.37}$$

Algorithm 2 (Time-domain Probe Method)**.** *Let $U^s(x,t)$ be given for all $x \in \Gamma_{h,A}$ and $t \in \mathbb{R}$. To identify points $x \in \Gamma$ or to calculate a reconstruction f_{rec} for the surface height function f on some compact subset Q of $\mathbb{R}^2$, respectively, we choose a constant h_λ and $\epsilon = 2h_\lambda$ to carry out the following steps:*

1. *For every $\tilde{x} \in Q$:*
2. *we successively investigate $\lambda = \lambda_\xi$ for $\xi = 0, 1, 2, ...$ given by (4.37):*
3. *with x_{λ_ξ} defined by (4.35) we reconstruct $U^s(x_{\lambda_\xi}, t)$ in the small interval $t \in (T, T + \epsilon)$ after the first hitting time $T = T(x_{\lambda_\xi})$ by Algorithm 1.*
4. *If $|U^s(x_{\lambda_\xi}, t)| = 0$ for all $t \in (T, T + \epsilon)$, then we set $\mu(\lambda_\xi) = 0$ and conclude that $x_{\lambda_\xi} \in \Omega$. If there are points t such that $|U^s(x,t)| > 0$ is in the time interval $(T, T + \epsilon)$, then we define $\mu(\lambda_\xi) = 1$ and we conclude that x_{λ_ξ} is close to Γ.*
5. *If $\mu(\lambda_\xi) = 1$ and $\mu(\lambda_\eta) = 0$ for all $\eta < \xi$, then we define the approximation*

$$f_{rec}(\tilde{x}) := h - \lambda_\xi \tag{4.38}$$

to the unknown surface given by f.

To achieve a numerical algorithm we will employ a grid of points in the rectangle $Q = (a_1, b_1) \times (a_2, b_2)$ with n_1 or n_2 points in the x_1 or x_2 direction, respectively, and we use the notation

$$x_{1,j} = a_1 + \frac{b_1 - a_1}{n_1 - 1}(j-1), \quad j = 1, ..., n_1 \tag{4.39}$$

$$x_{2,\ell} = a_1 + \frac{b_2 - a_2}{n_2 - 1}(\ell - 1), \quad \ell = 1, ..., n_2. \tag{4.40}$$

We denote our horizontal grid by Q_{n_1,n_2}. For every point $\tilde{x} \in Q_{n_1,n_2}$ we investigate the points x_{λ_ξ} for $\xi = 1, 2, 3, ...$ until $\mu(\lambda_\xi) = 1$. For the discrete version we need to make sure that we identify points which are close to the unknown boundary Γ. To this end we need to investigate appropriately chosen intervals $(T, T + \epsilon)$ depending on our discretisation for simulations. In the following example at the end of this chapter, we have used a fixed $\epsilon = 0.2$ which was chosen by trial and error.

4.4 Convergence

The goal of this chapter is to prove convergence of the time-domain Probe Method for the reconstruction of impenetrable rough surfaces.

We denote the reconstructed field of Algorithm 1 by $U^s_{B,\alpha}$ to indicate its dependence on the reconstruction parameter $\alpha > 0$ and its dependence on the truncation parameter $B > 0$. From now on U^s is the *true scattered field* in the time-domain. Before we discuss the convergence of Algorithm 2, we study the convergence of the reconstructed field $U^s_{B,\alpha}$ towards the true field U^s. We begin by considering the case $B = \infty$ in the sense that we choose $\varphi \in L^2(\Gamma^*)$ with support Γ^*. In particular, we consider Algorithm 1 where we replace the Tikhonov regularisation in step 2 by

$$\alpha\varphi(\cdot, \kappa) + S^* P_A S\varphi(\cdot, \kappa) = S^* P_A v(\cdot, \kappa) \text{ on } \Gamma_{h,A}. \tag{4.41}$$

THEOREM 4.4.1. *Let U^i be an incident pulse, given by (4.3), and U^s_α the reconstructed field by the use of Algorithm 1 based on a Tikhonov regularisation (4.41) with densities $\varphi \in L^2(\Gamma^*)$. If the test surface Γ^* is in Ω, then it holds that*

$$|U^s_\alpha(x,t)| \to |U^s(x,t)| \text{ for } \alpha \to 0, \tag{4.42}$$

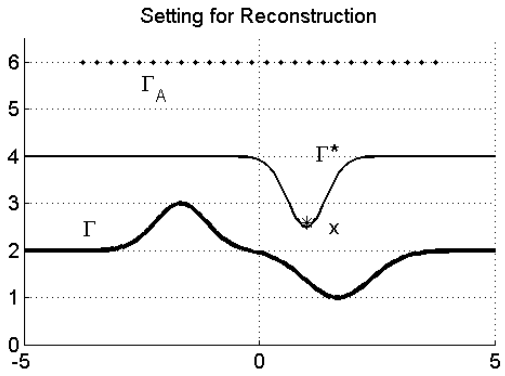

Figure 4.2: *We show the setting for the reconstruction of the scattered field $U^s(x,t)$. The surface Γ^* is supposed to be in the domain Ω, i.e. above the unknown surface Γ. The measurement surface is Γ_A. The figure shows a point x in which $U^s(x,t)$ is reconstructed close to or on the boundary of the test surface Γ^*.*

for every x above or on Γ^*.

Proof. This follows from $U^s_\alpha(x,t) = (\mathcal{F}u^s_\alpha(x,\cdot))(t)$ and the convergence

$$|u^s_\alpha(x,\kappa)| \to |u^s(x,\kappa)|$$

for $\alpha \to 0$ and points $x \in \Omega^*$ from the standard properties of the Tikhonov regularisation. In particular, the remainder v_α converges to the true solution v of Problem 1.2.3 with $\alpha \to 0$ and we use the bound (4.11) to obtain that $v(x,\cdot) \in L^2(\mathbb{R})$. Thus, applying the inverse Fourier transform we obtain convergence for the time-dependent fields as well. □

We recall that the support of $P_B\varphi$ is given by the truncated surface

$$\Gamma^*_B := \{x \in \Gamma^*, \max\{|x_1|, |x_2|\} \leq B\}. \tag{4.43}$$

for a truncation parameter $B > 0$. The next theorem states the convergence of the reconstructed fields $U^s_{B,\alpha}$ using that the choice of α depends on B.

THEOREM 4.4.2. *Consider the setting shown in Figure 4.2. Let U^i be an incident pulse and $U^s_{B,\alpha}$ the reconstructed field using the single-layer approach applied with the*

truncated surface (4.43). If the test surface Γ^* *is in* Ω *there exists a choice* $B_0(\alpha)$ *with*

$$B_0(\alpha) \to \infty, \quad \alpha \to 0 \tag{4.44}$$

such that for all $B(\alpha) \geq B_0(\alpha)$ *we obtain the convergence*

$$\left|U^s_{B,\alpha}(x,t)\right| \to |U^s(x,t)| \ \textit{for}\ \alpha \to 0, \tag{4.45}$$

for every x *above or on* Γ^*.

Proof. We first show the above statement for the frequency-domain, i.e. we show that $|u^s_{B,\alpha}(x,\kappa)| \to |u^s(x,\kappa)|$ respectively, $|v_{B,\alpha}(x,\kappa)| \to |v(x,\kappa)|$, for the ansatz (4.29), for every fixed $\kappa \in \mathbb{R}\setminus\{0\}$ and all x above Γ^*. To this end, we denote the Tikhonov operator for Γ^* by R_α, i.e.

$$R_\alpha := (\alpha I + S^* P_A S)^{-1} S^* P_A, \tag{4.46}$$

and the Tikhonov operator arising from Γ^*_B by

$$R^B_\alpha := (\alpha I + P_B S^* P_A S P_B)^{-1} P_B S^* P_A. \tag{4.47}$$

Let $\varphi_\alpha = R_\alpha v$ be the regularised density for Γ^*, for which we know the convergence $\varphi_\alpha \to \varphi$ towards the true solution φ of $S\varphi = v(\cdot,\kappa)$ on $\Gamma_{h,A}$ for $\alpha \to 0$ by the property of the Tikhonov regularisation. Then, we have pointwise convergence

$$R^B_\alpha v \to R_\alpha v,\ B \to \infty, \tag{4.48}$$

i.e.

$$\varphi^B_\alpha := R^B_\alpha v \to \varphi_\alpha,\ B \to \infty. \tag{4.49}$$

This now shows that for $\varepsilon > 0$ there exists an $\alpha_0 = \alpha_0(\varepsilon)$ and $B_0(\alpha,\varepsilon)$ such that

$$\begin{aligned} \left\|\varphi^{B(\alpha)}_\alpha - \varphi\right\|_{L^2(\Gamma^*)} &\leq \left\|R^{B(\alpha)}_\alpha v - R_\alpha v\right\|_{L^2(\Gamma^*)} + \left\|\varphi_\alpha - \varphi\right\|_{L^2(\Gamma^*)} \\ &< \frac{\varepsilon}{2} + \frac{\varepsilon}{2} \end{aligned}$$

for all $\alpha > \alpha_0(\varepsilon)$ and $B(\alpha) > B_0(\alpha,\varepsilon)$. Thus, we have $\varphi^{B(\alpha)}_\alpha \to \varphi$ when $B(\alpha)$ is chosen appropriately. Using Lemma 2.1.1, we find that for every $x \in \Omega^*$ there exists a constant

$c > 0$ with

$$\begin{aligned} |v_{B,\alpha}(x,\kappa) - v(x,\kappa)| &= |S(\varphi_\alpha^{B(\alpha)} - \varphi)(x,\kappa)| \\ &= |\int_{\Gamma_B^*} G(x,y,\kappa)(\varphi_\alpha^{B(\alpha)} - \varphi)(y)\, ds(y)| \\ &\leq \|G(x,\cdot,\kappa)\|^2_{L^2(\Gamma_B^*)} \left\|\varphi_\alpha^{B(\alpha)} - \varphi\right\|^2_{L^2(\Gamma_B^*)} \\ &\leq c \left\|\varphi_\alpha^{B(\alpha)} - \varphi\right\|^2_{L^2(\Gamma_B^*)} \end{aligned} \tag{4.50}$$

This implies that $|v_{B,\alpha}(x,\kappa)| \to |v(x,\kappa)|$ for $\alpha \to 0$ and $B(\alpha) \to \infty$ for all x above Γ^*. Finally, by the bound (4.11) of the remainder v we see that $v(x,\cdot) \in L^2(\mathbb{R})$. Thus, applying the Fourier transform we obtain convergence for the time-dependent fields as well. □

We recall the basic setup of the time-domain Probe method, see Figure 4.3. The following Lemma states that the scattered field cannot have a non-zero value in a point $x \in \mathbb{R}^3$ for any point in time before the first hitting time.

LEMMA 4.4.3. *Let U^i be an incident spherical pulse as given by (4.3) which is compactly supported in time. For every point $x \in \Omega$ we have that*

$$U^s(x,t) = 0 \text{ for all } t < T(x). \tag{4.51}$$

Proof. Let $x \in \Omega$. For all $t < T(x)$ we have $U^s(x,t) = U(x,t)$ by the definition of the first hitting time T. We can now consider the setting of Figure 4.1. For a spherical incident pulse the total field $U(x,t)$ is zero in space-time range of influence of $(x, T(x))$. Hence, the scattered field $U^s(x,t)$ can never be positive in x for all points in time $t < T(x)$. □

THEOREM 4.4.4 (Convergence of time-domain Probe Method). *The time-domain Probe Method as described in Algorithm 2 provides a complete reconstruction of the surface Γ above the compact set $Q \subset \mathbb{R}^2$ in the sense that for $h_\lambda \to 0$ we have convergence*

$$f_{rec,h_\lambda}(\tilde{x}) \to f(\tilde{x}), \;\; h_\lambda \to 0, \quad \tilde{x} \in Q. \tag{4.52}$$

Proof. Assume that $x = x_\lambda \in \Omega$ above Q. Then according to Lemma 4.4.3 the scattered field $U^s(x_\lambda, t)$ is zero for $t < T(x)$ and since $U^i(x,t)$ is zero for $t < T(x)$ the same is true for the total field.

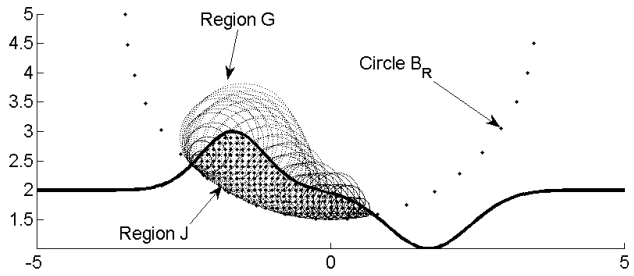

Figure 4.3: *We present the basic setup for the time-domain Probe Method. A time-dependent pulse at some time T is indicated by the dotted circle B_R. The pulse hits the surface and generates scattered pulses, here filling the region G. The basic idea of the time-domain Probe Method is to mark the points x on ∂B_R where the modulus of the time-domain scattered field $U^s(x,T)$ are positive in some set $(T, T+\epsilon)$ for some $\epsilon > 0$. All these points will then be on the unknown surface Γ. In two dimension we refer to [10] where $U^s(x,t)$ is reconstructed by the time-domain point source method. In this chapter we address the three-dimensional case and we will incorporate the potential method, which we presented in the previous chapter.*

Further, we want to show that $U^s(x,t)$ is zero even in a small neighbourhood $(T(x) - \epsilon, T(x)+\epsilon))$ of $T(x)$. We consider Figure 4.3, where the evolution of the field $U^s(x,t)$ is visualised. Let $R = T(x)$. Then, for $\varepsilon > 0$ we have that $U = U^i = 0$ for all $t < T(x)-\varepsilon$ and $x \in \mathbb{R}^3 \backslash B_R(z)$.

For any point $x \in \partial B_R(z)$ with $x \in \Omega$ the influence arising from the scattering of the incident pulse U^i on the rough surface needs some time $t > T(x)$ to reach the point x. This is due to the triangle inequality, which states that

$$|z - \tilde{x}| + |\tilde{x} - x| > |z - x| \tag{4.53}$$

for any point $\tilde{x} \in \overline{\Omega_f}$, and the propagation of the scattered field uniformly with the same wave speed $c = 1$ of the incident pulse. This proves that $\mu(\lambda) = 0$ for $x_\lambda \in \Omega$. Now, consider a point $x_\lambda \in \Gamma$. Then we know that the scattered field satisfies $U^s(x,t) = -U^i(x,t)$ and by definition of the first hitting time $T(x)$ we know that in some interval $(T(x), T(x)+\epsilon)$ we have $|U^i(x,t)| > 0$. This proves that $\mu(\lambda) = 1$ for this case. Finally, from both cases and the setup of the needle search which is starting with $\lambda = 0$ we obtain convergence of the time-domain Probe Method. □

4.5 Numerical study of the time-domain Probe Method

In this section we discuss the numerical realisation for the Probe Method. We have seen that the inverse Fourier transform of the solution of Problem 4.1.1 decays fast enough in κ, see (4.12), such that we can consider the truncation of the range of κ to a compact interval

$$\mathbb{K} = [-\kappa_{\max}, \kappa_{\max}] \tag{4.54}$$

for some maximal $\kappa_{\max} > 0$. We discretise the frequency interval $\mathbb{K}$ using a stepsize $h_\kappa = \kappa_{max}/N$ with $2N$ frequency points. Our frequency grid is thus given by

$$\kappa_n = n \cdot h_\kappa, \;\; n = -N, ..., N-1 \tag{4.55}$$

and we obtain a corresponding time grid by t_n by

$$t_n = n \cdot h_t, \;\; n = -N, ..., N-1 \tag{4.56}$$

with time-stepsize h_t. We use forward code developed by Heinemeyer, Lindner and Potthast [27] to calculate the scattered field in the time-domain $\boldsymbol{U}^s(x,t_n)$, $n=-N,...,N-1$, for a selection of grid points x in the measurement patch $\Gamma_{h,A}$.

We use an approximation of the incident pulse by choosing g as a truncated Gaussian function. In particular, we approximate U^i in the gridpoints t_n, $n=-N,...,N$ by

$$\boldsymbol{U}^i(x,t_n)=\frac{\sqrt{\pi}}{\sigma}\frac{1}{4\pi|x-z|}e^{-\frac{1}{4\sigma^2}(|x-y|-t_n)^2} \tag{4.57}$$

for $\|x\|_2<C$ for some truncation parameter $C>0$.

Simulations. We first present the relation between the scattering problems in time and frequency. The location of the point source for the simulation is $(-3,0,10)$ and we choose $\sigma=15$ for the Gaussian pulse density. We use forward code developed by Heinemeyer, Lindner and Potthast [27] to calculate the scattered field in the time-domain $\boldsymbol{U}^s(x,t_n)$, $n=-N,...,N-1$, for a selection of grid points x in the measurement patch $\Gamma_{h,A}$ at height $h=10$, where we used $A=5$. In Figure 4.4, we present a simulation where the unknown surface consists of a hill and a valley. We use frequencies from 0 to 6 with a stepsize $h=0.15$. In particular, we present a visualisation of the incident pulse in (a). The pictures (b), (c) and (d) show time slices of the scattered field at three different times t_1, ..., t_3. This confirms the arguments demonstrated in Figure 4.3.

Numerical examples. We choose $z=(0,0,13)$ as location of the point source and $\sigma=4$. For our numerical implementation we have realised a simplified version of the field reconstruction by a fixed choice of the auxiliary surface Γ^* below the unknown surface for the reconstruction of the scattered field u^s. We first calculate the frequency components by FFT from the time-domain measurements

$$\boldsymbol{u}^s(x,\kappa_n)=\mathcal{F}^{-1}(\boldsymbol{U}^s(x,\cdot))(\kappa_n)\,,\quad n=-N,...,N-1,\ x\in\Gamma_{h,A}\,. \tag{4.58}$$

Then, we reconstruct the scattered field $\boldsymbol{u}^s(x,\kappa_n)$ for $x\in\mathbb{Q}\subset\mathbb{R}^3$ where $\mathbb{Q}$ is a three-dimensional grid. For every fixed $x\in\mathbb{Q}$ we evaluate

$$\boldsymbol{U}^s(x,t_n)=\mathcal{F}(\boldsymbol{u}^s(x,\cdot))(t_n)\,. \tag{4.59}$$

The second part of the numerical implementation is the probing procedure. We chose some fixed constant $\epsilon=0.2$. For every point x in $\mathbb{Q}$ we evaluate the first hitting

time $T(x)$ and investigate $U^s(x,t)$ for $t \in J := (T(x), T(x) + \epsilon)$. We set $\mu(x) = 1$ for those points for which $|U^s(x,t)| > \rho$ in J, where ρ is some numerical threshold which we use to discriminate $U^s(x,t) = 0$ and $|U^s(x,t)| > 0$.

The points which are identified as boundary points by the time-domain Probe Method are visualised in Figure 4.6. In 4.6 (a) we show a slice plot along $x_2 = 0$. In 4.6 (b) we present a horizontal view onto the reconstructions which proves that the location and height of the hill and valley are correctly found. Finally, a complete reconstruction of the height function is visualised in Figure 4.5.

In Figure 4.7 we present an example for the reconstruction of a rough surface using the same setting as in the reconstruction before.

The numerical results confirm the feasibility of the time-domain Probe Method.

The reconstructions here are comparable to frequency-domain reconstructions for example by the point source method (c.f. [46], [44]) when we know and use the Dirichlet boundary condition. However, here we do not need to use this condition, so we are in a different setting where standard frequency-domain algorithms do not work. A comparison to methods like the *range test* or the *no-response test* (compare [46]) needs to be part of future research.

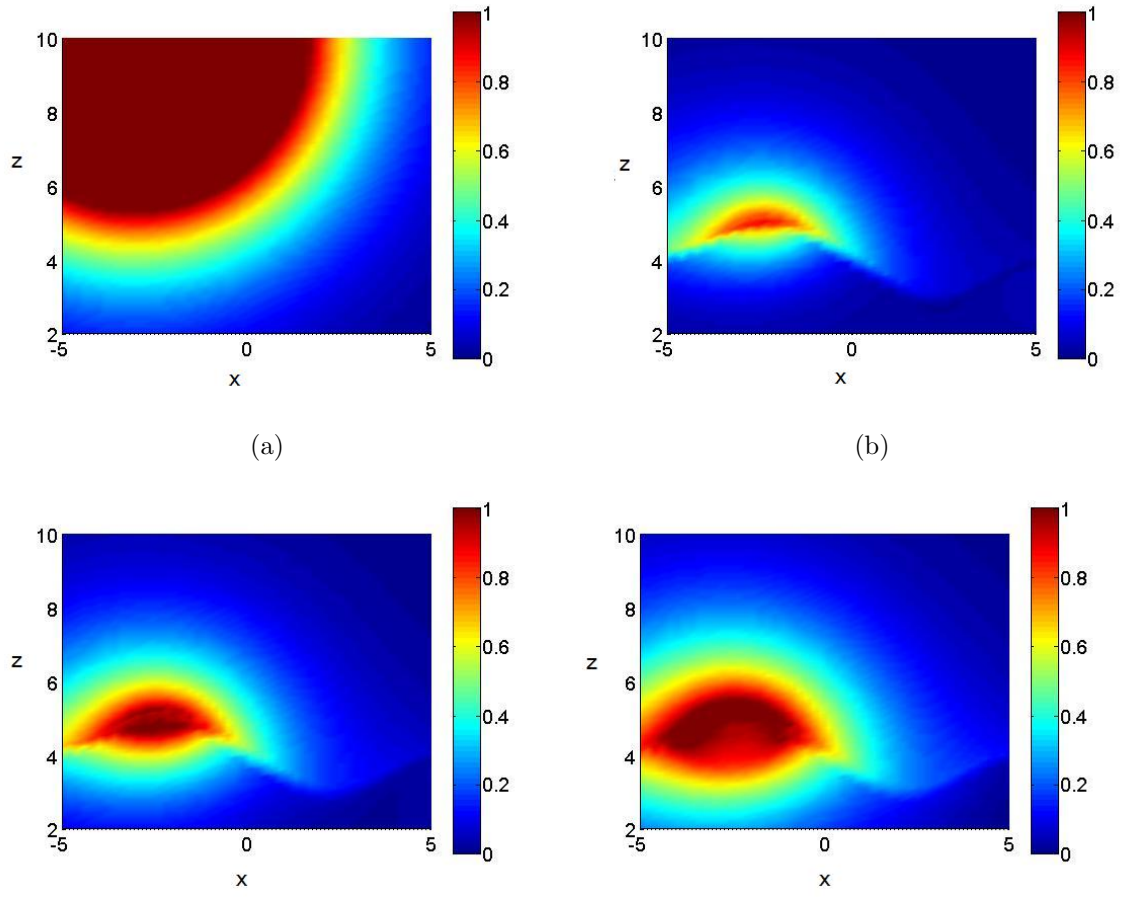

(a) (b)

(c) (d)

Figure 4.4: *Figure (a) shows the modulus of an incident pulse in the plane* $\{(x, y, z) \in \mathbb{R}^3 : y = 0\}$ *arising from a source located in* $z_0 = (-3, 0, 10)$ *at some time* t_1*, where we cut values with* $|U^s(x, t)| > 1$*. In (b) we show the modulus of the scattered field which is arising when the pulse is touching the scattering surface above* $(-3, 0)$*. The yellow color denotes some threshold of* $\rho = 0.6$ *which might be used to detect the surface. Figures (c) and (d) show the time-dependent scattered field at two later times* t_2 *and* t_3*. The intersection of the expanding yellow line from (a) with the yellow areas from the scattered field move along the unknown surface* Γ *and are used by the time-domain Probe Method to reconstruct* Γ*.*

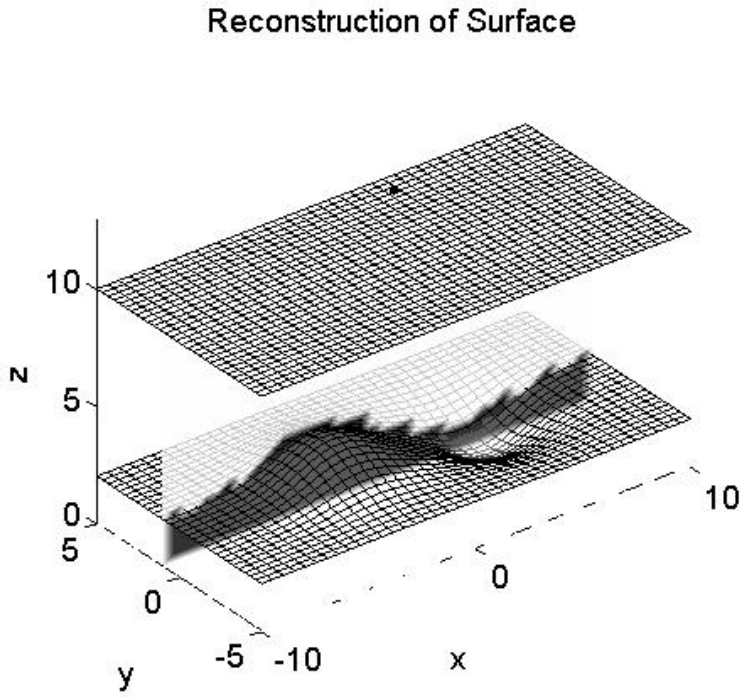

Figure 4.5: *We show a selection of points which are identified by the time-domain Probe Method as being on or below the unknown surface* Γ*. Here, we present reconstructions in one selected plane parallel to the* x_1*-*x_3 *plane. Measurements have been taken on the upper surface patch. The unknown surface is shown as a mesh, the points identified by the reconstruction method are colored black.*

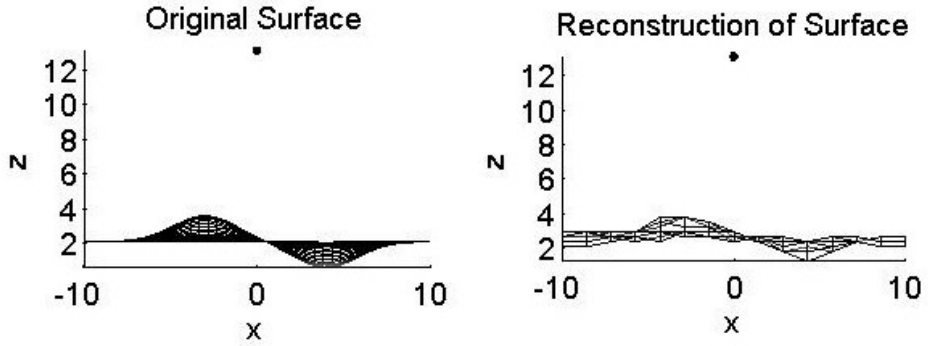

(a)

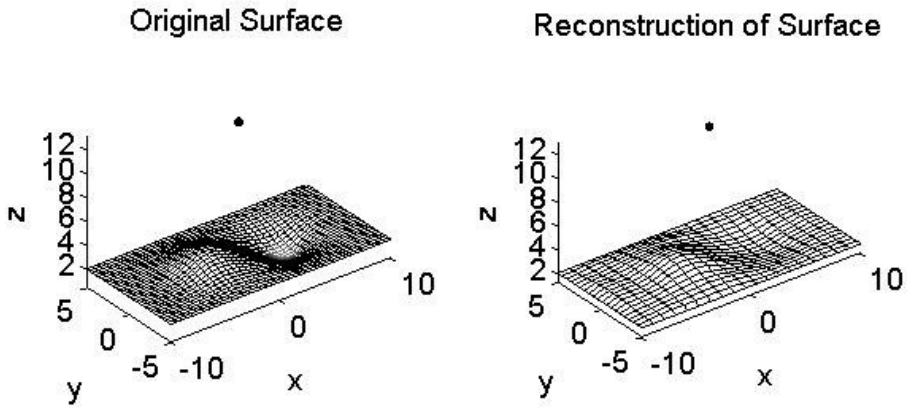

(b)

Figure 4.6: *Figure (a) shows a side view onto the original and the reconstructed surface, the hill and valley are correctly identified. In Figure (b) we demonstrate a complete reconstruction, where we applied some smoothing (convolution with a Gaussian kernel) before display of the reconstructed height function.*

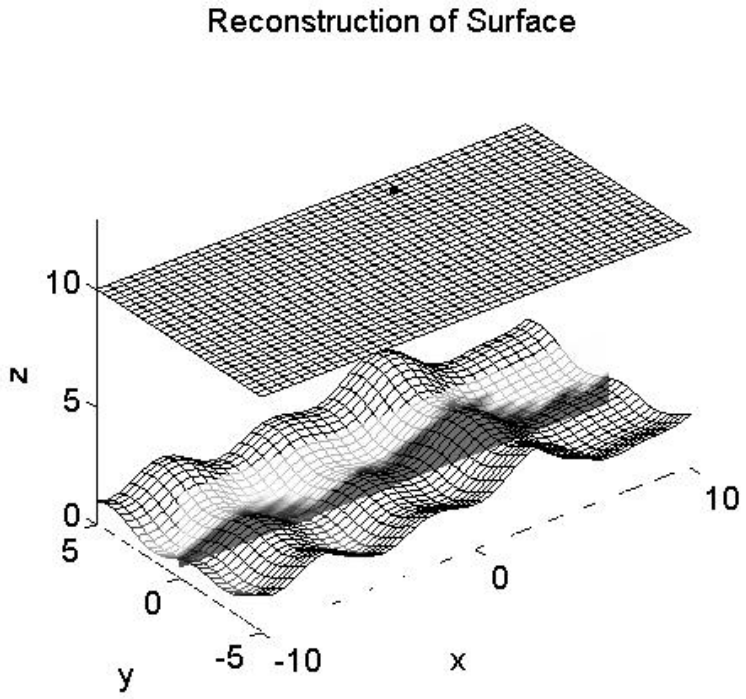

Figure 4.7: *In this example we present the reconstruction of a rough surface. As before, we show a selection of points which are identified by the time-domain Probe Method as being on or below the unknown surface* Γ*. Again, we present reconstructions in one selected plane parallel to the* x_1*-*x_3 *plane. Measurements have been taken on the upper surface patch. The unknown surface is shown as a mesh, the points identified by the reconstruction method are colored black.*

Part II

Anisotropic Electromagnetic Scattering

Chapter 5

Integral equation methods for scattering by three-dimensional anisotropic media

The goal of this part is to develop a numerical method for scattering of electromagnetic waves from an anisotropic inhomogeneous medium in three dimensions. We will employ an integral equation approach with a strongly singular volume integral equation system. Using the Fast Fourier Transform (FFT) we formulate a scheme which has compuational costs of $N \log(N)$ with the number of grid points of the three-dimensional grid given by N. In particular, we develop a numerical scheme for the strong singularity based on the FFT, which has high convergence order for smooth refractive indices.

This chapter is focused on the analysis of an *anisotropic* scattering problem. We first present a strongly singular integral equation system and provide the main results of uniqueness and existence shown in [43]. The proofs in [43] make use of a Fourier transform of the kernel and a related representation of the strongly singular operator. We provide a more detailed analysis of the representation of the strongly singular integral operator. In particular, we first investigate a Fourier transform based representation and then, based on these previous computations, we study a local representation of the strong singularity. This in turn will enable us to formulate a numerical scheme for the anisotropic scattering problem which deals with large amounts of unknowns.

5.1 Anisotropic scattering problem

Anisotropic materials are characterised by the property that the electrical excitations depend on the direction of the incoming electrical field. In particular, the refractive index is a mapping which maps every point in $\mathbb{R}^3$ onto a complex valued matrix, i.e. $x \in \mathbb{R}^3 \mapsto \mathbb{C}^{3\times 3}$. These materials could be interesting for the development for highly functionalised optical devices and we expect that they lead to scattering effects which cannot be obtained from isotropic materials. In [53], examples of dielectric *buried* grating microstructures are shown and we can imagine that also buried anisotropic grating structures could lead to similar or even more impressive scattering patterns.

5.1.1 Problem setting

The refractive index $N = N(x)$ is a complex 3×3 matrix given by

$$N(x) = \frac{1}{\epsilon_0}\left(\epsilon(x) + i\,\frac{\sigma(x)}{\omega}\right) \tag{5.1}$$

where $\epsilon = \epsilon(x)$ is the tensor of the electric permittivity and $\sigma = \sigma(x)$ is the tensor of the electric conductivity. The constant ϵ_0 is known as the dielectric constant of the vacuum and ω is the frequency of the electromagnetic wave.

We make the following assumptions about the refractive index.

(A1) The refractive index N is an at least twice continuously differentiable matrix function.

(A2) The support of the difference

$$M := I - N \tag{5.2}$$

is bounded in $\mathbb{R}^3$.

(A3) The refractive index N can be diagonalised with a unitary complex matrix U, i.e. N can be represented by $N(x) = U(x)N_D(x)U^*(x)$ with a diagonal matrix N_D and $U^*(x)U(x) = I$ for every $x \in \mathbb{R}^3$.

(A4) The real part of the diagonal elements of N_D are greater or equal to one.

(A5) The diagonal matrix N_D has positive semi-definite imaginary parts, i.e. $\sigma(x) \geq 0$.

These conditions are motivated from the isotropic case and are satisfied for a wide range of practical applications.

Problem 5.1.1. *Let $E^i, H^i \in H^{(1)}_{loc}(\mathbb{R}^3)$ be a solution of the Maxwell's equation for the background medium, i.e. E^i, H^i satisfy*

$$\nabla \times E^i - i\kappa H^i = 0, \tag{5.3}$$

$$\nabla \times H^i + i\kappa E^i = 0, \tag{5.4}$$

for a wavenumber $\kappa > 0$. Then, find a solution $E, H \in H^{(1)}_{loc}(\mathbb{R}^3)$ of

$$\nabla \times E - i\kappa H = 0, \tag{5.5}$$

$$\nabla \times H + i\kappa N(x) E = 0, \tag{5.6}$$

such that the scattered field E^s, H^s defined by

$$E = E^i + E^s, \tag{5.7}$$

$$H = H^i + H^s \tag{5.8}$$

satisfies the Silver-Müller radiation condition

$$\lim_{r\to\infty} H^s \times x - rE^s = 0 \tag{5.9}$$

uniformly for all directions $\hat{x} = x/|x|$ where $r = |x|$.

5.1.2 Main results

In this section we summarise the results obtained by Potthast, [42], for the anisotropic scattering problem. We start with an integral equation formulation and present uniqueness and existence. The proofs of the theorems can be found in [42] and in [44].

THEOREM 5.1.2. *Let $E, H \in H^1_{loc}(\mathbb{R}^3)$ be a solution of Problem 5.1.1. Then, E satisfies the volume-integral equation*

$$\begin{aligned} E(x) &+ \nabla \int_\Omega \nabla_x \Phi(x,y) \cdot (ME)(y)\, dy \\ &+ \kappa^2 \int_\Omega \Phi(x,y)(ME)(y)\, dy = E^i(x) \text{ for } x \in \mathbb{R}^3, \end{aligned} \tag{5.10}$$

for $\Omega \subset \mathbb{R}^3$, which contains the support of M and where $N = I - M$ satisfies the assumptions (A1) – (A5).

This integral equation can be reformulated as an integral equation system on the L^2-vector field $v := ME$. In particular, $v \in (L^2(\mathbb{C}^3))^3$ where $(L^2(\mathbb{C}^3))^3$ is the L^2-space with norm

$$\|v\| := \left(\sum_{i=1}^{3} \left\| v^{(i)} \right\|^2_{L^2(\mathbb{C})} \right)^{1/2}, \tag{5.11}$$

which is induced by the scalar product

$$\langle v, u \rangle = \sum_{i=1}^{3} \left\langle v^{(i)}, u^{(i)} \right\rangle_{L^2(\mathbb{C})}. \tag{5.12}$$

We define the multiplication operator $\mathcal{M}$ by

$$\mathcal{M} := M(I - \frac{1}{3}M)^{-1}. \tag{5.13}$$

With the assumptions (A1), (A2), (A3) and (A4), $\mathcal{M}$ is well-defined. Using the jump relation, see [44],

$$\begin{aligned} &\nabla \int_{\mathbb{R}^3} \nabla_x \Phi(x,y) \cdot (ME)(y)\, dy \\ &\quad = \int_{\mathbb{R}^3} \nabla \left(\nabla_x \cdot \{\Phi(x,y)(ME)(y)\} \right) dy - \frac{1}{3}(ME)(x) \end{aligned} \tag{5.14}$$

for L^2-densities, we obtain that $v = (v^{(1)}, v^{(2)}, v^{(3)})^T = (ME)$ solves the integral equation

$$\begin{aligned} v(x) \;&+\; \mathcal{M}(x) T_0 v(x) \\ &+\; \mathcal{M}(x)(T - T_0)v(x) + \kappa^2 \mathcal{M}(x) T_1 v(x) = \mathcal{M}(x) E^i(x), \quad x \in \mathbb{R}^3, \end{aligned} \tag{5.15}$$

where we have set

$$Tv(x) := \int_\Omega \nabla_x (\nabla_x \cdot \{\Phi(x,y)v(y)\})\, dy, \tag{5.16}$$

$$T_0 v(x) := \int_\Omega \nabla_x (\nabla_x \cdot \{\Phi_0(x,y)v(y)\})\, dy, \tag{5.17}$$

$$T_1 v(x) := \int_\Omega \Phi(x,y) v(y) dy. \tag{5.18}$$

Here, Φ_0 is the fundamental solution for the Laplace operator ($\kappa = 0$) in three dimensions, i.e.

$$\Phi_0(x,y) := \frac{1}{4\pi} \frac{1}{|x-y|^3}. \tag{5.19}$$

We recall that the kernel of the operator T and T_0 is a matrix of strongly singular functions, the integral is defined in the sense of a Cauchy principal value for Hölder-continuous vector fields and for L^2-vector fields by extending the operator, see [43].

In particular, we have that the kernel of T_0 is given by

$$k_0(x,y) = \frac{1}{4\pi} \begin{bmatrix} \frac{3(x_1-y_1)^2}{|x-y|^5} - \frac{1}{|x-y|^3} & \frac{3(x_1-y_1)(x_2-y_2)}{|x-y|^5} & \frac{3(x_1-y_1)(x_3-y_3)}{|x-y|^5} \\ \frac{3(x_2-y_2)(x_1-y_1)}{|x-y|^5} & \frac{3(x_2-y_2)^2}{|x-y|^5} - \frac{1}{|x-y|^3} & \frac{3(x_2-y_2)(x_3-y_3)}{|x-y|^5} \\ \frac{3(x_3-y_3)(x_1-y_1)}{|x-y|^5} & \frac{3(x_3-y_3)(x_2-y_2)}{|x-y|^5} & \frac{3(x_3-y_3)^2}{|x-y|^5} - \frac{1}{|x-y|^3} \end{bmatrix}. \tag{5.20}$$

The j-th component of $T - T_0$ is given by

$$((T-T_0)v(x))^{(j)} = \int_\Omega \frac{\partial}{\partial x_j} \sum_{k=1}^{3} \frac{\partial}{\partial x_k} \frac{1}{4\pi} \frac{1}{|x-y|} (e^{i\kappa|x-y|} - 1) v^{(k)}(y)\, dy, \tag{5.21}$$

where we recall that $v^{(k)}$ denotes the k-th component of v. Differentiation shows that

$$\begin{aligned} ((T-T_0)v(x))^{(j)} = \int_\Omega \Big(\sum_{k=1}^{3} \{ & \delta_{jk} \frac{1}{|x-y|^3} + \delta_{jk} \frac{i\kappa e^{i\kappa|x-y|}}{|x-y|^2} - \delta_{jk} \frac{e^{i\kappa|x-y|}}{|x-y|^3} \\ & -3\frac{(x_j-y_j)(x_k-y_k)}{|x-y|^5} - 3\frac{i\kappa(x_j-y_j)(x_k-y_k)e^{i\kappa|x-y|}}{|x-y|^4} \\ & +3\frac{(x_j-y_j)(x_k-y_k)e^{i\kappa|x-y|}}{|x-y|^5} \\ & -\frac{(x_j-y_j)(x_k-y_k)\kappa^2 e^{i\kappa|x-y|}}{|x-y|^3} \} \, v^{(k)}(y) \Big)^{(j)} dy, \end{aligned} \tag{5.22}$$

where δ_{ik} denotes the Kronecker delta. With Taylor series representation of the exponential function we see that the strongly singular parts cancel out and, noting that also $|(x_j-y_j)(x_k-y_k)| \le |x-y|^2$, $j,k = 1,2,3$, we find that $T - T_0$ is weakly singular. The same is true for the weakly singular operator T_1. Solvability and uniqueness for the strongly singular system of integral equations, (5.15), has been shown in [42] for $\mathcal{M} \in C_0^{\ell+1}(\mathbb{R}^3)$, $\ell \ge 2$.

THEOREM 5.1.3 (Uniqueness). *Assume that $M = I - N \in C_0^3(\mathbb{R}^3)$ is semi-coercive, i.e. for every $x \in \mathbb{R}^3$ we have that*

$$Im(a \cdot \overline{M(x)a}) \ge \gamma(x)|a|^2 \tag{5.23}$$

for every $a \in \mathbb{C}^3$ where $\gamma \ge 0$. Furthermore, we assume that N is elliptic, i.e. $a \cdot Na \ne 0$, $a \in \mathbb{R}^3$. Then, the anisotropic scattering problem Problem 5.1.1 has at most one solution.

For a matrix N, which satisfies the assumptions (A1) to (A5), the matrix M is semi-coercive, and N is elliptic.

THEOREM 5.1.4 (Existence). *Assume that $\mathcal{M} \in C_0^{\ell+1}(\Omega), \ell \geq 2$. Then, the scattering problem Problem 5.1.1 has one and only one solution $E, H \in H^1_{loc}(\mathbb{R}^3)$ and the field depends continuously on the incident field E^i and H^i.*

5.2 A Fourier representation for the strongly singular operator

In the following section we discuss another analytical representation of the strongly singular (matrix) integral operator $\mathcal{M}T_0$. This representation involves the Fourier transform and enables us to formulate a numerical interpolation scheme.

5.2.1 The symbol for specific singular kernels

In a first step, we consider the Fourier transform of

$$K_s(x-y) := \frac{1}{|x-y|^3} Y_n^{(k)}(\theta, \varphi), \tag{5.24}$$

for the spherical harmonic function $Y_n^{(k)}$ of degree n and order k and where θ and φ are the angles of the spherical coordinates for $y - x \in \mathbb{R}^3$ given by

$$y - x = r(\cos\varphi \sin\theta, \sin\varphi \sin\theta, \cos\theta). \tag{5.25}$$

We will see that the kernel of the strongly singular integral operator T_0 has a (matrix) kernel with components of the form (5.24). We note that in [40] the Fourier transform of (5.24) in higher dimensions is discussed and large parts of this section can be found therein.

Let $\hat{y} := \frac{y}{|y|}$ and $\xi \in \mathbb{R}^3 \backslash \{0\}$. In spherical coordinates, $\hat{y}$ is given by

$$\hat{y} = (\cos\varphi \sin\theta, \sin\varphi \sin\theta, \cos\theta)$$

and we identify the spherical harmonic $Y_n^{(k)}(\vartheta,\varphi)$ with $Y_n^{(k)}(\hat{y})$. We have for S being the unit sphere in three dimensions that

$$\begin{aligned}
(\mathcal{F}K_s(\cdot))(\xi) &= \lim_{\varepsilon\to 0,\, R\to\infty} \int_\varepsilon^R \frac{1}{|y|^3} \int_S Y_n^{(k)}(-\hat{y}) e^{-i|\xi||y|\,\hat{\xi}\cdot\hat{y}}\, d\hat{y}\, d|y| && (5.26)\\
&= \lim_{\varepsilon\to 0,\, R\to\infty} \int_\varepsilon^R \frac{1}{r^3} \int_0^{2\pi}\int_0^{\pi} Y_n^{(k)}(\pi+\theta,\pi+\varphi) \\
&\qquad e^{-i|\xi| r\hat{\xi}\cdot(\cos\varphi\sin\theta,\sin\varphi\sin\theta,\cos\theta)} r^2\sin\theta\, d\theta\, d\varphi\, dr && (5.27)\\
&= \lim_{\varepsilon\to 0,\, R\to\infty} \int_\varepsilon^R \frac{1}{r} \int_0^{2\pi}\int_0^{\pi} Y_n^{(k)}(\pi+\theta,\pi+\varphi) \\
&\qquad e^{-i|\xi|\hat{\xi}\cdot r\hat{y}} \sin\theta\, d\theta\, d\varphi\, dr. && (5.28)
\end{aligned}$$

We use the Funk-Hecke formula (see [17] and [40], page 250), which is given by

$$\int_S Y_n^{(k)}(\hat{y}) e^{ir\hat{\xi}\hat{y}}\, d\hat{y} = \frac{4\pi}{i^n} Y_n^{(k)}(\hat{\xi}) j_n(r). \tag{5.29}$$

Here, j_n is the spherical Bessel function of the first kind, which is related to the Bessel function J_n via

$$j_n(r) = \pi^{\frac{1}{2}} 2^{-\frac{1}{2}} r^{-\frac{1}{2}} J_{n+\frac{1}{2}}(r). \tag{5.30}$$

We have

$$\int_S Y_n^{(k)}(-\hat{y}) e^{-ir\hat{\xi}\hat{y}}\, d\hat{y} = r^{-\frac{1}{2}} (2\pi)^{\frac{3}{2}} i^n J_{n+\frac{1}{2}}(r)\, Y_n^{(k)}(\hat{\xi}), \tag{5.31}$$

and by substituting r by $|\xi| r$ we obtain

$$\begin{aligned}
(\mathcal{F}K_s(\cdot))(\xi) &= \lim_{\varepsilon\to 0,\, R\to\infty} \int_{|\xi|\varepsilon}^{|\xi|R} \frac{1}{r} \int_0^{2\pi}\int_0^{\pi} Y_n^{(k)}(-\hat{y}) e^{-ir\hat{\xi}\cdot\hat{y}} \sin\theta\, d\theta d\varphi dr \\
&= \lim_{\varepsilon\to 0,\, R\to\infty} \int_{|\xi|\varepsilon}^{|\xi|R} \frac{1}{r} \left(r^{-\frac{1}{2}} (2\pi)^{\frac{3}{2}} i^n J_{n+\frac{1}{2}}(r) \right) Y_n^{(k)}(\hat{\xi})\, dr && (5.32)\\
&= (2\pi)^{\frac{3}{2}} i^n Y_n^{(k)}(\hat{\xi}) \lim_{\varepsilon\to 0,\, R\to\infty} \int_{|\xi|\varepsilon}^{|\xi|R} \left(r^{-\frac{3}{2}} J_{n+\frac{1}{2}}(r) \right) dr && (5.33)\\
&= \gamma_n\, Y_n^{(k)}\!\left(\frac{\xi}{|\xi|}\right), && (5.34)
\end{aligned}$$

for

$$\gamma_n := \frac{i^n \pi^{\frac{3}{2}} \Gamma(n/2)}{\Gamma((3+n)/2)}, \tag{5.35}$$

where Γ denotes the Gamma function. In the last step we used the formula

$$\int_0^\infty r^{-m/2} J_{\frac{m}{2}+n-1}(r)\, dr = \frac{\Gamma(n/2)}{2^{m/2}\Gamma((n+m)/2)}, \tag{5.36}$$

for m being the space dimension. For $\xi \equiv 0$ the above calculations for the symbol cannot be done. We have, see Theorem 1.1 on page 221 in [40], that

$$(\mathcal{F}K_s(\cdot))(0) = \lim_{\varepsilon \to 0,\, R \to \infty} \int_\varepsilon^R \frac{1}{|y|^3} \int_S Y_n^{(k)}(-\hat{y})\, dy \tag{5.37}$$

$$= 0. \tag{5.38}$$

The Fourier transform of a strongly singular kernel is also denoted by the *symbol* of the integral operator. In particular, the *symbol* of a strongly singular integral operator

$$Kv(x) := \int_{\mathbb{R}^3} k(x,y)v(y)\, dy \tag{5.39}$$

with kernel

$$k(x,y) := \frac{f(x,\vartheta,\varphi)}{|x-y|^3}$$

where ϑ, φ are given by the spherical coordinates of $(y-x)$, is formally defined by the Fourier transform of the kernel and denoted by

$$\hat{K}(\xi) = \mathcal{F}k(\xi) \text{ for } \xi \neq 0, \tag{5.40}$$

and $\hat{K}(0) = 0$. The function f is also denoted by *characteristic function* of the strongly singular integral operator. For a detailed discussion of the symbol we refer to [40].

5.2.2 A symbol representation of the strongly singular operator

In this section we consider the strongly singular operator T_0. We rewrite the kernel k_0 of T_0 in spherical coordinates. To this end, let $x - y = r(\cos\varphi \sin\vartheta, \sin\varphi \sin\vartheta, \cos\vartheta)$. Then, we have

$$k_0(\varphi,\vartheta) = \frac{1}{4\pi r^3}\mathcal{K}(\vartheta,\varphi) \tag{5.41}$$

with

$$\mathcal{K}(\vartheta,\varphi) := \begin{bmatrix} 3\cos^2\varphi\sin^2\vartheta - 1 & 3\cos\varphi\sin^2\vartheta\sin\varphi & 3\cos\varphi\sin\vartheta\cos\vartheta \\ 3\cos\varphi\sin^2\vartheta\sin\varphi & 3\sin^2\varphi\sin^2\vartheta - 1 & 3\sin\varphi\sin\vartheta\cos\vartheta \\ 3\cos\varphi\sin\vartheta\cos\vartheta & 3\sin\varphi\sin\vartheta\cos\vartheta & 3\cos^2\vartheta - 1 \end{bmatrix}. \tag{5.42}$$

Every component of k_0 consists of spherical harmonics of order 2. In particular, we obtain from

$$\begin{aligned}\mathcal{K}_{11}(\vartheta,\varphi)+\mathcal{K}_{22}(\vartheta,\varphi) &= -(3\cos^2\vartheta-1) = -\mathcal{K}_{33}(\vartheta,\varphi) = -Y_2^{(0)}(\vartheta,\varphi) \text{ and}\\ \mathcal{K}_{11}(\vartheta,\varphi)-\mathcal{K}_{22}(\vartheta,\varphi) &= 3\sin^2\vartheta\,(1-2\sin^2\varphi) = \frac{1}{2}\left(Y_2^{(2)}(\vartheta,\varphi)+Y_2^{(2)}(\vartheta,\varphi)\right),\end{aligned}$$

that

$$\mathcal{K}_{11}(\vartheta,\varphi) = \frac{1}{4}\left(Y_2^{(2)}(\vartheta,\varphi)+Y_2^{(-2)}(\vartheta,\varphi)\right)-\frac{1}{2}Y_2^{(0)}(\vartheta,\varphi) \tag{5.43}$$

$$\mathcal{K}_{22}(\vartheta,\varphi) = -\frac{1}{4}\left(Y_2^{(2)}(\vartheta,\varphi)+Y_2^{(-2)}(\vartheta,\varphi)\right)-\frac{1}{2}Y_2^{(0)}(\vartheta,\varphi). \tag{5.44}$$

With similar computations to those above we obtain

$$\mathcal{K}_{12}(\vartheta,\varphi) = \mathcal{K}_{21}(\vartheta,\varphi) = \frac{1}{4i}\left(Y_2^{(2)}(\vartheta,\varphi)-Y_2^{(-2)}(\vartheta,\varphi)\right), \tag{5.45}$$

$$\mathcal{K}_{13}(\vartheta,\varphi) = \mathcal{K}_{31}(\vartheta,\varphi) = \frac{1}{2}\left(Y_2^{(1)}(\vartheta,\varphi)+Y_2^{(-1)}(\vartheta,\varphi)\right), \tag{5.46}$$

$$\mathcal{K}_{23}(\vartheta,\varphi) = \mathcal{K}_{32}(\vartheta,\varphi) = \frac{1}{2i}\left(Y_2^{(1)}(\vartheta,\varphi)-Y_2^{(-1)}(\vartheta,\varphi)\right). \tag{5.47}$$

We first consider the strongly singular matrix operator A, given by

$$Au(x) = \int_{\mathbb{R}^3} K(x,x-y)u(y)\,dy = \int_{\mathbb{R}^3}\frac{f(x,\theta)}{r^3}u(y)\,dy \text{ for } x\in\mathbb{R}^3, \tag{5.48}$$

where the characteristic function f can be expressed in a series with respect to spherical harmonics

$$f(x,\theta) = \sum_{n=1}^{\infty}\sum_{k=-n}^{n} a_n^{(k)}(x)Y_n^{(k)}(\theta), \quad \theta\in\mathbb{R}^3. \tag{5.49}$$

From [40], page 251, we have that the symbol of A is given by the expansion

$$\hat{A}(x,\psi) = \sum_{n=1}^{\infty}\sum_{k=-n}^{n}\gamma_n a_n^{(k)}(x)Y_n^{(k)}(\psi)\,, \tag{5.50}$$

where $\psi := \frac{\theta}{|\theta|}$ and γ_n given by (5.35).

The symbol of a strongly singular matrix operator is then defined by the matrix of symbols and we obtain that every component of the operator $\mathcal{M}T_0$ possesses a similar representation to (5.49). In particular, there exist functions $a^{(-2)}, a^{(-1)}, ..., a^{(2)} \in C^3(\mathbb{R}^3)$ such that $\mathcal{M}(x)k_0(\varphi,\theta)$ can be represented by

$$(\mathcal{M}k_0(\varphi,\theta))_{ij} = \frac{1}{4\pi r^3}\sum_{k=-2}^{2} a^{(k)}(x)\,Y_2^k(\varphi,\theta)\,. \tag{5.51}$$

We derive from this and the above computations, that the matrix operator $\mathcal{M}T_0$ possesses the symbol

$$\mathcal{M}(x)\widehat{(T_0)}(\xi) = -\frac{1}{3}\mathcal{M}(x)\,\mathcal{K}(\xi) \tag{5.52}$$

for ξ with spherical coordinates $|\xi|(\cos\varphi\sin\vartheta, \sin\varphi\sin\vartheta, \cos\vartheta)$. In cartesian coordinates we see that the symbol matrix can be rewritten as

$$\mathcal{K}(\xi) = \begin{bmatrix} \frac{3\xi_1^2}{|\xi|^2} - 1 & \frac{3\xi_1\xi_2}{|\xi|^2} & \frac{3\xi_1\xi_3}{|\xi|^2} \\ \frac{3\xi_2\xi_1}{|\xi|^2} & \frac{3\xi_2^2}{|\xi|^2} - 1 & \frac{3\xi_2\xi_3}{|\xi|^2} \\ \frac{3\xi_3\xi_1}{|\xi|^2} & \frac{3\xi_3\xi_2}{|\xi|^2} & \frac{3\xi_3^2}{|\xi|^2} - 1 \end{bmatrix}. \tag{5.53}$$

Hence, an analytical expression for the Fourier transform of the matrix kernel $\mathcal{M}k_0$ is given and it holds that

$$\begin{aligned} \mathcal{M}(x)\mathcal{F}(T_0 v)(\xi) &= \mathcal{M}(x)\widehat{(T_0)}(\xi)(\mathcal{F}v)(\xi) \\ &= -\frac{1}{3}\mathcal{M}(x)\,\mathcal{K}(\xi). \end{aligned} \tag{5.54}$$

We can now express the strongly singular matrix operator $\mathcal{M}T_0$ by

$$\begin{aligned} (\mathcal{M}T_0)v(x) &= -\frac{1}{3}\mathcal{M}(x)\mathcal{F}^{-1}\left(\mathcal{K}(\cdot)\mathcal{F}v(\cdot)\right)(x) \\ &= -\frac{1}{3}\mathcal{M}(x)\int_{\mathbb{R}^3}\mathcal{K}(z)\int_{\mathbb{R}^3} v(s)e^{isz}ds\,e^{-ixz}\,dz\,. \end{aligned} \tag{5.55}$$

To model optical variable security devices, we need to discuss the numerical solution of the anisotropic scattering problem. There are several issues to be overcome. One of these is the numerical evaluation of the strongly singular integral operator T_0. Also, due to the large number of unknowns related to the electromagnetic problem setting, we need an operator approximation which can be done in a fast way. For example, a direct discretisation of a volume integral operator for a grid of $10\times10\times10$ points would lead to a matrix of size 3000×3000. So far, we have seen that the strong singularity can be integrated via Fourier methods. Nevertheless, for the numerical evaluation of (5.55) we see that a truncation of the integrals over $\mathbb{R}^3$ is needed. That this is possible is part of the next sections. In particular, we will study a local representation of the strong singularity and formulate a numerical integration scheme for every $x \in \Omega$.

5.3 Three-dimensional Fourier analysis for multi-periodic functions

In this section we give a brief review of the classical Fourier analysis extended to multi-periodic functions. The case of multi-periodic functions is also presented in [26] for higher dimensions.

Let $v : \mathbb{R}^3 \to \mathbb{C}^3$ be p-periodic which means that there exists $p = (p_1, p_2, p_3) \in \mathbb{R}^3$ with $p_1, p_2, p_3 > 0$ such that for every component $v^{(k)}$ of v, $k = 1, 2, 3$, we have

$$v^{(k)}(x) = v^{(k)}(x + p_j \boldsymbol{e}_j), \quad j = 1, 2, 3, \text{ for all } x \in \mathbb{R}^3, \tag{5.56}$$

where $\boldsymbol{e}_j$ denotes the unit vector in direction x_j. We further assume that

$$\int_{[0,p_1]\times[0,p_2]\times[0,p_3]} |v^{(k)}(x)|^2 \, dx < \infty, \quad k = 1, 2, 3. \tag{5.57}$$

and write $[0, p]$ as a shorthand for $[0, p_1] \times [0, p_2] \times [0, p_3]$. We restrict our consideration to one component of v and suppress the exponent of $v^{(j)}$ in the following pages.

The space of all p-periodic functions $v : \mathbb{R}^3 \to \mathbb{C}$ which satisfy (5.57) is denoted by $(L^2([0, p]))$ and we denote that any function in $L^2([0, p])$ is uniquely determined by its values on $[0, p]$. We are now able to transfer the results from the classical Fourier analysis to the multi-dimensional space.

The space $L^2([0, p])$ is a Hilbert space with norm introduced by the scalar product defined by

$$\langle u, v \rangle := \int_{[0,p]} u(x) \, \overline{v(x)} \, dx. \tag{5.58}$$

We use the notation

$$\frac{1}{p} x := \left(\frac{x_1}{p_1}, \frac{x_2}{p_2}, \frac{x_3}{p_3}\right)$$

for $x \in \mathbb{R}^3$, and define the trigonometric monomials by

$$f_m(x) := e^{i \frac{2\pi}{p} m \cdot x}, \quad x \in \mathbb{R}^3, m \in \mathbb{Z}^3. \tag{5.59}$$

It holds that $\langle f_n, f_m \rangle = \delta_{mn}$, where $\delta_{mn} = 1$ if $n = m$ and zero otherwise, is the Kronecker symbol. Thus, the set $\{f_m : m \in \mathbb{Z}^3\}$ is an orthogonal system on $L^2([0, p])$.

Moreover, we note that the orthogonal system is complete, i.e. the *Fourier series* for a function $u \in L^2([0,p])$ given by

$$\sum_{m\in\mathbb{Z}^3} \hat{u}_m f_m(x) \tag{5.60}$$

with *Fourier coefficients*

$$\hat{u}_m = \frac{1}{p_1 p_2 p_3} \int_{[0,p]} u(x) e^{-2\pi i (m\cdot\frac{1}{p}x)}\, dx \text{ for } m \in \mathbb{Z}^3\,, \tag{5.61}$$

converges in the mean square norm to u,

$$\left\| \sum_{m\in\mathbb{Z}^3 : \|m\|_1 < N} \hat{u}_m f_m - u \right\|_{L^2([0,p])} \longrightarrow 0 \text{ for } N \to \infty. \tag{5.62}$$

We define the mapping, which maps $u \mapsto (\hat{u}_m)_{m\in\mathbb{Z}^3}$ by $\mathcal{F}_p$. By *Parseval's theorem* we have that

$$\langle u, v\rangle = \sum_{m\in\mathbb{Z}^3}\sum_{n\in\mathbb{Z}^3} \hat{u}_m \overline{\hat{v}_n} \langle f_n, f_m\rangle = \sum_{n\in\mathbb{Z}^3} \hat{u}_n \overline{\hat{v}_n} \tag{5.63}$$

and we see, inserting $u = v$ in the last equation, that

$$\|u\|_{L^2([0,p])} = \|\mathcal{F}_p u\|_{\ell^2(\mathbb{Z}^3)}\,,$$

i.e. $\mathcal{F}_p$ is a unitary operator and, thus, possesses a bounded inverse. The inverse operator $\mathcal{F}_p^{-1}$ maps a sequence $(u_m)_m \in \ell^2(\mathbb{Z}^3)$ onto $\sum_{m\in\mathbb{Z}^3} u_m f_m$ and we find that

$$u = \mathcal{F}_p^{-1}(\hat{u}_m)_m = \sum_{m\in\mathbb{Z}^3} \hat{u} f_m. \tag{5.64}$$

THEOREM 5.3.1 (Convolution theorem for multi-periodic functions). *Let $u, v \in L^2([0,p])$. Then, it holds that every Fourier coefficient of the convolution $u*v$ is given by the product of the Fourier coefficient of u with v,*

$$\widehat{(u*v)}_m = \hat{u}_m \cdot \hat{v}_m, \quad m \in \mathbb{Z}^3. \tag{5.65}$$

Proof. We follow the same arguments as in [26], Theorem 4.3, to find that

$$\begin{aligned}(u*v)(x) &= \int_{[0,p]} \left(\sum_{n\in\mathbb{Z}^3} \hat{u}_n e^{i\frac{2\pi}{p}n\cdot(x-y)}\right)\left(\sum_{m\in\mathbb{Z}^3} \hat{v}_m e^{i\frac{2\pi}{p}m\cdot(y)}\right) dy \\ &= \sum_{n,m\in\mathbb{Z}^3} \hat{u}_n\hat{v}_m \int_{[0,p]} e^{i\frac{2\pi}{p}m\cdot(y)+i\frac{2\pi}{p}n\cdot(x-y)}\, dy \\ &= \frac{1}{p_1p_2p_3}\sum_{m\in\mathbb{Z}^3} \hat{u}_m\hat{v}_m e^{i\frac{2\pi}{p}m\cdot x} \\ &= \frac{1}{p_1p_2p_3}\mathcal{F}_p^{-1}(a_m)_m(x). \end{aligned} \tag{5.66}$$

where the elemts of the sequence (a_m) are given by $a_m := \hat{u}_m\hat{v}_m$. We conclude $\widehat{(u*v)}_m = \hat{u}_m\hat{v}_m$ which was the assertion of the theorem. □

For $N = (N_1, N_2, N_3) \in \mathbb{N}^3$ we define

$$\mathcal{Z} := \{-N_1, ..., N_1 - 1\} \times \{-N_2, ..., N_2 - 1\} \times \{-N_3, ..., N_3 - 1\}. \tag{5.67}$$

Then, using a rectangular quadrature rule with an equidistant grid for the discretisation of the cube $[0, p]$ with $2N_\ell$ grid points in x_ℓ–direction, $\ell = 1, 2, 3$, i.e. the grid points are given by

$$x_j = (x_1^{(j_1)}, x_2^{(j_2)}, x_3^{(j_3)}), \quad j \in \mathcal{Z}, \tag{5.68}$$

with

$$x_\ell^{(j_\ell)} := j_\ell \frac{p_\ell}{2N_\ell}, \quad \ell = 1, 2, 3, \tag{5.69}$$

we find that

$$\begin{aligned}\hat{u}_m &\approx \frac{1}{p_1p_2p_3}\left(\frac{p_1}{2N_1}\,\frac{p_2}{2N_2}\,\frac{p_3}{2N_3}\right) \\ &\qquad \sum_{j_1=-N_1}^{N_1-1}\sum_{j_2=-N_2}^{N_2-1}\sum_{j_3=-N_3}^{N_3-1} u(x_1^{(j_1)}, x_2^{(j_2)}, x_3^{(j_3)}) e^{-i\frac{2\pi}{p}m\cdot x_j} \\ &= \frac{1}{\#N}\sum_{j\in\mathcal{Z}} u(x_j)e^{-i\frac{2\pi}{p}m\cdot x_j} =: \tilde{u}_m, \end{aligned} \tag{5.70}$$

where $\#N := 2^3N_1N_2N_3$. The coefficients $\tilde{u}_m$ are called 3-dimensional *discrete Fourier coefficients* of u. Using that

$$x_j = \left(\frac{p_1}{2N_1}j_1, \frac{p_2}{2N_2}j_2, \frac{p_1}{2N_3}j_3\right) \tag{5.71}$$

the discrete Fourier coefficients reduce to

$$\tilde{u}_m = \frac{1}{\#N} \sum_{j \in \mathcal{Z}} u(x_j) e^{-i \frac{2\pi}{2N} m \cdot j}, \quad m \in \mathbb{Z}^3. \tag{5.72}$$

The (uniquely determined) solution of the trigonometric interpolation problem for p-periodic u,

$$u_N(x_j) = u(x_j) \tag{5.73}$$

for $j \in \mathcal{Z}$ and for equidistant grid points $(x_j) \in [0, p]$, is given by the *trigonometric interpolation polynomial*

$$u_N(x) = \sum_{j \in \mathcal{Z}} \tilde{u}_j e^{i \frac{2\pi}{p} j \cdot x}, \quad x \in [0, p]. \tag{5.74}$$

Thus, we can view the trigonometric interpolation polynomial as a discretised version of the Fourier series. We call $(\tilde{u}_m)_{m \in \mathcal{Z}}$ the *discrete Fourier transform* of u, and u_N the *inverse discrete Fourier transform*. We note that

$$u_{N,\ell} := u_N(x_\ell) = \sum_{j \in \mathcal{Z}} \tilde{u}_j e^{i \frac{2\pi}{2N} j \cdot \ell}, \quad \ell \in \mathcal{Z}. \tag{5.75}$$

A fast evaluation of the *discrete Fourier transform* can be achieved via the *Fast Fourier Transform* which reduces the computational cost significantly from $O(N^2)$ to $O(N \log N)$ steps where N is the total number of unknowns. The basic idea of the *Fast Fourier Algorithm*, which dates back to Johann Friedrich Gauss and which is attributed to Cooley and Tukey (1965), is to split the one-dimensional discrete Fourier coefficient

$$\tilde{v}_k = \frac{1}{2n} \sum_{j=-n}^{n-1} v(x_j) e^{i \frac{2\pi}{2n} kj}, \quad k = -n, ..., n-1\,, \tag{5.76}$$

for $x_j = j \frac{2\pi}{n}$ and some fixed number of unknowns $n = 2^p$ for $p \in \mathbb{N}$ in the parts for j odd and j even. Then, both parts can be recognised to be Fourier transforms of length $\frac{n}{2}$. Recursively, the computational cost reduces to $O(n \log n)$. As the three-dimensional case is just a nested version of the one-dimensional Fourier representation we conclude that the Fast Fourier Transform reduces the computational cost to $O(N \log N)$ for N being the total amount of unknowns.

5.4 A local representation of the strong singularity

We have seen that we can represent the strongly singular operator by (5.55). Nevertheless, a numerical treatment of (5.55) leads to difficulties as a truncation of the infinite integrals must be sufficiently large to incorporate the symbol $\mathcal{K}$ and is not applicable for the amount of unknowns we aim to work with. In this section we present a local integration scheme for the strong singularity. In particular, we will formulate a decomposition of T_0 into a local and global part and study the local part which includes the strong singularity separately.

We consider the integral operator

$$Lv(x) := \int_{\mathbb{R}^3} \frac{1}{|x-y|^3} Y(x-y)v(y)\,dy, \quad x \in \Omega \tag{5.77}$$

where the kernel $\frac{1}{|x-y|^3}Y(x-y)$ is one of the entries of the kernel of T_0 given in (5.20) and $v : \mathbb{R}^3 \to \mathbb{C}$ lies in $L^2(\mathbb{R}^3)$. Furthermore, we assume that the density v is compactly supported in a ball $\Omega \subset B_R(0)$ where $B_R(0)$ denotes a ball with radius $R > 0$ and centre 0. With the symbol matrix (5.53) we see that

$$\begin{aligned} Lv(x) &= \int_{\mathbb{R}^3} \left(\int_{\mathbb{R}^3} \frac{1}{|y|^3} Y(-\hat{y}) e^{i|y|\hat{y}\cdot z}\,dy \right) \left(\int_{\mathbb{R}^3} v(s) e^{isz} ds \right) e^{-izx} dz \\ &= \int_{\mathbb{R}^3} \mathcal{K}_Y(z) \left(\int_{\mathbb{R}^3} v(s) e^{isz} ds \right) e^{-izx} dz, \end{aligned} \tag{5.78}$$

for the symbol $\mathcal{K}_Y$ of Y given by the appropriate entry of (5.53). Here, we first split L into two parts, in the *local* operator

$$L_{loc}v(x) := \int_{\mathbb{R}^3} (1 - \chi(|x-y|)) \frac{1}{|x-y|^3} Y(x-y)v(y)\,dy, \quad x \in \Omega, \tag{5.79}$$

and *global* operator

$$L_{glob}v(x) := \int_{\mathbb{R}^3} \chi(|x-y|) \frac{1}{|x-y|^3} Y(x-y)v(y)\,dy, \quad x \in \Omega, \tag{5.80}$$

using the cut-off function given by (2.14). It holds that

$$Lv(x) = L_{loc}v(x) + L_{glob}v(x), \tag{5.81}$$

and the local operator is strongly singular and the global operator possesses a continuous kernel. To cope with the singularity of L_{loc} we now construct for every $x_0 \in \Omega$ an

operator and a density, which, on the one hand, coincides with $L_{loc}v(x_0)$ in x_0 and, on the other hand, represents a convolution with a kernel whose Fourier coefficients can be exactly evaluated. We conclude this section with a Fourier series representation of $L_{loc}v(x_0)$.

Let $x_0 \in \Omega$. Using that

$$\text{supp}_{\,y\in\mathbb{R}^3}\{(1-\chi(|x_0-y|))\} = B_1(x_0), \tag{5.82}$$

for the ball $B_1(x_0)$ with radius 1 and centre x_0, we see that

$$L_{loc}v(x_0) = \int_{B_1(x_0)} (1-\chi(|x_0-y|))\frac{1}{|x_0-y|^3}Y(x_0-y)v(y)\,dy.$$

Let $\rho > 2$ and let Q_{x_0} be the cube

$$Q_{x_0} := \left\{x \in \mathbb{R}^3 : \exists z \in [-\rho,\rho]^3 : x = x_0 + z\right\}. \tag{5.83}$$

We define the *multiplication operator* $\Xi = \Xi^{\lfloor x_0 \rfloor} : L^2(Q_{x_0}) \to L^2(Q_{x_0})$ by

$$\Xi v(x) = \Xi^{\lfloor x_0 \rfloor}v(x) := (1-\chi(|x_0-x|))v(x), \quad x \in Q_{x_0}, \tag{5.84}$$

and set v_ρ as the 2ρ-periodically extended image of Ξv given by

$$v_\rho(y+y_{2\rho}) = v_\rho(y) \text{ for } y \in Q_{x_0} \text{ and for all } (y_{2\rho,j} \mod 2\rho) = 0,\ j = 1,2,3, \tag{5.85}$$

where $y_{2\rho,j}$ denotes the components of $y_{2\rho}$. In the same way, we extend the kernel k_ρ defined for $x, y \in Q_{x_0}$ via

$$k_\rho(x-y) := \begin{cases} \frac{1}{|x-y|^3}Y(x-y) & , (x-y) \in B_\rho(0), \\ 0 & , (x-y) \in [-\rho,\rho]^3 \backslash \overline{B_\rho(0)}. \end{cases} \tag{5.86}$$

2ρ-periodically. We have

$$\begin{aligned} (L_\rho v_\rho)(x_0) &= \int_{Q_{x_0}} k_\rho(x_0-y)v_\rho(y)\,dy \\ &= \int_{B_\rho(x_0)} \frac{1}{|x_0-y|^3}Y(x_0-y)v_\rho(y)\,dy \\ &= \int_{B_1(x_0)} (1-\chi(|x_0-y|))\frac{1}{|x_0-y|^3}Y(x_0-y)v(y)\,dy \\ &= (L_{loc}v)(x_0), \end{aligned} \tag{5.87}$$

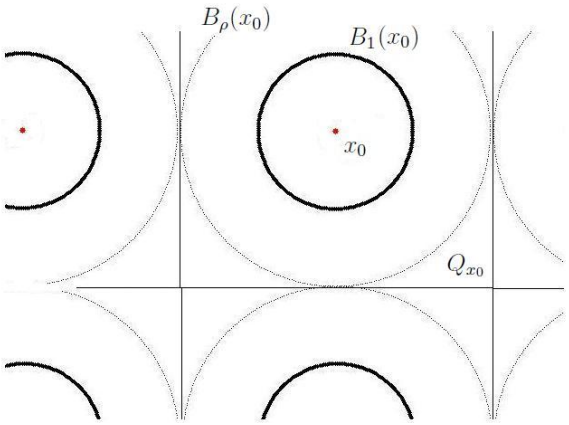

Figure 5.1: *The setting for the periodically extended operator L_ρ. The support of $(v_\rho)|_{Q_{x_0}}$ is contained in the ball $B_1(x_0)$ whereas we construct the periodical kernel k_ρ such that the support of $(k_\rho(x_0 - \cdot)|_{Q_{x_0}}$ lies within the ball $B_\rho(x_0)$. Both functions are 2ρ-periodic.*

and thus, we have found a *multi-periodic* integral operator L_ρ which incorporates the strong singularity. The application of the convolution theorem for 2ρ-periodic functions, Theorem 5.3.1, leads to

$$\widehat{(L_\rho v_\rho)}_m = \left(\frac{1}{(2\rho)^3}\int_{Q_{x_0}} k_\rho(x_0-y)e^{-\frac{2\pi}{2\rho}i(x_0-y)\cdot m}\,dy\right) \left(\frac{1}{(2\rho)^3}\int_{Q_{x_0}} v_\rho(s)e^{-\frac{2\pi}{2\rho}is\cdot m}\,ds\right), \quad m\in\mathbb{Z}^3. \tag{5.88}$$

By the definition of k_ρ, it holds that

$$\int_{Q_{x_0}} k_\rho(x_0-y)e^{-\frac{2\pi}{2\rho}i(x_0-y)\cdot m}\,dy = \int_{B_\rho(0)}\frac{1}{|y|^3}Y(-\hat{y})e^{-\frac{2\pi}{2\rho}i|y|\hat{y}\cdot m}\,dy, \tag{5.89}$$

where Y consists of spherical harmonics of order 2, see (5.41). We proceed analogously as in Chapter 5.2.1 and consider

$$\begin{aligned}&\lim_{\varepsilon\to 0}\int_{B_\rho(0)\setminus B_\varepsilon(0)}\frac{1}{|y|^3}Y_2^{(k)}(-\hat{y})e^{-i\frac{2\pi}{2\rho}|y|\hat{y}\cdot m}\,dy\\ &=\lim_{\varepsilon\to 0}\int_\varepsilon^\rho\frac{1}{r}\int_0^{2\pi}\int_0^\pi Y_2^{(k)}(-\hat{y})e^{-i\frac{2\pi}{2\rho}r\hat{y}\cdot m}\,\sin\theta\,d\theta\,d\varphi\,dr.\end{aligned} \tag{5.90}$$

We now substitute r by $\frac{2\pi}{2\rho}r$ to obtain from (5.29) - (5.31) that

$$\begin{aligned}
&\lim_{\varepsilon\to 0}\int_{B_\rho(0)\setminus B_\varepsilon(0)} \frac{1}{r^3}Y_2^{(k)}(-\hat{y})e^{-i\frac{2\pi}{2\rho}r\hat{y}\cdot m}\, r^2\, dr\, d\hat{y}\\
&= \lim_{\varepsilon\to 0}\int_{\varepsilon\frac{2\pi}{2\rho}|m|}^{\pi|m|}\frac{1}{r}\int_0^{2\pi}\int_0^{\pi} Y_2^{(k)}(-\hat{y})e^{-ir\hat{y}\cdot\hat{m}}\,\sin\theta\, d\theta\, d\varphi\, dr\\
&= (2\pi)^{\frac{3}{2}}i^2\, Y_2^{(k)}(\frac{m}{|m|})\lim_{\varepsilon\to 0}\int_{\varepsilon\frac{2\pi}{2\rho}|m|}^{\pi|m|}\frac{1}{r^{\frac{3}{2}}}J_{\frac{5}{2}}(r)\, dr. \qquad (5.91)
\end{aligned}$$

We use

$$\int \frac{J_{5/2}(r)}{r^{3/2}}\, dr = -\sqrt{\frac{2}{\pi}}\left[\frac{\sin r}{r^3} - \frac{\cos r}{r^2}\right],$$

and we get from

$$\lim_{\varepsilon\to 0}\frac{\sin\varepsilon - \varepsilon\cos\varepsilon}{\varepsilon^3} = \frac{1}{3}, \qquad (5.92)$$

that

$$\lim_{\varepsilon\to 0}\int_{\varepsilon}^{\pi|m|}\frac{J_{5/2}(r)}{r^{3/2}}\, dr = \sqrt{\frac{2}{\pi}}\left(\frac{1}{3} - \frac{1}{\pi|m|^3}(\sin\pi|m| - \pi|m|\cos\pi|m|)\right).$$

Since the kernel Y consists of spherical harmonics of order 2 we have an exact representation of the Fourier coefficients of the convolution $L_\rho v_\rho$. In particular, from (5.89), we have that

$$\int_{Q_{x_0}} k_\rho(x_0 - y)e^{-\frac{2\pi}{2\rho}i(x_0-y)\cdot m}\, dy = \widehat{Y}_m, \qquad (5.93)$$

where

$$\begin{aligned}
\widehat{Y}_m := \quad & \frac{1}{(2\rho)^3}(2\pi)^{3/2}i^2 Y(m/|m|)\\
& \sqrt{\frac{2}{\pi}}\left(\frac{1}{3} - \frac{1}{\pi|m|^3}(\sin\pi|m| - \pi|m|\cos\pi|m|)\right), \qquad (5.94)
\end{aligned}$$

and, by (5.92), $\widehat{Y}_m$ is also defined in $m \equiv 0$. From the representation (5.88) we see that

$$\widehat{(L_\rho v_\rho)}_m = \left(\widehat{Y}_m\right)\cdot\widehat{(v_\rho)}_m,\ m\in\mathbb{Z}^3,$$

for the Fourier coefficients

$$\widehat{(v_\rho)}_m = \frac{1}{(2\rho)^3}\int_{Q_{x_0}} v_\rho(s)e^{-i\frac{2\pi}{2\rho}m\cdot s}ds, \qquad (5.95)$$

of v_ρ. We obtain

$$L_\rho v_\rho(x) = \frac{1}{(2\rho)^3}\mathcal{F}_p^{-1}(\widehat{Y}_m\cdot\widehat{(v_\rho)}_m)(x), \qquad (5.96)$$

and, by (5.87), the *local* operator can be pointwise evaluated,

$$L_{loc}v(x_0) = L_\rho v_\rho(x_0) = \frac{1}{(2\rho)^3}\mathcal{F}_p^{-1}\left(\widehat{Y}_m \cdot \widehat{(v_\rho)}_m\right)(x_0) \tag{5.97}$$

$$= \frac{1}{(2\rho)^3}\sum_{m\in\mathbb{Z}^3} \widehat{Y}_m \cdot \widehat{(v_\rho)}_m \, e^{2\pi i \frac{1}{2\rho}x_0\cdot m}. \tag{5.98}$$

We return to the original (matrix-) operator $\mathcal{M}T_0$ where the kernel of T_0 is a matrix given by k_0 with entries $k_0^{(j,\ell)}$, $j,\ell = 1,2,3$, given through (5.41). The above computations yield

$$\begin{aligned}&(\mathcal{M}T_0 v)^{(j)}(x_0)\\ &= \mathcal{M}(x_0)\sum_{\ell=1}^{3} L_{glob}^{(j,\ell)} v^{(\ell)}(x_0) + \mathcal{M}(x_0)\sum_{\ell=1}^{3} L_{loc}^{(j,\ell)} v^{(\ell)}(x_0),\ x_0\in\Omega,\end{aligned} \tag{5.99}$$

for $L_{glob}^{(j,\ell)}$ being the integral operator with kernel $\chi k_0^{(j,\ell)}$ and $L_{loc}^{(j,\ell)} = L_{loc}$ where the kernel Y takes the form $k_0^{(j,\ell)}$. Hence, for every $x\in\Omega$ we have found a representation of the strongly singular integral and this will enable us to evaluate every component of T_0 successively for every point $x\in\Omega$.

Chapter 6

Operator approximations and Nyström method

In this chapter we address the treatment of the large system of unknowns in the anisotropic scattering problem and the incorporation of a scheme to handle the strong singularity. In the following we present a domain decomposition approach which relies on a geometrical decomposition of the domain Ω which contains the support of M. It enables us to handle several million unknowns by a parallelisation of the FFT-based operator evaluations on subdomains of Ω.

We begin this chapter with the quadrature schemes used for the weakly singular and strongly singular parts. Then, we present a domain decomposition approach and discuss details of the numerical implementation.

At the end, we provide numerical examples and test the feasibility of the domain decomposition scheme.

6.1 Quadrature of the weakly singular parts

In this section we present the application of the Fast Fourier transform for a numerical scheme to evaluate the convolution operators $T - T_0$ and T_1. Here, we restrict our presentation to the case where the integration kernel is smooth. In particular, we present a simplified numerical discretisation for the weakly singular part where the

singularity is cut-off by a smooth cut-off function. This in turn means that we can only achieve linear convergence. Nevertheless, the FFT-based evaluation can be used by the same arguments for higher order schemes for the weak singularity. For example, such a high order scheme is presented in [52] for the Lippmann-Schwinger equation with the use of the Fourier transform.

Let us consider the integral operator

$$Kv(x) = \int_{\mathbb{R}^3} k(x-y)v(y)\,dy \tag{6.1}$$

for $x \in \mathbb{R}^3$ and kernel k, where k is one of the three components of the weakly singular integral operator $\mathcal{M}(T-T_0)+\kappa^2\mathcal{M}T_1$ and $v \in L^2(\mathbb{R}^3)$. By assumption, M and hence, also $\mathcal{M}$, is compactly supported and we assume that the support lies within a cuboid, supp $\mathcal{M} \subset Q_R$, given by

$$Q_R := [-R_1, R_1] \times [-R_2, R_2] \times [-R_3, R_3], \tag{6.2}$$

for $R \in \mathbb{R}^3_+$. We set Q_{2R} to be the cuboid with doubled sidelengths, i.e. $Q_{2R} := [-2R_1, 2R_1] \times [-2R_2, 2R_2] \times [-2R_3, 2R_3]$. As $v = ME$ has compact support in Q_R, we find that the density

$$v_{2R}(x) := v(x) \text{ for } x \in Q_{2R}, \tag{6.3}$$

possesses a uniquely determined $2R$-periodic extension which coincides with v in every point $x \in Q_{2R}$ and for simplicity we denote this $2R$-periodic extension by v_{2R}. Similarly, the kernel k is extended to a $2R$-periodic function with

$$k_{2R}(x) := k(x) \text{ for } x \in Q_{2R}. \tag{6.4}$$

The multi-periodic integral operator

$$K_{2R}v_{2R}(x) = \int_{B_{2R}(0)} k_{2R}(x-y)v_{2R}(y)\,dy, \quad x \in Q_{2R}, \tag{6.5}$$

coincides with (6.1) for all $x \in Q_R$ and thus, it suffices to consider a quadrature scheme for K_{2R}. It is possible to consider the sequence of operators given by $(K_{2R,\chi}) = (K_{2R,\chi,n})_{n\in\mathbb{N}}$ with corresponding $2R$-periodic kernel $k_{2R,\chi}$ given by

$$k_{2R,\chi}(x) := (\chi(n|x|))k_{2R}(x), \quad x \in Q_{2R}, \tag{6.6}$$

to approximate $K_{2R}v_{2R}$. Here, χ is the cut-off function given by (2.14). The integral $(K_{2R,\chi}v)$ represents a convolution of two $2R$-periodic functions in $L^2(Q_{2R})$. By the

same arguments as in the proof of Theorem 5.3.1 we can approximate the convolution by replacing the kernel $k_{2R,\chi}$ and the density v_{2R} by its trigonometric interpolation polynomials k_N and v_N. We have for $x \in Q_{2R}$,

$$\begin{aligned}(K_{2R,\chi}v_{2R})_{\text{fft}}(x) &:= \int_{Q_{2R}} \sum_{m\in\mathcal{Z}} \left(\widetilde{(k_{2R,\chi})}_m e^{i\frac{2\pi}{p}m\cdot(x-y)}\right)\left(\sum_{\ell\in\mathcal{Z}} \widetilde{(v_{2R})}_\ell e^{i\frac{2\pi}{2R}\ell\cdot y}\,dy\right)\\ &= \frac{1}{\#N}\sum_{m\in\mathcal{Z}} \widetilde{(k_{2R,\chi})}_m \widetilde{(v_{2R})}_m\, e^{i\frac{2\pi}{2R}m\cdot x}\\ &= \frac{1}{\#N}\sum_{m\in\mathcal{Z}} \widetilde{(k_{2R,\chi})}_m \widetilde{(v_{2R})}_m\, e^{i\frac{2\pi}{2N}m\cdot \ell}, \quad \ell\in\mathcal{Z}, \end{aligned} \tag{6.7}$$

where $\#N = (2N_1)(2N_2)(2N_3)$ is the total amount of unknowns and the grid $\mathcal{Z}$ is given by (5.67).

LEMMA 6.1.1. *It holds that*

$$(K_{2R,\chi}v_{2R})_{\text{fft}}(x_\ell) = \frac{1}{N_1N_2N_3}\sum_{m\in\mathcal{Z}} k_{2R,\chi}(x_\ell - x_m)v_{2R}(x_m), \tag{6.8}$$

in every gridpoint $x_\ell \in Q_R$.

Proof. This is shown in [26], Chapter 8. □

6.2 Quadrature scheme for the strongly singular part

The discretisation of the strongly singular (matrix) operator T_0 is based on the decomposition of every component in local and global part. We first consider

$$Lv(x) = L_{loc}v(x) + L_{glob}v(x) \tag{6.9}$$

where Lv is one of the three components of T_0v and the local and global parts are given by (5.79) and (5.80). With exactly the same arguments as at the beginning of Section 6.1, we find that there exists a $2R$-periodic operator

$$L_{2R}v_{2R}(x) = L_{glob}v(x) \text{ for all } x \in Q_R \tag{6.10}$$

with continuous $2R$-periodic kernel k_{2R} and density satisfying the periodicity assumptions (6.4) and (6.3). In particular, we have the $2R$-periodic kernel given by

$$k_{2R}(x) := k_{2R}^{(m,n)}(x) = \chi(|x|)k_0^{(m,n)}(x), \quad x \in Q_{2R}, \quad m,n = 1,2,3, \tag{6.11}$$

for χ defined by (2.14) and kernel k_0 given by (5.20), and the density defined via

$$v_{2R}^{(n)}(x) = v^{(n)}(x), \quad x \in Q_{2R}. \tag{6.12}$$

We obtain a fully discretised version of the m-th component of the global part $(L_{glob}v)^{(m)}$ by

$$(L_{glob}v)_{\text{fft}}^{(m)}(x_\ell) = \sum_{n=1}^{3}\Big(\frac{1}{\#N}\sum_{j\in\mathcal{Z}}\widetilde{(k_{2R}^{(m,n)})}_j\widetilde{(v_{2R}^{(n)})}_j\, e^{i\frac{2\pi}{2N}j\cdot\ell}\Big),\ \ell\in\mathcal{Z} \text{ s.t. } x_\ell \in Q_R.$$

Lemma 6.2.1. *It holds that*

$$\sum_{k=1}^{3}(L_{glob}v)_{\text{fft}}^{(m)}(x_\ell) = \sum_{k=1}^{3}\frac{1}{N_1N_2N_3}\sum_{m\in\mathcal{Z}}\chi(|x_\ell - x_\xi|)k_0^{(m,n)}(x_\ell,x_\xi)v^{(n)}(x_\xi). \tag{6.13}$$

Proof. This follows from [26], Chapter 8. □

We have seen that the local operator can be pointwise represented by (5.98). Now, we proceed similarly as in the weakly singular case. We choose an equidistant quadratic grid for Q_{x_0} with $2N_j'$ grid points in the j-th direction given by

$$x_j = x_0 + j\frac{2\rho}{\#N'} \text{ for } j \in \mathcal{Z}', \tag{6.14}$$

where

$$\mathcal{Z}' := \{-N_1', ..., N_1' - 1\} \times \{-N_2', ..., N_2' - 1\} \times \{-N_3', ..., N_3' - 1\}, \tag{6.15}$$

and replace the density v_ρ of the operator $L_\rho v_\rho$, recalling the relation (5.87), by its trigonometric interpolation polynomial

$$v_{N',\rho}(x) = \sum_{m\in\mathcal{Z}'}\widetilde{(v_\rho)}_m e^{i\frac{2\pi}{2\rho}m\cdot x}, \quad x \in Q_{x_0},$$

with discrete Fourier coefficients

$$\widetilde{(v_\rho)}_m = \left(\frac{1}{\#N'}\sum_{j\in\mathcal{Z}'}(1-\chi(|x_0-x_j|))v(x_j)e^{-i\frac{2\pi}{2N'}m\cdot j}\right), \quad m \in \mathcal{Z}'.$$

Let now

$$V_j := \begin{cases} \widetilde{(v_\rho)}_j, & j \in \mathcal{Z}', \\ 0, & j \in \mathbb{Z}^3 \backslash \mathcal{Z}'. \end{cases} \tag{6.16}$$

From (5.88), (5.93) and from (5.98), we find that

$$\begin{aligned} (L_\rho v_\rho)(x) &\approx (L_\rho v_{N',\rho})(x) \\ &= \sum_{j \in \mathbb{Z}^3} \widehat{Y}_j \, V_j \, e^{i\frac{2\pi}{2\rho} n \cdot x} \\ &= \frac{1}{(2\rho)^3} \sum_{j \in \mathcal{Z}'} \widehat{Y}_j \, \widetilde{(v_\rho)}_j \, e^{i\frac{2\pi}{2\rho} j \cdot x}. \end{aligned} \tag{6.17}$$

A fully discretised version of the strongly singular local part is then given by

$$(L_{loc} v)_{\mathrm{fft}}(x_0) := \sum_{j \in \mathcal{Z}'} \widehat{Y}_j \, (\widetilde{\Xi^{\lfloor x_0 \rfloor} v})_j \, e^{i\frac{2\pi}{2\rho} j \cdot x_0}. \tag{6.18}$$

In particular, the local part of $T_0 v$ with kernel Y replaced by $\mathcal{K}^{(m,k)}$, $m, k \in \{1, 2, 3\}$ defined in (5.42), is given by

$$(L_{loc} v)^{(m)}_{\mathrm{fft}}(x_\ell) = \sum_{n=1}^{3} \Big(\frac{1}{\#N'} \sum_{j \in \mathcal{Z}'} (\widehat{\mathcal{K}^{(m,n)}})_j \, (\widetilde{\Xi^{\lfloor x_\ell \rfloor} v^{(n)}})_j \, e^{i\frac{2\pi}{2\rho} j \cdot x_\ell} \Big), \tag{6.19}$$

for $x_\ell \in \Omega$ and where $(\widehat{\mathcal{K}^{(m,n)}})_j$ is given by

$$\begin{aligned} (\widehat{\mathcal{K}^{(m,n)}})_j := \quad & \frac{1}{(2\rho)^3} (2\pi)^{3/2} i^2 \mathcal{K}^{(m,n)}(j/|j|) \\ & \sqrt{\frac{2}{\pi}} \left(\frac{1}{3} - \frac{1}{\pi |j|^3} (\sin \pi |j| - \pi |j| \cos \pi |j|) \right), \end{aligned} \tag{6.20}$$

for $j \in \mathcal{Z}'$, see (5.94)). We note that the computational cost for the evaluation of the local operator, using $\#N'$ gridpoints for Q_{x_0}, is of the order $(\#N)(\#N') \log \#N'$. We also remark that we never have to save any matrix of size $(\#N)(\#N')$ and the above scheme is possible for all N only restricted by the amount of available memory and time.

6.3 The Nyström method

We solve the strongly singular integral equation system, (5.15), which is given by

$$v(x) + \mathcal{M}(x) T_0 v(x) + K v(x) = f(x), \quad x \in \Omega \tag{6.21}$$

with f defined by

$$f(x) := \mathcal{M}(x)E^i(x), \tag{6.22}$$

and K given by $K = \mathcal{M}(T - T_0) + \kappa^2 \mathcal{M}T_1$, by the direct application of the above quadrature schemes, which is known as Nyström method. Using approximations based on the numerical integration of the strongly and weakly singular parts the strongly singular integral equation system reduces to solving a finite dimensional linear system,

$$(I + A)v_N = f_N \tag{6.23}$$

where A represents the discretisation of the operators $\mathcal{M}(\cdot)T_0 + K$ and v_N and f_N denote the 3-tupels of tensors $v_N^{(k,j)} := v^{(k)}(x_j)$, $f_N^j := f^{(k)}(x_j)$, $k = 1, 2, 3$, for the N gridpoints $x_j \in Q_R$. Here, we never implement a matrix A, but use the Fast Fourier Transform for the evaluation of Av_N. In particular, for a grid $\mathcal{G}$ of $Q_R \supset \operatorname{supp} \mathcal{M}$ with a total number of N_j grid points in the j-th direction, the computational cost of Lv is of order $O(\#N \log \#N + (\#N)(\#N') \log \#N')$ operations for N' being the vector of the amount of discretisation points for the (strongly singular) local part.

We solve the finite dimensional linear system due to the anisotropic system by an iterative method. In particular, we use the *conjugate gradient method* formulated for operator equations $\mathcal{A}x = f$ where $\mathcal{A} : X \to Y$ is a bounded, linear and injective operator between Hilbert spaces X and Y with adjoint $\mathcal{A}^* : Y \to X$. The algorithm is presented in [30], see Algorithm 6.1. We further apply the FFT-algorithm of Matlab for the *matrix-vector* evaluations.

6.4 Domain Decomposition

In this section we describe parallel or successive implementations based on an integral equation domain decomposition approach which can deal with problems of size $m \cdot N$, where the computational cost increases to $m^2 N \log(N)$. Here, m denotes the number of subdomains used in the domain decomposition and N is the total number of discretisation points per subdomain. This second scheme is limited only by computing time and the size of available storage space.

To solve equation (6.21) numerically, we apply a gradient method. We use the notation

$$A := \mathcal{M}T_0 + \mathcal{M}(T - T_0) + \kappa^2 \mathcal{M}T_1, \quad f = \mathcal{M}E^i. \tag{6.24}$$

Algorithm 6.1 The conjugate gradient method: Original Version

initialize $v^0 \equiv 0$;
if $\mathcal{A}^* v = f$ **then**:
    Stop;
end if
initialize $p^0 = -\mathcal{A}^* y$;
for m=0,...,M **do**:
    $t_m := \frac{(\mathcal{A}v^m - f, \mathcal{A}p^m)}{\|\mathcal{A}p^m\|^2}$;
    $v^{m+1} := v^m - t_m p^m$;
    if $\mathcal{A}^*(\mathcal{A}v^{m+1} - f) = 0$ **then**:
        Stop;
    end if
    $\gamma_m := \frac{\left\|\mathcal{A}^*(\mathcal{A}v^{m+1} - f)\right\|^2}{\|\mathcal{A}^*(\mathcal{A}v^m - f)\|^2}$;
    $p^{m+1} := \mathcal{A}^*(\mathcal{A}v^{m+1} - f) + \gamma_m p^m$;
    $m \leftarrow m + 1$;
end for
return v^M;

We recall that A is a mapping from $(L^2(\mathbb{C}^3))^3$ to $(L^2(\mathbb{C}^3))^3$, and we set A^* to be its adjoint operator. In particular, we can make use of the Fast Fourier transform based discretisations of the previous sections for the evaluation of the adjoint since

$$\langle \mathcal{M}T_0 v, u\rangle = \left\langle v, T_0^*(\overline{\mathcal{M}^t}u)\right\rangle, \tag{6.25}$$

for the complex conjugate transpose $\overline{\mathcal{M}^t}$ of $\mathcal{M}$ and for the adjoint T_0^* of T_0 with the complex conjugate of the transposed matrix kernel $\overline{k_0^t}$ as kernel. Similarly, we find that $(\mathcal{M}(T-T_0))^* v = (T-T_0)^*(\overline{\mathcal{M}^t}v)$ and $(\mathcal{M}T_1)^* v = T_1^*(\overline{\mathcal{M}^t}v)$ with the complex conjugate of the kernel of T_1 as kernel of T_1^* and the complex conjugate of the transposed (matrix-) kernel of $T - T_0$ as kernel of $(T-T_0))^*$.

We write $\boldsymbol{A}$, $\boldsymbol{f}$ and $\boldsymbol{v}$ for the discretised versions of A, f and v in the sense of the Fourier Transform based evaluations. We also write

$$\boldsymbol{L} := \boldsymbol{I} + \boldsymbol{A} \tag{6.26}$$

for the discretisation of $(I + A)$.

We define the functional

$$\mu(\boldsymbol{v}) = \|\boldsymbol{L}\boldsymbol{v} - \boldsymbol{f}\|^2 \tag{6.27}$$

for the discretised function $\boldsymbol{v}$ of v. The Fréchet derivative of μ can then be computed by simply rewriting the complex parts $\boldsymbol{v}^{(i)} \in \mathbb{C}^N$, $i = 1, 2, 3$ as a function in $\mathbb{R}^{2N}$. We have

$$(\nabla_{\boldsymbol{v}}\mu)(\boldsymbol{v}) = 2\boldsymbol{L}^*(\boldsymbol{L}\boldsymbol{v} - \boldsymbol{f}), \tag{6.28}$$

and a possible gradient method with adaptive stepsize h_n is given by

$$\boldsymbol{v}^{n+1} = \boldsymbol{v}^n - h_n(\nabla_{\boldsymbol{v}}\mu)(\boldsymbol{v}^n), \tag{6.29}$$

with

$$\boldsymbol{v}^n = (\boldsymbol{v}^{n,(1)}, \boldsymbol{v}^{n,(2)}, \boldsymbol{v}^{n,(3)}) \in (\mathbb{C}^N)^3. \tag{6.30}$$

To simulate the scattering of, for example, terahertz waves (wavelengths between 0.1 mm to 1mm) on the anisotropic medium the amount of unknowns is already very large. Choosing at least 5 points per wavelength and the wavelength to be 1 mm, we already reach the capacity of a personal computer with 2 GB. In particular, for the wavelength of 1 mm ($\kappa = 2\pi/\lambda$) we need $200 \times 200 \times 10$ points to model an anisotropic medium of size $4 \times 4 \times 0.2$ cm^3. Thus, for high frequencies, i.e. smaller wavelengths, we need to consider another approach for the gradient method.

1. We suggest a *domain decomposition*, which uses a geometrical decomposition of the domain Q_R, which includes the support of $M = I - N$, for the refractive index N. A geometrical decomposition of Q_R implies a decomposition of the integral operators. We will see that the introduced numerical discretisation schemes are still applicable and the scattering problem can be solved for higher wave numbers even on a personal computer.

2. We solve the finite-dimensional system by the conjugate gradient method, see Algorithm 6.1, which we also apply to the domain decomposition approach.

We decompose the cuboid $Q_R = [-R_1, R_1] \times [-R_2, R_2] \times [-R_3, R_3]$ into $m_1 \times m_2$ equal sized subdomains $D_{1,1}, ..., D_{m_1,m_2}$ given by

$$D_{i,j} = [R_{1,j}, R_{1,j+1}] \times [R_{2,i}, R_{2,i+1}] \times [-R_3, R_3], \tag{6.31}$$

with

$$R_{1,j} = -R_1 + (j-1)\frac{2R_1}{m_1} \text{ and } R_{2,i} = -R_2 + (i-1)\frac{2R_1}{m_2}. \tag{6.32}$$

For $k(i,j) := (j-1)m_1 + i$ we define $\tilde{D}_k := D_{ij}$. We see that the domain Ω is a composition of m subdomains where $m = m_1 m_2$ is the total amount of subdomains,

$$\Omega = \tilde{D}_1 \cup \tilde{D}_2 \cup ... \cup \tilde{D}_m \tag{6.33}$$

with $\tilde{D}_k \cap \tilde{D}_{k+2} = \varnothing$ and $\tilde{D}_k \cap \tilde{D}_{k+1} = \partial\tilde{D}_k \cap \partial\tilde{D}_{k+1}$. We denote the kernel of $T_0 + (T - T_0) + \kappa^2 T_1$ by k. Then, A can be written as a composition of

$$A_{ij}v|_{\tilde{D}_j}(x) := \mathcal{M}|_{\tilde{D}_i}(x) \int_{\tilde{D}_j} k(x,y)v|_{\tilde{D}_j}(y)\, dy \text{ for } x \in \tilde{D}_i, \tag{6.34}$$

given by

$$Av(x) = \sum_{j=1}^{m} A_{ij}v|_{\tilde{D}_j}(x) \text{ for } x \in \tilde{D}_i\,, \tag{6.35}$$

for $i = 1, ..., m$. We define the kernel of A_{ij} by

$$k_{ij} := k|_{\tilde{D}_i \times \tilde{D}_j}. \tag{6.36}$$

For $i = j$, A_{jj} is sum of a weakly and a strongly singular convolution operator with kernel k_{jj} and we can apply the methods of the previous sections to evaluate $A_{jj}v$ on $\tilde{D}_j$. For $i \neq j$ there exists a unique *translation* vector $x_{ij} \neq 0 \in \mathbb{R}^3$ with

$$\tilde{D}_i = \tilde{D}_j + x_{ij} \tag{6.37}$$

and we find that for $x \in \tilde{D}_i$,

$$\begin{aligned} A_{ij}v|_{\tilde{D}_j}(x) &= \int_{\tilde{D}_j} k_{ij}(x,y)v|_{\tilde{D}_j}(y)\,dy \\ &= \int_{\tilde{D}_j} k_{ij}(x_{ij}+z,y)v|_{\tilde{D}_j}(y)\,dy \text{ for } z \in \tilde{D}_j. \end{aligned} \tag{6.38}$$

The kernel

$$h_{ij}(z,y) := k_{ij}(x_{ij}+z,y) : \tilde{D}_j \times \tilde{D}_j \to \mathbb{C}^3 \tag{6.39}$$

is a continuous convolution kernel and, thus, for the numerical evaluation of A_{ij}, $i \neq j$ we can use FFT methods similar to the discretisation described in the first section of this chapter. Every component of the sum in (6.35) is a convolution operator and we can evaluate every component A_{ij} of A by the Fast Fourier transform. In particular, for $i = j$ we apply the methods decribed in Sections 6.1 and 6.2.

The domain decomposition gradient method can be rewritten for the components of A. In particular, we set $\boldsymbol{v}_j^n$ to be the n-th iteration of v in the domain $\tilde{D}_j$ and $\boldsymbol{f}_i := \boldsymbol{f}|_{\tilde{D}_i}$. Then, we obtain the domain-decomposition gradient method

$$\boldsymbol{v}^0 = 0, \tag{6.40}$$

$$\boldsymbol{v}_j^{n+1} = v_j^n - h_n \sum_{i=1}^{m} \boldsymbol{A^*}_{ji} \sum_{k=1}^{m} (\boldsymbol{A}_{ik}\boldsymbol{v_k^n} - \boldsymbol{f}_i), \quad j = 1,2,...,M. \tag{6.41}$$

This formulation enables us now to work with larger systems of unknowns by using an iterative evaluation of the sums and only loading the actual needed components to the main memory while storing the new components $\boldsymbol{v}_j^{n+1}, j = 1,...,m$ successively. The decomposed domain approach for the gradient method is formulated in pseudocode, see Algorithm 6.2. Here, we use an adaptive stepsize h_n. The algorithm provides sequences v_j^n for $n \to \infty$ and $j = 1,...,m$, which coincide with the non-decomposed iterative solution on every subdomain provided that the operator approximation on a subdomain does not differ from the operator approximation on the whole domain Ω. For a fast method we apply these ideas to the conjugate gradient method.

Algorithm 6.2 Domain Decomposition Scheme: Realisation of a simple gradient method

Define the size of Ω and decompose the domain into m subdomains $D_1, ..., D_m$.
for all $j = 1, ..., m$ **do**:
    successively save $f_j = (ME^i)|_{D_j}$;
end for
for all $N = 1, ...$ **do**:
    for all $\eta = 1, ..., m$ **do**:
        initialize $S_3 = 0$.
        for all $i = 1, ..., m$ **do**:
            initialize $S_1 = 0$;
            for all $k = 1, ..., m$ **do**:
                load the n-th iterate $v_k^n := (v^{n,(1)}, v^{n,(2)}, v^{n,(3)})|_{D_k}$ on domain D_k;
                evaluate $A_{ik} v_k^n$;
                $S_1 \leftarrow S_1 + A_{ik} v_k^n$;
            end for
            load f_i;
            $S_{2,i} \leftarrow S_1 - f_i$;
            evaluate $A_{\eta,i}^* S_{i,2}$;
            $S_3 \leftarrow S_3 + A_{\eta,i}^* S_{i,2}$;
        end for
        load v_η^n;
        $v_\eta^{n+1} \leftarrow v_\eta^n - 2h_n S_3$;
        save v_η^{n+1};
    end for
end for

Domain decomposition for the evaluation of the scattered field

Let v be the solution of the anisotropic volume integral equation system (5.15). The scattered field can then be evaluated by, ((5.15)),

$$\begin{aligned} E^s(x) &= M^{-1}v(x) - E^i(x) && (6.42)\\ &= (I - \frac{1}{3}M)^{-1}(E^i(x) - T_0 v(x) \\ &\quad -(T - T_0)v(x) - \kappa^2 T_1 v(x)) - E^i(x) && (6.43) \end{aligned}$$

for every point $x \in \text{supp } M$. For $x \notin \text{supp } M$ we use (5.10), noting that now

$$\nabla \int_\Omega \nabla_x \Phi(x,y) \cdot (ME)(y)\, dy = \int_\Omega \nabla_x (\nabla_x \Phi(x,y), \cdot (ME)(y))\, dy$$

and we obtain

$$E^s(x) = -T_0 v(x) - (T - T_0)v(x) - \kappa^2 T_1 v(x), \tag{6.44}$$

for every $x \notin \text{supp } M$. From (6.43) and (6.44), we see that

$$\begin{aligned} E^s(x) &= (I - \frac{1}{3}M)^{-1}(E^i(x) - T_0 v(x) && (6.45)\\ &\quad -(T - T_0)v(x) - \kappa^2 T_1 v(x)) - E^i(x) \end{aligned}$$

for every $x \in \mathbb{R}^3$.

For any domain $\Lambda := Q_R + t$ for a fixed $t \in \mathbb{R}^3$ such that $\Lambda \cap Q_R = \varnothing$ we want to evaluate the scattered field by the use of the Fast Fourier transform and the domain decomposition. We recall that $\Omega \subset Q_R$ and that Q_R was defined as the cube containing the support of M.

Let $x = z + t \in \Lambda$ for a fixed $z \in Q_R$. As before we denote the kernel of A, defined in (6.24) by k. The scattered field on the domain Λ possesses the representation

$$\begin{aligned} E^s|_\Lambda(x) &= (I - \frac{1}{3}M)^{-1}|_\Lambda \Big(E^i|_\Lambda(x) - \int_{Q_R} k(t+z,y) v(y)\, dy \Big) && (6.46)\\ &\quad -E^i|_\Lambda(x) \\ &= -\int_{Q_R} k(t+z,y) v(y)\, dy, && (6.47) \end{aligned}$$

since M vanishes outside of Ω. Recalling the domain decomposition of Q_R we find that

$$\Lambda = \bigcup_{k \in \{1,2,\ldots,m\}} t + \tilde{D}_k,$$

where the subdomains $\tilde{D}_k$, $k = 1, ..., m$ are defined after (6.31). We have

$$E^s|_{(t+\tilde{D}_i)}(x) = -\sum_{j=1}^{m} \int_{\tilde{D}_j} k(t+z,y)v|_{\tilde{D}_j}(y)\, dy, \tag{6.48}$$

where $x \in (t + \tilde{D}_i)$ is represented by $x = t + z$ for some $z \in \tilde{D}_i$. Now, we use the translation (6.37) to rewrite the scattered field on $(t+\tilde{D}_i)$ as the image of a convolution on $\tilde{D}_j$. In particular, we obtain

$$E^s|_{(t+\tilde{D}_i)}(x) = -\sum_{j=1}^{m} \int_{\tilde{D}_j} k(t+x_{ij}+z_j,y)v|_{\tilde{D}_j}(y)\, dy \text{ for } z_j \in \tilde{D}_j, \tag{6.49}$$

where $z \in \tilde{D}_i$ is given by $z = x_{ij} + z_j$ for some $z_j \in \tilde{D}_j$. The kernel $\tilde{k}_{ij}(z_j, y) := k(t + x_{ij} + z_j, y) : \tilde{D}_j \times \tilde{D}_j \to \mathbb{C}$ is a continuous convolution kernel since $t \neq 0$ and we can evaluate the scattered field on Λ via a Fast Fourier transform coupled with the domain decomposition.

6.5 Numerical implementation of the conjugate gradient method for a domain decomposition

As fast method to solve the singular integral equation system we use the conjugate gradient method, given by Algorithm 6.1, and transfer the steps of Algorithm 6.1 to the domain decomposition setting. To this end, we introduce functions which use as input parameters the (string) names of *global variables*. A global variable is available in every function and during the whole running time. By the use of these input parameters we can transfer the conjugate gradient method to the domain decomposition scheme. In particular, we implement the functions

1. `matVecD.m`: Generalises a matrix-vector product to an operator evaluation on either the whole grid or by using a domain decomposition appoach.

2. `normD.m`: This function generalises the usual Euler-norm to a discretised L^2-norm for a discretised field $v \in L^2(\Omega)^3$, see Algorithm 6.3 and (5.11).

3. `numVecPlusNumVecD.m`: Sum of two matrix-vector products.

4. `numMatVecD.m`: Multiplication of a constant with a matrix-vector product.

5. `scalComplVecD.m`: Generalisation of the usual scalar product for tensors.

As an example we present the code for `normD.m`, Algorithm 6.3. The input parameters are the strings of names of the required global variables. In particular, one of the input parameters is the string 'name1' which refers to the global variable whose norm we want to compute, say v. Then, for `mycase = 1` we show the numerical evaluation of the norm for the density v with discretised components $v.comp1$ for $v^{(1)}$, $v.comp2$ for $v^{(2)}$ and $v.comp3$ for $v^{(3)}$. In the case `mycase = 2`, the implementation of the domain decomposition is shown. We use the eval-operation which executes a string containing a MATLAB expression.
As opposed to Algorithm 6.3 the functions `matVecD.m`, `numVecPlusNumVecD.m` and `numVecPlusNumVecD.m` do not have a seperate output variable. We pass the string specifiying the name of the global variable to the function as an input parameter and assign the result of the function to this global variable. For example by calling the function `matVecD` with input paramters `matVecD('A', namev, 'Av', nameParam, mycase);`, see line 8 of Algorithm 6.4, the operator evaluation of Av is assigned to the global variable Av with string name $'Av'$. Here, also `namev` and `nameParam` are strings specifying the names of the density v and the parameters like wave number, number of discretisation points etc. which are defined as global variables. Moreover, in the case of a domain decomposition, we stored the momentarily unused data and the string $'Av'$ refers to the name of the saved data.
In Algorithm 6.4 we present the conjugate gradient method which incorporates the domain decomposition scheme.

6.6 Numerical results

In the following examples we present the illumination of an anisotropic thin (finite) layer by an incident plane wave given by

$$E^i(x;d,p) := i\kappa\,(d\times p)e^{i\kappa\,x\cdot d}\,, \tag{6.50}$$

for both a non-decomposed domain and a domain decomposition. The direction of the incident plane wave is $d = (0,0,1)$ and possesses polarisation $p = (0,1,0)$. For the

Algorithm 6.3 This code presents the evaluation of the norm of v, given by (5.11), with string name 'name1' and with components `v.comp1`, `v.comp2` and `v.comp3`, for a simple non-decomposition case (case 1) and the domain decomposition approach (case 2). Here, in case 2, we use additional storage space and load the components step-by-step.

```
1: function nf = normD(name1, nameParam, mycase)
2: switch( mycase )
3: case 1
4: nor1 = 0; nor2 = 0; nor3 = 0;
5: eval(['global ' name1]); eval(['v =' name1 ';']);
6: nor1 = nor1 + sum(sum(sum(abs(v.comp1).^ 2)));
7: nor2 = nor2 + sum(sum(sum(abs(v.comp2).^ 2)));
8: nor3 = nor3 + sum(sum(sum(abs(v.comp3).^ 2)));
9: nf = sqrt(nor1 + nor2 + nor3);
10: case 2
11: nor1 = 0; nor2 = 0; nor3 = 0;
12: eval(['global ' name1]); eval(['global ' nameParam]);
13: eval(['Ncomp = ' nameParam '.Ncomp;']);
14: for j=1:Ncomp do
15:     var = [name1, '_', num2str(j)];
16:     load([var '.mat']); eval(['v =' var ';']);
17:     nor1 = nor1 + sum(sum(sum(abs(v.comp1).^ 2)));
18:     nor2 = nor2 + sum(sum(sum(abs(v.comp2).^ 2)));
19:     nor3 = nor3 + sum(sum(sum(abs(v.comp3).^ 2)));
20: end for
21: nf = sqrt(nor1 + nor2 + nor3);
22: end switch
```

Algorithm 6.4 The conjugate gradient method: Incorporating functions which use global variables to enable an easy transfer to the domain decomposition scheme:

```
1: function cgfuncD(nameA, nameAast, namef, tol, L, namev, nameParam, mycase)
2: initializeSolutionD(namev, nameParam, mycase);
3: err = zeros(L,1);
4: numMatVecD(-1, 'Aast', namef, 'pgradD', nameParam, mycase);
5: nf = normD(namef, nameParam, mycase);
6: np = normD('pgradD', nameParam, mycase);
7: for l = 1 : L do:
8:     matVecD('A', namev, 'Av', nameParam, mycase);
9:     numVecPlusNumVecD(1, 'Av', -1, namef, 'Avminf', nameParam, mycase);
10:    nAvminf = normD('Avminf', nameParam, mycase);
11:    err(l) = nAvminf/nf;
12:    matVecD('A', 'pgradD', 'Ap', nameParam, mycase);
13:    nAp = normD('Ap', nameParam, mycase);
14:    resAp = scalComplD('Avminf', 'Ap',nameParam, mycase);
15:    tstepD = real(resAp)/nAp.^2;
16:    numVecPlusNumVecD(1, namev, -tstepD, 'pgradD', namev, nameParam, mycase);
17:    matVecD('Aast', 'Avminf', 'r1', nameParam, mycase);
18:    nr1 = normD('r1', nameParam, mycase);
19:    if nr1 <= tol then:
20:        L = l;
21:        return;
22:    end if
23:    matVecD('A', namev, 'Av', nameParam, mycase);
24:    numVecPlusNumVecD(1, 'Av', -1, namef, 'Avminf', nameParam, mycase);
25:    matVecD('Aast', 'Avminf', 'r2', nameParam, mycase);
26:    nr2 = normD('r2', nameParam, mycase);
27:    gammaD = (nr2^2)/(nr1^2);
28:    numVecPlusNumVecD(1, 'r2', gammaD, 'pgradD', 'pgradD', nameParam, mycase);
29: end for
```

anisotropy we use the rotation matrix

$$U(x) := \begin{bmatrix} \cos x_1 & \sin x_1 & 0 \\ \sin x_1 & -\cos x_1 & 0 \\ 0 & 0 & 1 \end{bmatrix} \tag{6.51}$$

and set the anisotropy by choosing

$$(I - N)(x) = U(x) \cdot D(x) \cdot U(x), \tag{6.52}$$

for some diagonal matric $D : \mathbb{R}^3 \to \mathbb{C}^{3\times 3}$.

The numerical examples were executed on a personal computer with 2 GB RAM.

Example 1.

We start with the total domain

$$\Omega := [-2, 2] \times [-2, 2] \times [-1, 1],$$

which includes the support of M, and set the wave number $\kappa = 4$. In this example we set

$$d_{11}(x_1, x_2, x_3) = -\frac{1}{2}(e^{-(2x_1^2+2x_2^2+6x_3^3)}), \tag{6.53}$$

$$d_{22}(x_1, x_2, x_3) = -2(e^{-(2x_1^2+2x_2^2+6x_3^3)}), \tag{6.54}$$

$$d_{22}(x_1, x_2, x_3) = -\frac{1}{2}(e^{-(2x_1^2+2x_2^2+6x_3^3)}), \tag{6.55}$$

for the diagonal entries of D. In Figure 6.1 we visualise the anisotropy. We proceed now as follows.

(1.A) We first discretize the domain Ω with $50 \times 50 \times 20$ grid points and start the Conjugate Gradient Method without any domain decomposition. We stop the algorithm as soon as the relative residual error is smaller than 0.01 with a maximal number of iterations of 300.

(1.B) In a second example we test our domain decomposition by decomposing Ω in 2 subdomains given by $D_1 = [-2, 0] \times [-2, 2] \times [-1, 1]$ and $D_2 = [0, 2] \times [-2, 2] \times [-1, 1]$. Every subdomain is discretised with $25 \times 50 \times 20$ points. We again stop our Conjugate Gradient Method as soon as the relative residual error is smaller than 0.01.

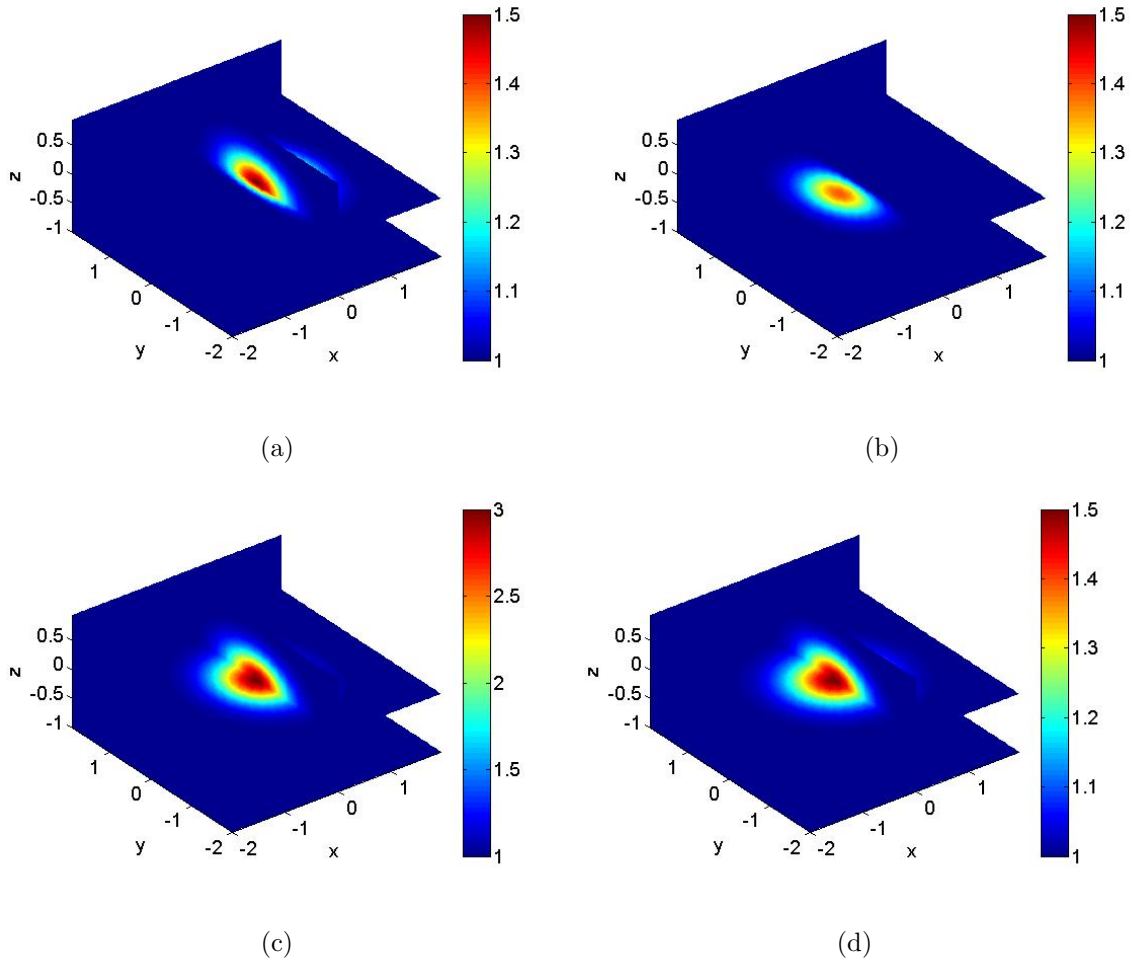

(a) (b)

(c) (d)

Figure 6.1: *Anisotropy of Example 1: In Figure (a) we plot the real part of* N_{11}*. Figure (b) shows the real part of the component* N_{12} *and* N_{21}*, (d)* N_{22} *and (e) shows* N_{33} *of* N*.*

In Figure 6.2 we show the results for the domain decomposition approach.

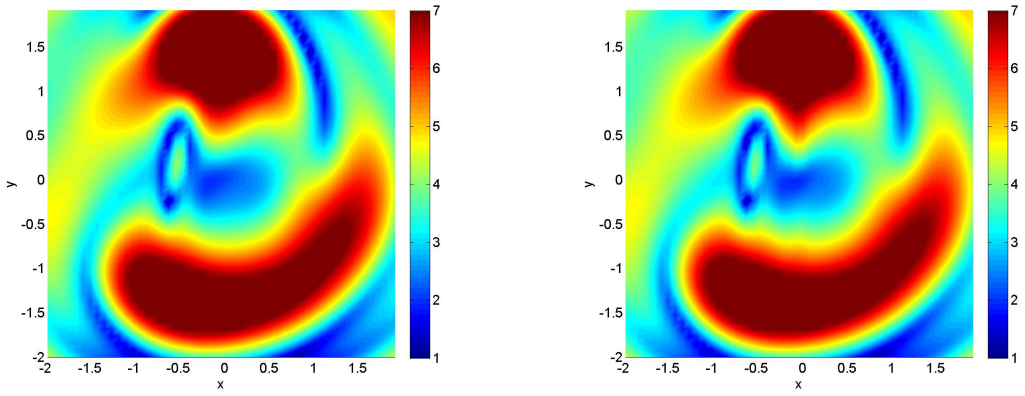

(a) (b)

Figure 6.2: *Results of Example 1: Figure (a) shows the front view of the modulus of the total field for a non-decomposed domain. In (b) we show the modulus of the total field derived from a domain decomposition in* 2×1 *subdomains, again with a total of* $50 \times 50 \times 20$ *discretisation points.*

Example 2.

In this example we set the wave number $\kappa = 5$ and

$$d_{11}(x_1, x_2, x_3) = -\frac{1}{2}(e^{-(2x_1^2+2x_2^2+6x_3^3)}), \tag{6.56}$$

$$d_{22}(x_1, x_2, x_3) = -\frac{1}{5}(e^{-(2x_1^2+2x_2^2+6x_3^3)}), \tag{6.57}$$

$$d_{22}(x_1, x_2, x_3) = -\frac{1}{2}(e^{-(2x_1^2+2x_2^2+6x_3^3)}), \tag{6.58}$$

for the diagonal entries of D. We proceed as in Example 1. In particular,

(2.A) We first discretize the domain Ω with $60 \times 60 \times 30$ grid points and start the Conjugate Gradient Method without any domain decomposition.

(2.B) In a second example we test our domain decomposition by decomposing Ω in 4 subdomains given by $D_1 = [-2, 0] \times [-2, 0] \times [-1, 1]$, $D_2 = [-2, 0] \times [0, 2] \times [-1, 1]$, $D_3 = [0, 2] \times [-2, 0] \times [-1, 1]$ and $D_4 = [0, 2] \times [0, 2] \times [-1, 1]$. Every subdomain is discretised with $15 \times 15 \times 30$ points.

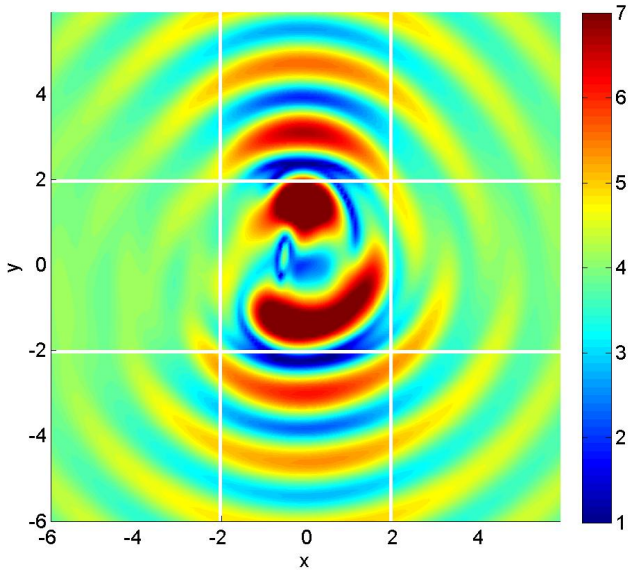

(a)

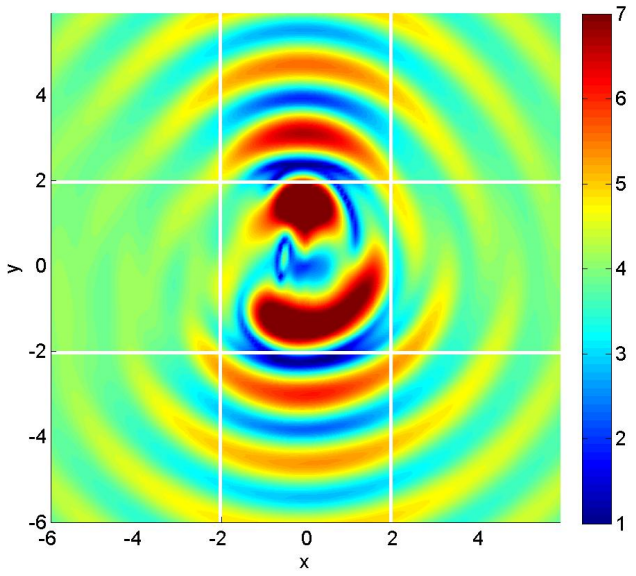

(b)

Figure 6.3: *Example 1: Figure (a) and (b) show the front view of the modulus of the total field. In both figures the scattered field is successively evaluated in the translated domains* $t+\Omega$ *for the translation vector* t*, see (6.49), and we show the total field in the total domain* $[-6,6]\times[-6,6]\times[-1,1]$*. The white lines indicate the translated domains. Figure (a) uses the non-domain decomposition. In Figure (b) the total field is evaluated by a domain decomposition approach.*

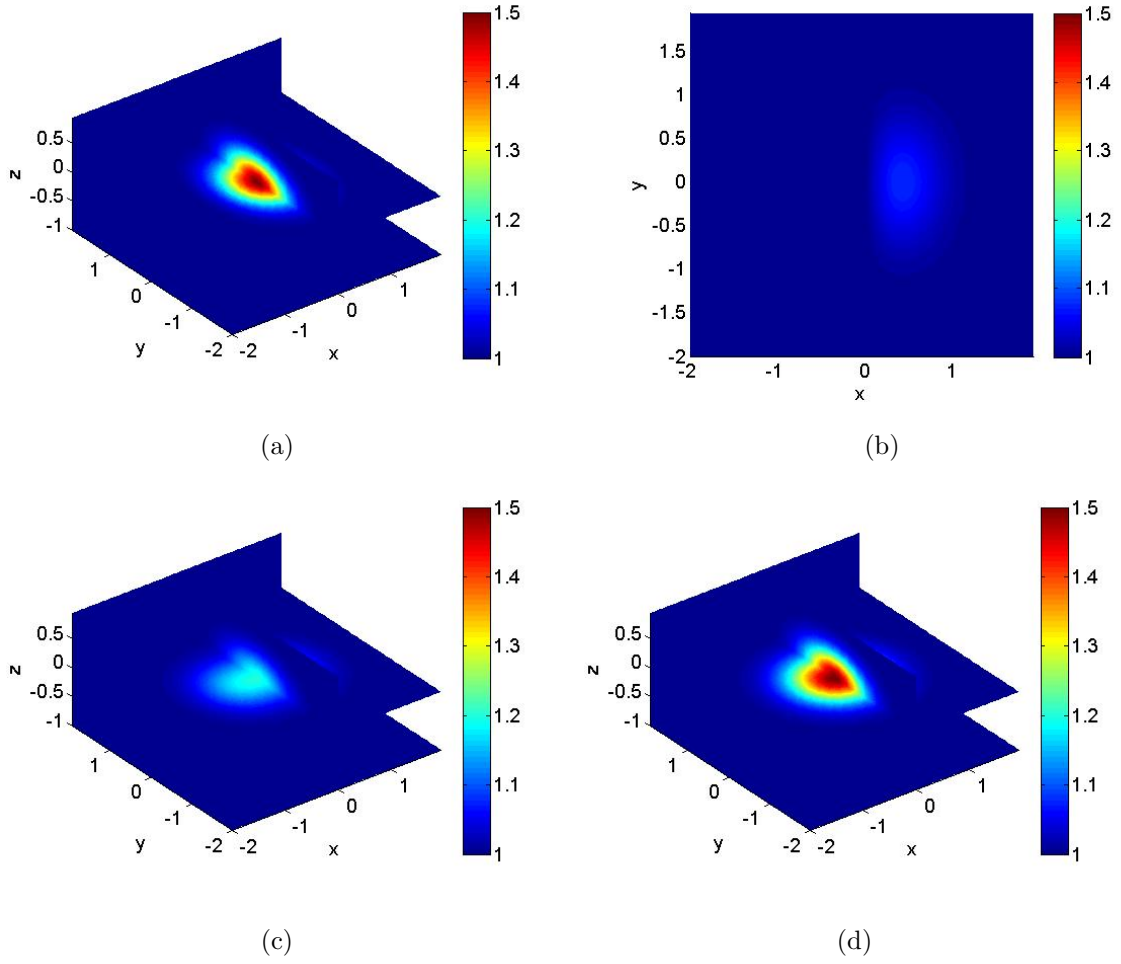

Figure 6.4: *Anisotropy of Example 2: In Figure (a) we plot the real part of* N_{11}*. Figure (b) shows the real part of the component* N_{12} *which equals* N_{21}*, (d) is* N_{22} *and (e) shows* N_{33} *of* N*.*

Figure 6.5 shows a front view of the total field in the domain $[-6,6] \times [-6,6] \times [-1,1]$ for both - a domain decomposition and a non-decomposed problem setting.

In Table 6.1 we test the performance of the direct approach for an increasing number of unknowns. We show that the amount of main memory required by the Fast Fourier transform for the evaluation of the involved integral operators limits the direct *no-decomposition* approach. In particular, we denote by *required main memory* the amount of bytes which we need for the evaluation of the Fast Fourier Transform of a data matrix of size $2N_1 \times 2N_2 \times 2N_3$ multiplicated by three, due to the three components of the electromagnetic field. We find that the domain decomposition algorithm enables

Number of gridppoints: $N_1 \times N_2 \times N_3$	Total number of unknowns	Required Main Memory	Direct (no domain decomposition)
$70 \times 70 \times 20$	294000	37.6MB	2.4min
$100 \times 100 \times 20$	600000	76.8MB	5.48min
$120 \times 120 \times 20$	846000	110.4MB	8.83min
$140 \times 140 \times 20$	1176000	150.5MB	OUT OF MEMORY

Table 6.1: *The performance of the non-decomposition Conjgate Gradient Method. In the last column we give the running time per iteration.*

Number of gridppoints: $N_1 \times N_2 \times N_3$	Total number of unknowns	Required Main Memory	Domain decomposition into 2×2 subdomains
$70 \times 70 \times 20$	294000	9.4MB	9.3 min
$100 \times 100 \times 20$	600000	19.2MB	15.8 min
$120 \times 120 \times 20$	846000	27.7MB	27.7 min
$140 \times 140 \times 20$	1176000	37.6MB	51.22min
$210 \times 210 \times 20$	2646000	84.7MB	89.82min

Table 6.2: *The performance of the domain decomposition Conjgate Gradient Method. In the last column we give the running time per iteration.*

us to compute the scattering by an anisotropic medium for an increasing number of

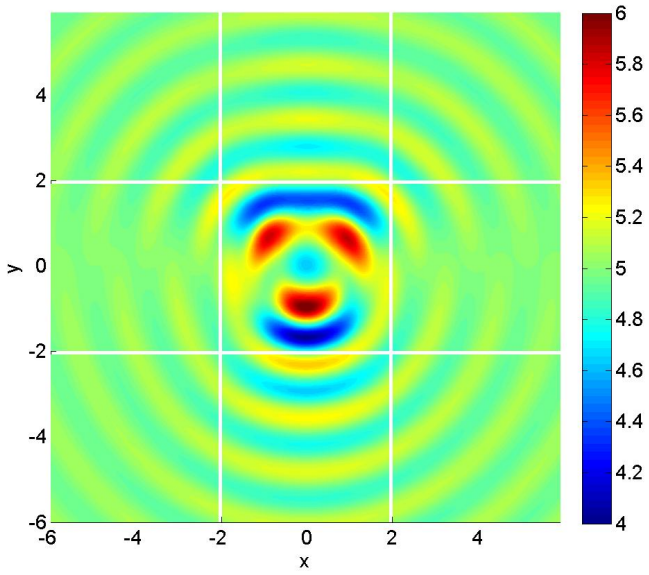

(a)

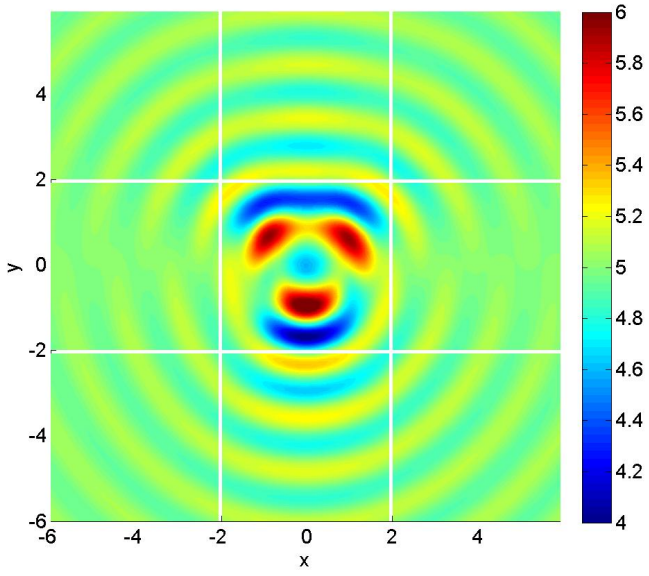

(b)

Figure 6.5: *Example 2: Figure (a) shows the front view of the modulus of the total field of Example 2 in the domain* $[-6,6] \times [-6,6] \times [-1,1]$ *for the non-decomposed domain* Ω *with* $60 \times 60 \times 30$ *discretisation points. In (b) we present the result for a domain decomposition in* 2×2 *domain.*

unknowns which cannot be numerically solved by a non-decomposition approach using a personal computer, see Table 6.2.

Optical Security Devices - Conclusions

In this thesis we have investigated optical security devices by considering the inverse acoustic rough surface scattering problem and the anisotropic electromagnetic scattering problem.

In Part 1 we considered those devices which particularly consist of a rough profile and formulated the inverse problem as the task to reconstruct the rough surface from frequency- resp. time-data given on a finite surface patch above the unknown surface. We saw that the key difficulties of the direct problem are due to the non-compactness and unboundedness of the scattering surface and these difficulties appear similarly in the inverse problem.

The main achievement of Chapter 3 was the transfer of a potential approach for the bounded domain case to the three-dimensional rough surface case. As a main result we showed the convergence of the potential approach combined with a multi-section approach. We pointed out that a rigorous analysis for the fully-infinite approach based on an optimisation problem over the non-compactly supported density and a non-compact surface cannot be carried out directly. We proved the convergence of the multi-section approach indirectly by incorporating the convergence of a semi-finite approach. For the numerical realisation of the method we used the forward code developped by E. Heinemeyer and R. Potthast, [26], [27], and we provided an example at the end of Chapter 3.

In Chapter 4 we turned to a time-domain problem formulation. As, in practice, time-data is usually collected, we were interested in the discussion of an inverse reconstruction scheme for the rough surface case from given time-data. We described a time-domain scheme which only relies on the causality principle of the wave equation

in contrast to recent results from work by Chandler-Wilde and Lines [10] and by Luke and Potthast [38] in which the two-dimensional rough surface case and the bounded domain case are discussed. We formulated the time-domain problem such that it corresponds to the frequency-domain rough surface scattering problem, which we discussed in Chapter 1 to 3, via Fourier transforms. Here, we used a non-timeharmonic scattering from pulses to apply Fourier transform techniques. We incorporated the ideas of the potential approach of Chapter 3 to formulate a reconstruction scheme which was based on time-data instead of a single frequency-data given on a surface patch above the unknown surface.

In Part 2 we considered the three-dimensional electromagnetic scattering problem. In particular, we discussed the scattering of electromagnetic plane waves by an anisotropic medium. Materials which include anisotropic scattering effects could be potentially interesting for optical applications as in optical security devices. In Chapter 5 we introduced the anisotropic scattering problem and its formulation in a strongly singular integral equation system in three dimensions. We presented the results of [43] and studied the strongly singular operator. In particular, we wished to implement a fast method to solve the strongly singular integral equation system. The key difficulties we needed to overcome had been the large amount of unknowns due to the three-dimensional scattering problem and the use of higher wavenumbers, and the numerical treatment of the strong singularity. In Chapter 6, we were able to use the symbol of the strongly singular operator to formulate a numerical exact integration scheme in terms of the exact Fourier transform evaluation of the involved strongly singular kernel. Furthermore, we formulated a geometrical domain decomposition scheme for the integral equation system. By this domain decomposition approach it is possible to handle several million unknowns by a parallelisation of the FFT-based operator evaluations on subdomains of Ω. Here, the corresponding data vectors do not need to fit in the main memory of a personal computer. The domain decomposition incorporates the usage of additionally available storage space and it permits the realisation of anisotropic scattering problems on a personal computer with computation times on the scale of hours.

We implemented a domain-decomposition-based Conjugate Gradient Method. At the end of Chapter 6 we presented examples to show the feasibility of using the domain decomposition approach for an anisotropic medium.

A possible extension to Part 1 would be the incorporation of high-frequency scattering. Moreover, we studied the time-domain Probe Method in Chapter 4 only for the case of Dirichlet boundary condition and we note that the case of other boundary conditions is open for future research. In Part 2 we observed that the domain decomposition method slows down the computations with the size of the domain and the number of subdomains and a useful next step could be the incorporation of parallel or distributed systems. In particular, we also investigated if starting the Conjugate Gradient Method on a coarse grid to obtain an approximate solution to start the CG-Method on a finer grid could accelerate the computations. We observed that this idea does work for small wavenumbers. In particular, we tested $\kappa = 1$. As soon as the wavenumber is larger we see that the minimum amount of grid points is already very large and we are forced to use the domain decomposition approach. This means that by a double amount of discretisation points in each direction also more subdomains are needed and therefore, we are in a better position if we stay with a minimum amount of unknowns for the particular wavenumber. We conclude that again a further extension of this work would lead to the involvement of distributed and parallel systems to solve the large system of unknowns. Based on a fast solver of the direct problem, the numerical realisation of the inverse problem of reconstruction of the refractive index from a given near field pattern, see for example [18], would be an interesting future investigation. Furthermore, coupling multiple small anisotropic scatterers located in the same isotropic strip could provide a novel security device and lead to the interesting topic of inverse high-frequency and multi-scattering problems.

Appendix A

Convolution operators

In this section we provide the main tools from Fourier analysis for convolution operators which we use particularly in Part 1 of the thesis. Some of the following results for convolution integral operators are proven in the thesis of Heinemeyer, [26], and we also refer to functional analysis and calculus books, for example, see [23].

A *convolution operator* or simply *convolution* is an integral operator of the type

$$K\varphi = k * \varphi(x) := \int_{\mathbb{R}^d} k(x-y)\varphi(y)\,dy, \quad x \in \mathbb{R}^d. \tag{A.1}$$

For example, the single and double layer potentials are convolutions. The existence of the above defined convolution is shown in the next theorem.

THEOREM A.0.1. *Let* $1 \leq p, q, r \leq \infty$ *with*

$$\frac{1}{p} + \frac{1}{q} = 1 + \frac{1}{r}. \tag{A.2}$$

If $k \in L^p(\mathbb{R}^d)$ *and* $\varphi \in L^q(\mathbb{R}^d)$ *then* $k * \varphi$ *exists almost everywhere in* $\mathbb{R}^d$ *and belongs to* $L^r(\mathbb{R}^d)$ *with*

$$\|k * \varphi\|_{L^r} \leq \|k\|_{L^p} \|\varphi\|_{L^q}. \tag{A.3}$$

Proof. For a proof see Theorem 3.1 in [39]. □

For a function $\ell \in L^1(\mathbb{R}^d)$ we define the *Fourier transform* of ℓ by

$$\mathcal{F}\ell(\xi) := \int_{\mathbb{R}^d} e^{-i\xi\cdot x}\ell(x)\,dx, \quad \xi \in \mathbb{R}^d. \tag{A.4}$$

The Fourier transform for a function $\ell \in L^1(\mathbb{R}^d)$ is bounded and continuous.

We present some basic theorems concerned with the mapping properties of $\mathcal{F}$. The following theorems can be found in classical analysis books, for example see [23].

COROLLARY A.0.2. *Let ℓ be a function in $C_c^n(\mathbb{R}^d), n \in \mathbb{N}$, the space of compactly supported n-times continuously differentiable functions. Then, there exists a constant $c \geq 0$ with*

$$|\mathcal{F}\ell(\xi)| \leq c(1 + \|\xi\|^{-n}) \text{ for all } \xi \in \mathbb{R}^d. \tag{A.5}$$

Proof. See [23], §12, Corollary 1. □

THEOREM A.0.3. *If $\ell \in L^1(\mathbb{R}^d) \cap L^2(\mathbb{R}^d)$, then $\mathcal{F}\ell \in L^2(\mathbb{R}^d)$ and*

$$\|\ell\|_{L^2} = (2\pi)^{\frac{d}{2}} \|\mathcal{F}\ell\|_{L^2}. \tag{A.6}$$

Proof. For a proof see for example Theorem 3, §12, in [23]. □

Based on the property that $L^1 \cap L^2$ is dense in L^2 it is possible to show the theorem of Plancherel.

COROLLARY A.0.4 (Theorem of Plancherel). *There exists a uniquely determined isomorphism $T : L^2(\mathbb{R}^d) \to L^2(\mathbb{R}^d)$ with the following properties:*

1. $\|T\ell\|_{L^2} = (2\pi)^{\frac{d}{2}} \|\ell\|_{L^2}$ *for all* $\ell \in L^2(\mathbb{R}^d)$,
2. $T\ell = \frac{1}{(2\pi)^{\frac{d}{2}}} \mathcal{F}\ell$ *for all* $\ell \in L^1(\mathbb{R}^d) \cap L^2(\mathbb{R}^d)$,
3. $T^{-1} = \frac{1}{(2\pi)^{\frac{d}{2}}} \mathcal{F}^*\ell$ *for all* $L^1(\mathbb{R}^d) \cap L^2(\mathbb{R}^d)$, *where*

$$\mathcal{F}^*\ell := \int_{\mathbb{R}^d} e^{i\xi \cdot x} \ell(x)\, dx, \quad \xi \in \mathbb{R}^d.$$

Proof. See for example [23]. □

THEOREM A.0.5 (Convolution Theorem). *Let $\ell, h \in L^1(\mathbb{R}^d)$. Then,*

$$\mathcal{F}(\ell * h) = \mathcal{F}\ell\, \mathcal{F}h. \tag{A.7}$$

Furthermore, let $\ell, h \in L^2(\mathbb{R}^d)$ *and define the convolution operator* $L : L^2(\mathbb{R}^d) \to L^2(\mathbb{R}^d)$ *which maps* h *to* $\ell * h$*. Then, (A.7) still holds. If* $\mathcal{F}\ell \in L^\infty(\mathbb{R}^d)$*, we have that* L *is a bounded operator with norm*

$$\|Lh\|_{L^2} \leq c \|\mathcal{F}\ell\|_{L^\infty} \tag{A.8}$$

Proof. See for example [23] for the first part of the theorem. The second part of the theorem is shown in Lemma 1.44 in [26]. □

LEMMA A.0.6. *Let* $m_1, m_2 \in BC(\mathbb{R}^d)$ *and* $\ell \in L^2(\mathbb{R}^d)$ *such that* $\mathcal{F}\ell \in L^\infty(\mathbb{R}^d)$*. Let the integral operator* L *be defined by*

$$L\varphi(x) := \int_{\mathbb{R}^d} m_1(x)\ell(x-y)\varphi(y)m_2(y)\,dy,\ x \in \mathbb{R}^d. \tag{A.9}$$

Then, we have that L *is a bounded operator with bound*

$$\|L\|_{L^2 \to L^2} \leq \|m_1\|_{BC} \|\mathcal{F}\ell\|_{L^\infty} \|m_2\|_{BC} \tag{A.10}$$

and further, $L\varphi \in L^2(\mathbb{R}^d) \cap BC_\infty(\mathbb{R}^d)$*.*

Proof. See for example Lemma 1.46 in [26]. □

In [8] it is shown that the single layer and double layer potentials are bounded operators on $L^2(\Gamma)$ by using a Taylor series expansion of the kernel G_3 with respect to y_3 and the incorporation of the estimate of Lemma A.0.6. At the beginning of Part 1 we use these tools and consider the single layer potential as an operator from $L^2(\Gamma) \to L^2(\tilde{\Gamma})$ for rough non-intersecting surfaces $\tilde{\Gamma}$ and Γ.

Appendix B

Ill-posed problems and Tikhonov regularisation

In Part 1 we discuss the reconstruction of the shape of a rough surface in three dimensions from given *measurements* above the unknown surface. The mathematical model of such a problem leads to an inverse problem. In this section we provide the main tools to discuss the inverse problem and present the *Tikhonov regularisation*. The following results can be found in the books of Kirsch, [30], and of Colton and Kress, [17].

Firstly, we need to explain what we understand by an *ill-posed* problem as most inverse problems are ill-posed. To this end, we follow Hadamard, [25], and start with the definition of a *well-posed* problem.

Definition B.0.7. *We call a problem well-posed if*

1. *there exists a solution,*
2. *the solution is unique,*
3. *the solution depends continuously on the data.*

If one or more of these properties fail to hold, the problem is called ill-posed.

Many inverse problems lead to an *ill-posed* operator equation $A\varphi = f$.

DEFINITION B.0.8 (Well-posedness). *Let X, Y be normed spaces and $A : X \to Y$ be a linear mapping. Then, the equation*

$$A\varphi = f \tag{B.1}$$

is well-posed if

- *The equation (B.1) is solvable for all right hand sides $f \in Y$ (Existence).*
- *The operator A is injective (Uniqueness).*
- *The inverse operator $A^{-1} : Y \to X$ is continuous (Stability).*

If at least one of these properties is not satisfied the problem (B.1) is called ill-posed.

In other words, the equation (B.1) is well-posed, if the operator is bijective and the inverse operator is continuous. Many inverse problems of the form $A\varphi = f$ are ill-posed as the inverse of A is not uniformly bounded. To solve the operator equation $A\varphi = f$ we need some *regularisation method*.

But first, we note that an operator equation $A\varphi = f$ with a compact linear operator $A : X \to Y$ is always ill-posed in an infinite dimensional space:
Suppose that A is compact and possesses a bounded inverse A^{-1}. Then, we have that $A^{-1}A\varphi = I\varphi$ for the identity operator I and, because the product $A^{-1}A$ must be compact, see for example [35], so is the idenity. As the identity can only be compact if X is finite-dimensional, [35], this is a contradiction, and thus, A^{-1} cannot be bounded.

DEFINITION B.0.9 (Regularisation Method). *Let X and Y be normed spaces and let $A : X \to Y$ be an injective bounded linear operator. Then, a family of linear bounded operators $\{R_\alpha\}_{\alpha>0}$ is a regularisation scheme for the operator A if the pointwise convergence to the identity operator*

$$R_\alpha A\varphi \to \varphi \text{ for } \alpha \to 0 \tag{B.2}$$

holds for every $\varphi \in X$.

From now on we denote by X and Y Hilbert spaces if no other comment is given and by $\langle \cdot, \cdot \rangle$ the scalar product in X resp. Y. Let $A : X \to Y$, then we denote by A^* its adjoint. $N(A)$ is the nullspace of A, i.e.

$$N(A) := \{\varphi \in X : A\varphi = 0\}. \tag{B.3}$$

LEMMA B.0.10 ([30], Lemma 2.10). *Let X and Y be Hilbert spaces and let $A : X \to Y$ be a linear and bounded operator. Then, there exists $\varphi^* \in X$ with*

$$\|A\varphi^* - f\| \leq \|A\varphi - f\| \text{ for all } \varphi \in X \tag{B.4}$$

if and only if φ^* is a solution of the normal equation

$$A^*A\varphi^* = A^*f. \tag{B.5}$$

Let us consider X to be an infinite dimensional Hilbert space and let $A : X \to Y$ be a compact operator. In this case, also A^*A is compact and $A^*A\varphi = A^*f$ remains ill-posed. The above lemma now implies that the minimization of the residual $\|A\varphi - f\|$ with respect to φ in some norm in Y corresponds to solving the (ill-posed) normal equation $A^*A\varphi^* = A^*f$.

A possible approach is to replace equation (B.5) by

$$\alpha\varphi + A^*A\varphi = A^*f, \tag{B.6}$$

where $\alpha > 0$ is called the *regularisation parameter* and equation (B.6) is referred as *Tikhonov normal equation*. That the operator $R_\alpha := (\alpha I + A^*A)^{-1}A^*$ is indeed a regularisation scheme is the statement of the following theorem.

LEMMA B.0.11 ([17]). *Let $A : X \to Y$ be an injective and compact operator. Then for each $\alpha > 0$ the operator $(\alpha I + A^*A) : X \to X$ is bijective and has a bounded inverse and*

$$R_\alpha := (\alpha I + A^*A)^{-1}A^* : Y \to X \tag{B.7}$$

is a regularisation scheme.

THEOREM B.0.12 ([17]). *Let $A : X \to Y$ be a compact linear operator and $\alpha > 0$. Then, for each $f \in Y$ there exists a unique $\varphi_\alpha \in X$ s.t.*

$$\|A\varphi_\alpha - f\|^2 + \alpha \|\varphi_\alpha\|^2 = \inf_{\varphi \in X} \left\{ \|A\varphi - f\|^2 + \alpha \|\varphi\|^2 \right\} \tag{B.8}$$

and, furthermore, $\varphi_\alpha \in X$ is the solution of

$$\alpha\varphi + A^*A\varphi = A^*f. \tag{B.9}$$

The functional

$$J_\alpha(\varphi) := \|A\varphi - f\|^2 + \alpha \|\varphi\|^2 \tag{B.10}$$

is called *Tikhonov functional*. We discuss the behavior for $\alpha \to 0$ in the following theorem.

THEOREM B.0.13. *Let A be injective and the range of A dense in Y. Let φ_0 be the exact solution of $A\varphi = f$. Then, either*

(i) if $f \in A(X)$, then $\lim_{\alpha\to 0} \|\varphi_\alpha\| = \|\varphi_0\| < \infty$, or

(ii) if $f \notin A(X)$, then $\|\varphi_\alpha\| \longrightarrow \infty$ for $\alpha \to 0$.

Proof. This is proven in [49]. □

We include in this section the following properties, which are used in the proof of Theorem B.0.13 and which we also need throughout the first part of this thesis.

LEMMA B.0.14. *Let X, Y be Hilbert spaces. The following statements hold.*

(i) Every bounded sequqence $(\varphi_n)_{n\in\mathbb{N}} \subset X$ possesses a weakly convergent subsequence $(\varphi_{n(j)})_{j\in\mathbb{N}}$ with $\varphi_{n(j)} \rightharpoonup \tilde{\varphi} \in X$ for $j \to \infty$, i.e.

$$\left\langle \varphi_{n(j)}, z \right\rangle \rightharpoonup \langle \tilde{\varphi}, z \rangle \,,\ j \to \infty, \text{ for all } z \in X.$$

(ii) Every weakly convergent sequence is bounded.

(iii) A compact operator maps a weakly convergent sequence in a strongly convergent sequence.

Proof. (i): For a proof we refer to [39], Theorem 2.31.
(ii): This is proven in [54].
(iii): Let $(\varphi_n) \subset X$ and $\varphi \in X$ with $\varphi_n \rightharpoonup \varphi$. Let further $A : X \to Y$ be a compact operator. Then,

$$\langle A\varphi_n - A\varphi, z\rangle = \langle \varphi_n - \varphi, A^* z\rangle \to 0 \text{ for all } z \in Y,$$

i.e. $A\varphi_n \rightharpoonup A\varphi$. Suppose now that $(A\varphi_n)$ does not strongly converge to $A\varphi$, i.e. there exists a subsequence $(A\varphi_{n(j)})$ with

$$\left\|A\varphi_{n(j)} - A\varphi\right\| > \varepsilon \text{ for } j > j_0 \text{ for some } j_0 \in \mathbb{N}. \tag{B.11}$$

By the foregoing we have $A\varphi_{n(j)} \rightharpoonup A\varphi$. Further, as A is compact, and (φ_n) is bounded from (ii), there exists a strongly convergent subsequence of $(A\varphi_{n(j)})$. Let this subsequence for simplicity be denoted by $(A\varphi_{n(j)})_{j\in\mathbb{N}}$ with limit $f_0 \in Y$. On the one hand, we have $A\varphi_{n(j)} \rightharpoonup f_0$ for $j \to \infty$, and on the other hand, $A\varphi_{n(j)} \rightharpoonup A\varphi$ for $j \to \infty$, hence, $f_0 = A\varphi$. This is a contradiction to (B.11) and we have shown the statement. □

At the end of this section we want to study the Tikhonov regularisation in the view point of so-called *filters*. Let from now on A be a *compact* operator.

Definition B.0.15 (Singular Values). *The square roots*

$$\mu_j = \sqrt{\lambda_j}, \quad j \in J \subseteq \mathbb{N}$$

of the eigenvalues λ_j of the self-adjoint operator $A^*A : X \to X$ are called singular values of A.

Theorem B.0.16 (Singular Value Decomposition). *Let $\mu_1 \geq \mu_2 \geq ... > 0$ be the ordered sequence of the (positive) singular values of A, counted relative to its multiplicity. Then, there exist orthonormal systems $(\varphi_j) \subset X$ and $(f_j) \subset Y$ with the properties*

$$A\varphi_j = \mu_j f_j \text{ and } A^* f_j = \mu_j \varphi_j \text{ for all } j \in J. \tag{B.12}$$

The system (μ_j, φ_j, f_j) is called singular system for A. Every $\varphi \in X$ has the representation

$$\varphi = \varphi_0 + \sum_{j\in J} \langle \varphi, \varphi_j \rangle \, \varphi_j \tag{B.13}$$

for some $\varphi_0 \in N(A)$ and

$$A\varphi = \sum_{j\in J} \mu_j \langle \varphi, \varphi_j \rangle \, f_j \tag{B.14}$$

Proof. See for example [30]. □

Theorem B.0.17 (Picard). *The equation*

$$A\varphi = f \tag{B.15}$$

is solvable if and only if

$$f \in N(A^*)^\perp \text{ and } \sum_{j\in J} \frac{1}{\mu^2} |\langle f, f_j \rangle|^2 < \infty. \tag{B.16}$$

In this case, φ can be represented by

$$\varphi = \sum_{j \in J} \frac{1}{\mu_j} \langle f, f_j \rangle \varphi_j. \tag{B.17}$$

Proof. See [30]. □

By Picard's Theorem, we see that every solution of the operator equation $A\varphi = f$ has a representation (B.17). Suppose that the right hand side f is replaced by $f^\delta := f + \delta f_n$ for an arbitrary but fixed $n \in J$, i.e. we solve the slightly perturbed equation $A\varphi^\delta = f^\delta$. The solution φ^δ has the representation

$$\varphi^\delta = \sum_{j \in J} \frac{1}{\mu_j} \langle f, f_j \rangle \varphi_j + \frac{1}{\mu_n} \delta \varphi_n. \tag{B.18}$$

Then, whenever μ_n is very small, the noise $\delta > 0$ strongly adulterates the solution φ^δ compared to the true solution of $A\varphi = f$. The idea is to construct a regularisation strategy by damping the factors $\frac{1}{\mu_j}$, i.e. we look for a *regularisation filter* $q : (0, \infty) \times (0, \|A\|] \to \mathbb{R}$ for which the operator R_α defined by

$$R_\alpha f := \sum_{j=1}^{\infty} \frac{q(\alpha, \mu_j)}{\mu_j} \langle f, f_j \rangle \varphi_j \tag{B.19}$$

is a regularisation strategy. The solution φ_α of the Tikhonov normal equation has the representation

$$\begin{aligned} \varphi_\alpha &= (\alpha I + A^* A)^{-1} A^* f \\ &= \sum_{j=0}^{\infty} \frac{\mu_j}{\alpha + \mu_j^2} \langle f, f_j \rangle \varphi_j, \end{aligned} \tag{B.20}$$

where (μ_j, φ_j, f_j) is a singular system for the operator A. As we have seen, the Tikhonov regularisation is a regularisation scheme and (B.20) explains the damping of the singular values on which it relies on.

Bibliography

[1] T. Arens and A. Kirsch. The factorization method in inverse scattering from periodic structures. *Inverse Problems*, 19:1195–1211, 2003.

[2] A. Bamberger and T. Ha-Duong. Formulation variationelle pour le calcul de la diffraction d'une onde acoustique par une surface rigide. *Math. Meth. in the Appl. Sci.*, 8:598–608, 1986.

[3] G. Bao and A. Friedmann. Inverse problems for scattering by periodic structure. *Arch. Rat. Mech. Anal.*, 132:49–72, 1995.

[4] C. Burkard and R. Potthast. A time-domain probe method for three-dimensional rough surface reconstructions. *Inverse Problems and Imaging (IPI)*, 3(2):259 – 274, 2009.

[5] C. Burkard and R. Potthast. A multi-section approach for rough surface reconstruction via the Kirsch-Kress scheme. *Inverse Problems*, 26(4):045007 (23pp), 2010.

[6] F. Cakoni and D. Colton. *Qualitative methods in inverse scattering theory.* Springer, 2006.

[7] S. N. Chandler-Wilde, E. Heinemeyer, and R. Potthast. A well-posed integral equation formulation for three-dimensional rough surface scattering. *Proc. R. Soc. A*, 462(2076):3683–3705, 2006.

[8] S. N. Chandler-Wilde, E. Heinemeyer, and R. Potthast. Acoustic scattering by mildly rough unbounded surfaces in three dimensions. *SIAM Journal on Applied Mathematics*, 66(3):1002–1026, 2006.

[9] S. N. Chandler-Wilde and M. Lindner. Boundary integral equations on unbounded rough surfaces: Fredholmness and the finite section method. *Journal of Integral Equations and Applications*, 20:13–48, 2008.

[10] S. N. Chandler-Wilde and C. D. Lines. A Time Domain Point Source Method for Inverse Scattering by Rough Surfaces. *Computing*, 75:157–180, 2005.

[11] S. N. Chandler-Wilde and P. Monk. Existence, Uniqueness, and Variational methods for scattering by unbounded rough surfaces. *SIAM Journal on Mathematical Analysis*, 37(2):598–618, 2005.

[12] S. N. Chandler-Wilde and R. Potthast. The Domain Derivative in Rough Surface Scattering and Rigorous Estimates for First Order Perturbation Theory. *Proc. R. Soc. Lond. A*, 458:2967–3001, 2002.

[13] S. N. Chandler-Wilde and C. R. Ross. Uniqueness results for direct and inverse scattering by infinite surfaces in a lossy medium. *Inverse Problems*, 10:1063–1067, 1995.

[14] S. N. Chandler-Wilde and C. R. Ross. Scattering by Rough Surfaces: the Dirichlet Problem for the Helmholtz Equation in a Non-locally Perturbed Half-plane. *Mathematical Methods in the Applied Sciences*, 19(12):959–976, 1996.

[15] S. N. Chandler-Wilde and B. Zhang. A generalised collectively compact operator theory with an application to second kind integral equations on unbounded domains. *Journal of Integral Equations and Applications*, 14:11–52, 2002.

[16] S. N. Chandler-Wilde, B. Zhang, and C. R. Ross. On the Solvability of Second Kind Integral Equations on the Real Line. *Journal of Mathematical Analysis and Applications*, 245:28–51, 2000.

[17] D. Colton and R. Kress. *Inverse acoustic and electromagnetic scattering theory*, volume 93 of *Applied Mathematical Sciences*. Springer-Verlag, Berlin, second edition, 1998.

[18] D. Colton and R. Potthast. The inverse electromagnetic scattering problem for an anisotropic medium. *Q. J. Appl. Math*, 52:349–372, 1999.

[19] P. Davies and D. Duncan. Stability and convergence of collocation scheme for retarded potential integral equations. *SIAM J. Numer. Anal.*, 42, 3:1167–1188, 2004.

[20] J. A. DeSanto and R. J. Wombell. Reconstruction of rough surface profiles with the kirchhoff approximation. *Journal of the Optical Society of America A A -Optics Image Science and Vision*, 8 (12):1892–1897, 1991.

[21] J. A. DeSanto and R. J. Wombell. The reconstruction of shallow rough-surface profiles from scattered field data. *Inverse Problems*, 7:L7–L12, 1991.

[22] J. Elschner and M. Yamamoto. An inverse problem in periodic diffractive optic: reconstruction of lipschitz grating profiles. *Appl. Anal.*, 81 (20):1307–1328, 2002.

[23] O. Forster. *Analysis 3.* vieweg+teubner, 5. aktualisierte Auflage, 2009.

[24] N. Grinberg and A. Kirsch. The factorization method for inverse problems. *Oxford Lecture Series in Mathematics and Its Applications*, 36, 2008.

[25] J. Hadamard. Lectures on cauchy's problem in linear partial differential equations. Yale University Press, 1923.

[26] E. Heinemeyer. *Integralgleichungsmethoden für Streuprobleme an rauhen Oberflächen in drei Dimensionen.* PhD thesis, Georg-August Universitaet Goettingen, 2008.

[27] E. Heinemeyer, M. Lindner, and R. Potthast. Convergence and numerics of a multi-section method for scattering by three-dimensional rough surfaces. *SIAM J. Numerical Analysis*, 46(4):1780–1798, 2008.

[28] M. Ikehata. The probe method and its applications. In *Inverse problems and related topics (Kobe, 1998)*, volume 419 of *Chapman & Hall/CRC Res. Notes Math.*, pages 57–68. Chapman & Hall/CRC, Boca Raton, FL, 2000.

[29] H. Kersten. Grenz- und Sprungrelationen für Potentiale mit quadratsummierbarer Dichte. *Resultate der Mathematik*, 3:17–24, 1980.

[30] A. Kirsch. *An introduction to the mathematical theory of inverse problems*, volume 120 of *Applied Mathematical Sciences.* Springer-Verlag, New York, 1996.

[31] A. Kirsch and R. Kress. On an integral equation of the first kind in inverse acoustic scattering. In *Inverse problems (Oberwolfach, 1986)*, volume 77 of *Internat. Schriftenreihe Numer. Math.*, pages 93–102. Birkhäuser, Basel, 1986.

[32] A. Kirsch and R. Kress. A numerical method for an inverse scattering problem. In *Inverse and ill-posed problems (Sankt Wolfgang, 1986)*, volume 4 of *Notes Rep. Math. Sci. Engrg.*, pages 279–289. Academic Press, Boston, MA, 1987.

[33] A. Kirsch and R. Kress. An optimization method in inverse acoustic scattering (invited contribution). In *Boundary elements IX, Vol. 3 (Stuttgart, 1987)*, pages 3–18. Comput. Mech., Southampton, 1987.

[34] R. Kress. *Linear Integral Equations*. Springer, 1989.

[35] R. Kress. *Linear integral equations*, volume 82 of *Applied Mathematical Sciences*. Springer-Verlag, New York, second edition, 1999.

[36] C. Lines. *Inverse scattering by rough surfaces*. PhD thesis, Departement of Mathematics, Brunel University, 2003.

[37] C. Lubich. On the multistep time discretization of linear intitial-boundary value problems and their boundary integral equations. *Numer. Math.*, 67:365–389, 1994.

[38] D. R. Luke and R. Potthast. The point source method for inverse scattering in the time domain. *Math. Meth. Appl. Sci.*, 29, Issue 13:1501–1521, 2006.

[39] W. McLean. *Strongly Elliptic Systems and Boundary Integral Equations*. Cambridge University Press, 2000.

[40] S. Mikhlin and S. Proessdorf. *Singular integral operators*. Springer, 1980.

[41] A. Neubauer, B. Kaltenbacher, and O. Scherzer. Iterative regularization methods for nonlinear ill-posed problems. In *Radon Series on Computational and Applied Mathematics*. de Gruyter, 2008.

[42] R. Potthast. Integral equation methods in electromagnetic scattering from anisotropic media. *Mathematical Methods in the Applied Sciences*, 23:1145–1159, 2000.

[43] R. Potthast. Integral equation methods in electromagnetic scattering from anisotropic media. *Math. Meth. Appl. Sci*, 23:1145–1159, 2000.

[44] R. Potthast. *Point sources and multipoles in inverse scattering theory*, volume 427 of *Chapman & Hall/CRC Research Notes in Mathematics*. Chapman & Hall/CRC, Boca Raton, FL, 2001.

[45] R. Potthast. Sampling and Probe Methods — An Algorithmical View. *Computing*, 75(2-3):215–235, 2005.

[46] R. Potthast. A survey on sampling and probe methods for inverse problems. *Inverse Problems*, 22(2):R1–R47, 2006.

[47] R. Potthast, F. M. Fazi, and P. A. Nelson. Source splitting methods via the point source method. *submitted for publication*, 2009.

[48] R. Potthast and J. Schulz. From the Kirsch-Kress potential method via the range test to the singular sources method. *J. Phys.: Conf. Ser.*, 12:116–127, 2005.

[49] R. Potthast, J. Sylvester, and S. Kusiak. A 'range test' for determining scatterers with unknown physical properties. *Inverse Problems*, 19(3):533–547, 2003.

[50] R. S. Strichartz. *A guide to distribution theory and Fourier transforms*. World Scientific Publishing Co Pte Ltd, second edition edition, 2003.

[51] M. Thomas. *Analysis of rough surface scattering problems*. PhD thesis, Department of Mathematics, University of Reading, 2006.

[52] G. Vainikko. Fast Solvers of the Lippmann-Schwinger Equation. Technical Report A387, Helsinki University of Technology, Institute of Mathematics, August 1997.

[53] R. L. van Renesse. *Optical document security*. Springer Netherlands, 1994.

[54] D. Werner. *Funktionalanalysis*. Springer-Verlag, third edition, 2000.

[55] B. Zhang and S. N. Chandler-Wilde. Integral equation methods for scattering by infinite rough surfaces. *Mathematical Methods in the Applied Sciences*, 24:463–488, 2003.

[56] A. Zinn. On an optimization method for the full- and limited aperature problem in inverse acoustic scattering for a sound-soft obstacle. *Inverse Problems*, 5:239–253, 1998.

Index